The Thesis Committee for Ruohan Li
Certifies that this is the approved version of the following Thesis:

Correlating Pavement Texture, Noise and Friction Properties

APPROVED BY
SUPERVISING COMMITTEE:

Jorge A. Prozzi, Supervisor

Joaquin Hernandez, Reader

Correlating Pavement Texture, Noise and Friction Properties

by

Ruohan Li

Thesis

Presented to the Faculty of the Graduate School of

The University of Texas at Austin

in Partial Fulfillment

of the Requirements

for the Degree of

Master of Science in Engineering

The University of Texas at Austin

August, 2020

Acknowledgements

I would like to thank my parents, Hailin Li and Xuan Liu, for the unceasing care and support they have given to me throughout the years. I would like to thank my supervisor, Dr. Jorge A Prozzi, for the encouragement and guidance on the various tasks and projects I have been working on as I explored my interest in transportation research and as I worked towards the completion of this thesis. I would like to thank Joaquin Hernandez, for kindly agreeing to be the reader for it and providing a great multitude of valuable feedbacks. Last but not least, I would like to thank Christian Sabillon, as he and Joaquin laid a solid foundation with data collection, processing, and preliminary analysis, patiently introduced me to the project as I was starting and explained to me how previous work had been done prior to my joining. The completion of this work would not have been made easy without all the efforts aforementioned, and I just cannot sufficiently express my gratitude to all these wonderful people above, for not only making it possible, but an enjoyable and unforgettable experience for me as well.

Abstract

Correlating Pavement Texture, Noise and Friction Properties

Ruohan Li, MSE

The University of Texas at Austin, 2020

Supervisor: Jorge A. Prozzi

This thesis uses texture, friction, and noise data collected along eight asphalt pavements with different surface types across Texas to explore the intercorrelation between the three properties, both within each pavement surface type and across different types. It was found that across all surface types, the entire frequency band of noise from 400 to 5000 Hz correlates the strongest with texture of wavelengths from 31.5 mm to 2.5 mm positively. This means that regardless of the surface type, pavements with a higher texture level in the wavelength spectrum of 31.5 mm to 2.5 mm tend to generate a higher level of noise in the frequency band of 400 to 5000 Hz. When noise is broken down into 1/3 octave bands in frequency, the strongest positive correlation is found between noise of 630 Hz and texture of 50 mm wavelength. A negative correlation, however, is found between higher frequency ($f > 1000$ Hz) noise and shorter wavelength ($\lambda < 10$ mm) texture. The slope of noise vs. texture is similar across different pavements, but the intercept can be different, indicating that with a unit increase in texture level, the additional noise generated by different pavement types is of similar magnitude, but they might be at different levels of loudness given the same texture level. Across all pavement types, when texture level is the same, pavements surfaced with thin overlay mixtures (TOM) tend to generate a consistently

lower level of noise at both high and low frequencies. While no strong correlation was found between noise and friction, this finding is consistent with the conclusions from studies by previous researchers. The correlation between friction and texture using the original data has not been found to be strong, which can be partially due to the inconsistency in location of the corresponding measurements. With the capability of measuring texture and friction simultaneously to ensure that the data are collected under the same condition and location using the equipment developed at UT Austin, a much stronger correlation between friction in terms of Grip Number (GN) and texture in terms of root mean square (RMS) was found. Speed, meanwhile, also plays an important role in predicting friction, with a significantly negative coefficient in the model. Statistically different friction levels are also observed among different mix types of pavement surface when other variables are held constant, indicating that different surface types can provide different levels of friction given the same texture at the same speed.

Table of Contents

List of Tables

List of Figures

Chapter 1: Introduction

According to Federal Highway Administration's (FHWA) 23 Code of Federal Regulations (CFR) 626.3 (2011), *"pavement shall be designed to accommodate current and predicted traffic needs in a safe, durable, and cost-effective manner."* As the roadway network system evolves to meet the requirements from both real-life demands and regulations issued by highway agencies, designing pavements that provide traffic mobility alone is no longer sufficient. Domenichini et al. (1999) pointed out that pavement characteristics are to be designed to fulfill structural (capacity), environmental (noise and vibrations) and safety (friction, hydroplaning, splash and spray) requirements. Hoerner and Smith (2002) described the two components of pavement performance as follows: while structural performance is the ability to carry traffic loads, functional performance is the ability to provide a smooth, safe, and comfortable ride to the travelers. Flinsch et al. (2003) define a good level of ride quality as the combination of good friction, low levels of roughness, and low levels of noise. Ahammed and Tighe (2010) cited Descornet (1989) in identifying the characteristics to be considered while designing the optimized pavement surface: safety in terms of skid resistance, splash and spray, visibility of road aor markings, and tire grip; economy in terms of fuel consumption, vehicle aor tire wear, and extra dynamic loads (vertical oscillation) on pavements; and comfort of users or residents in terms of noise and vibration inside and outside the vehicles. To provide satisfactory ride quality to the highway users, all factors should be well considered during the pavement design process, among which friction, texture, and noise are three major ones to include.

Though friction and noise have traditionally been believed to be conflicting characteristics, numerous studies have shown that they do not necessarily have to be incompatible (Elsenaar, 1977; Sandberg and Descornet, 1980). Chandler et al., (2003) cited

Abbott and Phillips (1996) that the relationship between road surface texture and tire noise differs depending on whether the surface texture is predominantly transverse (brushed concrete), or random (hot rolled asphalt or exposed aggregate concrete surface). A better understanding of the intercorrelation between texture, noise, and friction can help transportation agencies better make decisions in terms of pavement type selection based on the need of the specific site.

Chapter 2: Background

TEXTURE

Road surface texture is important as it controls different tire/road interactions such as skid resistance, noise, vibrations of the suspension, tire wear, and tire rolling resistance (Ejsmont et al., 2017). It is defined by the irregularities on a pavement surface that deviate from a true perfectly flat surface (Maguire and Carme, 2015).

Texture Classification

Pavement texture is categorized, based on wavelength, into microtexture, macrotexture, and megatexture (Henry, 2000). Texture with a wavelength longer than the upper limit of megatexture is classified as unevenness or roughness. Microtexture is defined by wavelengths ranging from 0.0 to 0.5 mm, macrotexture from 0.5 to 50 mm, megatexture from 50 to 500 mm, and unevenness from 500 mm to 50 m. Out of these ranges of texture, micro- and macro-texture are the two components primarily contributing to tire-pavement friction via different mechanisms. Microtexture interacts with the tire on a molecular scale and provides the adhesion component of friction, necessary at any speed. Though its importance is regardless of whether it is under dry or wet conditions, it plays a key role when the pavement is wet as it helps cut through the water film between the pavement surface and the tire. Macrotexture is the determining factor for skid resistance on wet pavements, especially when the vehicle travels at above 90 km/h. As it affects water drainage from the tire pattern, it is considered to be responsible for the hysteresis component of friction at high speeds. Pavement texture is dependent on the pavement surface properties, out of which maximum aggregate size, course and fine aggregate types, mix binder content and viscosity, mix gradation and mix air content are the ones affecting

macrotexture, and the coarse aggregate type mainly affects microtexture (Kogbara et al, 2016).

Each category is a function of the domains of texture wavelengths or spatial frequency, given that they are related by the relation $f_s = 1/\lambda$ (Serigos et al., 2016). Figure 4-1: Definition of fundamental texture classes, as a function of the wavelengths or spatial frequency illustrates the surface texture spectrum with the four main texture components and their respective wavelength or spatial frequency domain.

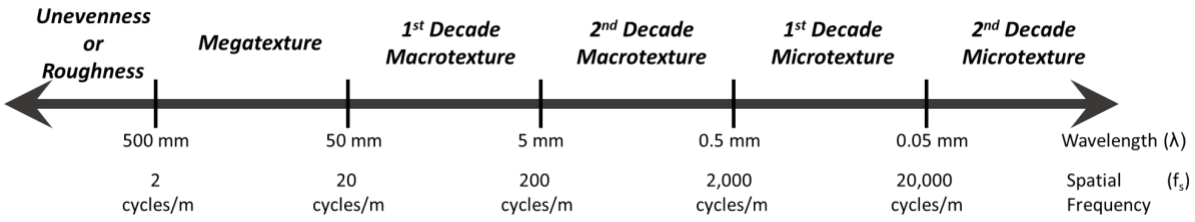

Figure 4-1: Definition of fundamental texture classes, as a function of the wavelengths or spatial frequency

Each of the four components influences tire/pavement to varying degrees. Smit (2008) reported that the unevenness of the pavement plays a significant role in the rolling resistance of the pavement, while the megatexture influences both rolling resistance and tire/pavement noise. Hall et al. (2009) summarized the pavement-tire interaction phenomena and the texture wavelength ranges upon which each of them primarily depends, based on findings from Henry (2000) and Sandburg and Ejsmont (2002), as shown in Figure 4-2.

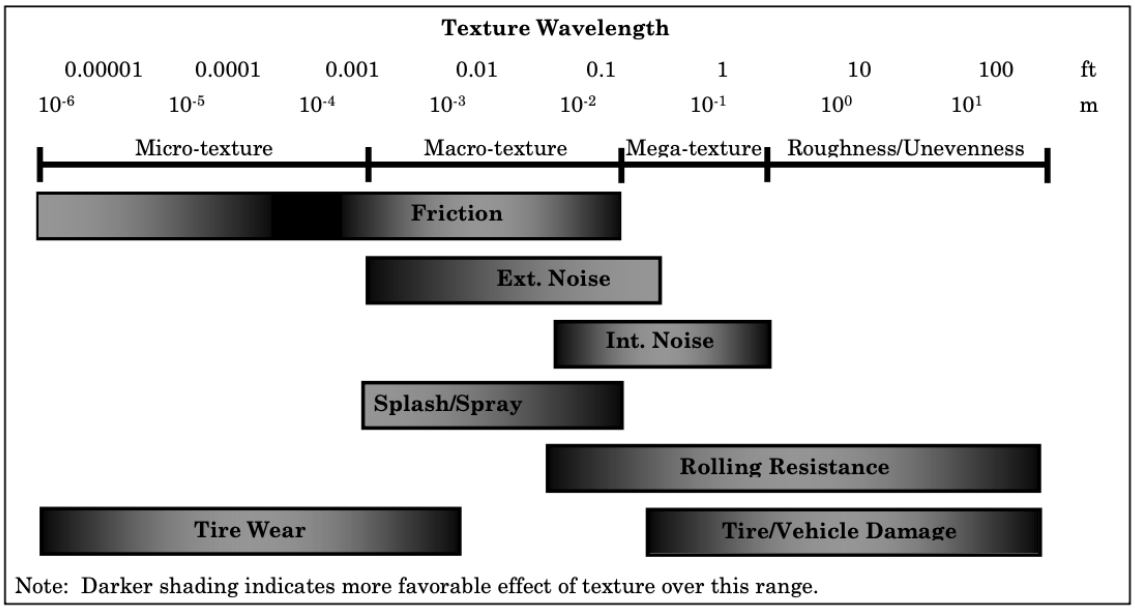

Figure 4-2: Texture Wavelength Influence on Pavement–Tire Interactions (Hall et al., 2009)

Texture Measurement

As described by Sabillon et al. (2020), in terms of texture, there are multiple techniques and equipment used to measure texture based on the texture component of interest. Typically, transportation agencies collect data for unevenness, megatexture and macrotexture for road maintenance and rehabilitation decisions. As pointed out by FHWA's Technical Advisory T 5040.36 (2005), microtexture and macrotexture are the two pavement surface characteristics that provide wet weather friction, and are the major components influencing tire/pavement noise. However, since no standard has been developed to measure microtexture on the road, significant effort has been dedicated to develop an affordable, efficient and reliable way to measure microtexture (Zuniga, 2017).

A topological survey can be used at the unevenness level to describe the pavement texture by obtaining the International Roughness Index (IRI). The IRI was developed in

1986 by the World Bank as one the first standardized primary indicator for the serviceability of highway network to road users (Sayers et al., 1986). The index calculates pavement roughness in inches per mile (in/mi.) or meters per kilometer (m/km) based on a surface profile measured by a laser sensor mounted on a profiler van. It was developed to capture the movement of the vehicle as felt by the driver. Figure 4-3 shows a schematic of a Road Surface Tester (RST), a vehicle that can be used to measure IRI. These measurements of IRI are typically within a wavelength range of 1.3 to 30 meters. (Sayers et al., 1986). Similarly, IRI measurements can also be used to characterize the pavement in the megatexture level using the highest resolution possible. Furthermore, using the same equipment, other parameters such a rut depth can also be measured to characterize megatexture.

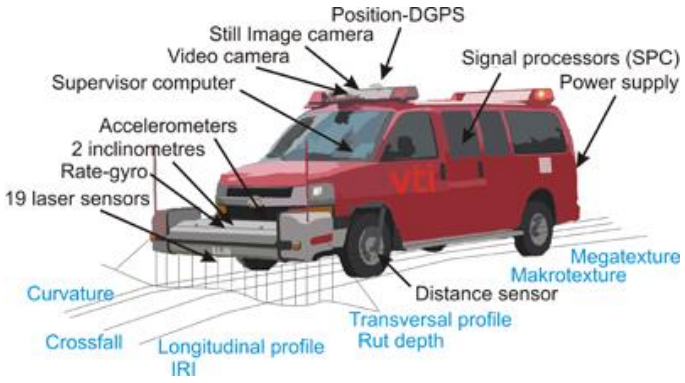

Figure 4-3: Schematic of a RST used to measured IRI and rut depth

Measurements taken at the macrotexture level can be taken in two different ways: with on-spot or in motion measurements. On-spot measurements typically require traffic control in order for technicians to collect the data in a safe manner and a significant number of measurements to get a representative sample for the pavement. Examples of on-spot measurements involve volumetric techniques such as the Sand Patch Test (SPT) or non-contact measurements such as the Circular Track Meter (CTM). In motion testing typically

involves taking continuous measurements on the pavement as a vehicle or trailer equipped with proper instrumentation drives on the road. While the latter procedures do not require traffic control, they are unable to collect microtexture data. Examples of in motion testing methods include Laser Crack Measurement System (LCMS) and the V-Texture. The latter one is the method used by Texas Department of Transportation (TxDOT).

Sand Patch Test (SPT)

Some of the most common volumetric techniques used to measure pavement macrotexture are the Sand Patch, the Grease Patch and the Outflow Meter Test. Out of the three, the Sand Patch Test is the simplest and most commonly used by transportation agencies. The method involves applying a known volume, which is typically 25 mm^3, of either solid glass spheres of uniform size or Ottawa natural silica sand on a relatively uniform, not distressed section of the pavement surface. The sand is spread in a circular motion with a spreading tool, as shown in Figure 4-4. Once the roughly circular patch of sand is made, four equally spaced diameters are measured and averaged to compute the area of the sand patch. The known volume of sand is then divided by the area of the circle using Equation 2.1 and reported as the Mean Texture Depth (MTD) (ASTM E965, 2015). The Grease Patch method is a variation used by NASA in which grease is used instead of sand or glass spheres (Zuniga, 2017). The Outflow Meter is a transparent vertical cylinder that is located on the top of the pavement surface, it is filled with water and the time for the water level to fall by a fixed amount is measured and reported as the outflow time (OFT) (ASTM E2380, 2015).

$$MTD = \frac{4V}{\pi D^2} \qquad 4\text{-}1$$

Where,

V = Material sample volume (mm^3)

D = Average diameter covered by material (mm)

Figure 4-4: (left) Sand Patch test equipment, and (right) field data collection

Circular Track Meter (CTM)

An alternative to indirect measurements of the texture profiles involves more modern techniques using non-contact lasers, such as the Circular Track Meter (CTM) or the Laser Texture Scanner model 9300 (LTS). The information collected from these devices can be used to compute various profile statistics such as the Mean Profile Depth (MPD).

The CTM is a device used to measure mean profile depth (MPD) and root mean square (RMS). It consists of a laser displacement sensor that is mounted on an arm that rotates clockwise at a fixed elevation from the measured surface and a portable computer that is used to control the device and save all the processed data as shown in Figure 4-5(a). The device measures a 2-D profile of a circle 284 mm in diameter. The profile is divided into eight segments with an arc length of 111.5 mm, as shown in Figure 4-5(b). The MPD is determined for each of the segments of the circle and the MPD reported as the average of the eight segments (ASTM 2157, 2015). The device later proceeds to calculate the RMS

for the profile using the equation for RMS provided in Table 4-1. A major drawback of the CTM arises when measuring textures of concrete pavement. Given that the system measures texture along a circumference, it makes it difficult to measure longitudinal or traverse texture separately. These two types of textures are very different for rigid pavements due to the surface anisotropy, hence, it is recommended that other techniques be used for that type of analysis.

Figure 4-5: (a) Circular Track Meter (CTM), and (b) CTM segments

Parameter	Calculation
Mean Profile Depth (MPD)	$MPD = \frac{1}{2}[\max\left(h_1, \dots, h_{\frac{N}{2}}\right) + \max\left(h_{\frac{N}{2}+1}, \dots, h_N\right)]$
Second Moment	$M_2 = \frac{1}{N}\sum_{i=1}^{N} h_i^2$
Third Moment	$M_3 = \frac{1}{N}\sum_{i=1}^{N} h_i^3$
Fourth Moment	$M_4 = \frac{1}{N}\sum_{i=1}^{N} h_i^4$
Root Mean Square (RMS)	$RMS = \sqrt{M_2}$

Skewness (R_{sk})	$R_{sk} = \frac{1}{RMS^3}\sqrt{M_3}$
Kurtosis (R_{ku})	$R_{ku} = \frac{1}{RMS^4}\sqrt{M_4}$

Table 4-1: Spatial texture parameters used for pavement texture characterization

Laser Texture Scanner (LTS)

The LTS is a lightweight and portable equipment designed to scan pavement surfaces in order to characterize its texture. It uses a laser sensor to scan the surface coordinate of parallel straight lines with a sampling rate of one point every 0.015 mm and a maximum scan area of 100 by 75 mm. The LTS computes the MPD, RMS, texture profile index (TPI), and estimated texture depth (ETD), which is an estimation of MTD based on MPD using an empirical equation, as shown in Equation 3.2. The resolution of the device allows it to measure and describe the two decades of macrotexture (wavelengths from 50 to 5 mm and from 5 to 0.5 mm) and the first decade of microtexture (wavelengths from 0.5 to 0.05 mm). However, scans performed at the highest resolution can take approximately two hours, making it impractical for field studies (Serigos et al., 2014). Zuniga (2017) also reports that the device is also not as reliable as the CTM and operators have experienced many operational problems in multiple occasions. Figure 2-6 illustrates the LTS device along with the scanned 3D surface profile plot.

$$ETD = 0.2 + 0.8 * MPD \qquad 4\text{-}2$$

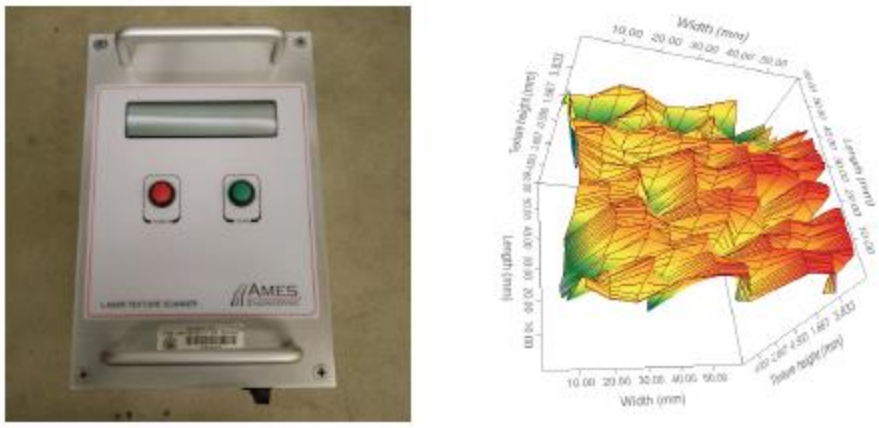

Figure 4-6: (left) Laser Texture Scanner (LTS), and (right) 3D plot of measured surface (Zuniga, 2017)

Currently, there are no standard methods to measure microtexture of pavements. Nevertheless, due to the high correlation between microtexture and low speed friction, some agencies replace microtexture measurements for low-speed-friction tests. It should be noted though, that most of the research dealing with the measurement of microtexture is based on the use of laser scanners and image analysis techniques. Some of the methods used to quantify microtexture statically include the LTS, the Line Laser Scanner (LLS) and the Aggregate Imaging System (AIMS).

Aggregate Imaging System (AIMS)

The AIMS is a system that uses image analysis techniques to analyze the particle geometry of coarse and fine aggregate through three independent properties: form, angularity and surface texture. The equipment consists on a camera, two different types of lighting schemes and microscope technology (Masad, 2005), as shown in Figure 4-7. AIMS analyzes the captured images of the aggregates using different techniques for each of the independent properties. The Wavelet method (Energy Signature) is used to analyze the aggregate texture; the gradient method and radius method are used to analyze the angularity

of the aggregate (Angularity Index), and the three-dimensional form of the aggregate is analyzed using sphericity and shape factors (Masad, 2005). The AIMS is an optical system so its main limitation is its precision. All laser systems evaluated in this research are superior than the optical system.

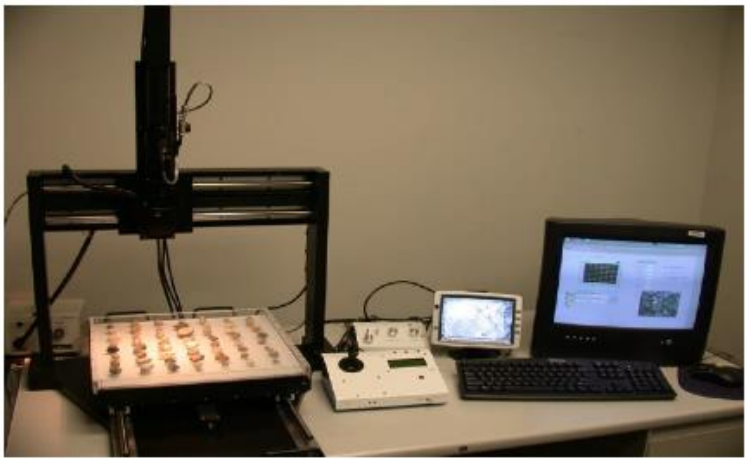

Figure 4-7: AIMS device (Mahmoud et al., 2010)

Line Laser Scanner (LLS)

The LLS is a surface profiling system developed to characterize macro- and microtexture. The device consists of a high-resolution laser scanner and a translation stage. The LLS is capable of collecting a maximum of 800 points in the transversal direction and a move up to 600 mm in the longitudinal direction. The equipment has an improved sampling rate that allows for the characterization of the decades of macrotexture (wavelengths of 0.5 to 50 mm) and the first decade of microtexture (wavelengths of 500 to 50 microns) (Zuniga, 2017). The main advantage that the LLS has over the LTS is its speed. The LLS is capable of scanning a wider area at a very high resolution in 15 seconds as opposed to two hours as is the case of the LTS. In addition, Zuniga states that not only is

the LLS more reliable than the CTM and the LTS but it also has a higher vertical resolution of 0.5 microns compared to the 3 microns in the CTM and 15 microns in the LTS. The equipment is suitable to be used out in the field (Zuniga, 2017).

Figure 4-8: (left) Line Laser Scanner (LLS), and (right) field operation

FRICTION

Friction is the resistance to motion between two surfaces in contact. Its magnitude is quantified by the coefficient of friction: the ratio of the friction force, whose direction is parallel to the plane in which the surface of contact lies and opposite to the direction of motion, and the normal force, which is perpendicular to the surface of contact, as calculated by

$$\mu = \frac{F_t}{F_v} \qquad 4\text{-}3$$

Where,

$\mu =$ Friction coefficient,

$F_t =$ Tangential (tractive) force applied at the tire/pavement interface, and

$F_v =$ Dynamic load on the tire perpendicular to the pavement.

Friction and Safety

According to Elsenaar et al. (1977), there are several reasons for measuring skid resistance of pavements: to predict the safety performance on wet pavements, to determine the priority level for road systems maintenance, to manage road systems and allocate budget, and to gather information on pavement skid properties for setting standards. With increasing traffic volumes and speeds during the late 1940s and early 1950s, a constant increase in number of crashes and traffic fatalities drew civil engineers' attention towards pavement safety in the highway system. Though there are numerous factors that lead to crashes, two primary causes were found to be uncontrolled skidding due to inadequate surface friction, which contribute to 15% to 35% of all wet weather crashes, and poor visibility due to splash and spray, which accounts for 10% of all wet weather crashes (Hoerner and Smith, 2002).

Many studies have documented the relationship between pavement skid resistance and safety. Fwa et al. (2003) identified the skid resistance of roadway surfaces as one of the fundamental requirements for highway engineers to consider in order to ensure safety in the process of pavement design. It is important in directional control and stopping ability on a pavement (Msallam et al., 2017), especially under wet pavement conditions. According to FHWA, over the decade between 2007 and 2016, 15% of vehicle crashes and 12% of crash fatalities occurred on wet pavements.

Giles et al. (1962) conducted a study on the correlation between skid number and skidding crashes. The skid resistance was measured by the Portable Skid-Resistance Tester (SRT) pendulum (shown in Figure 4-10) at selected sites of frequent skidding crashes, as well as a set of sites randomly chosen for comparing purposes. The average skid number for the frequent skidding crash sites was 45, and the average for the random sample was 60. Their distribution by site type is shown in Figure 4-9.

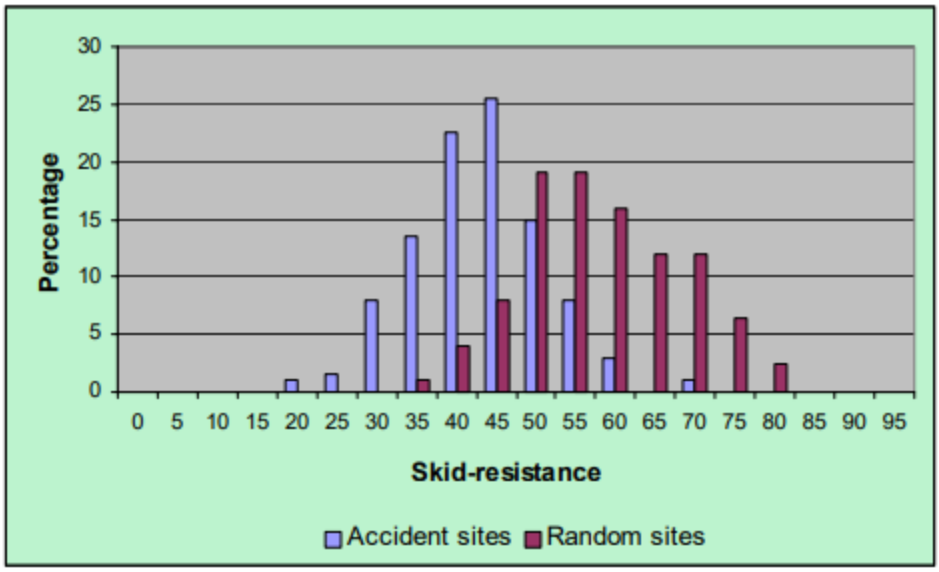

Figure 4-9: Skid Resistance Distribution of Frequent Crash Sites and Random Sites

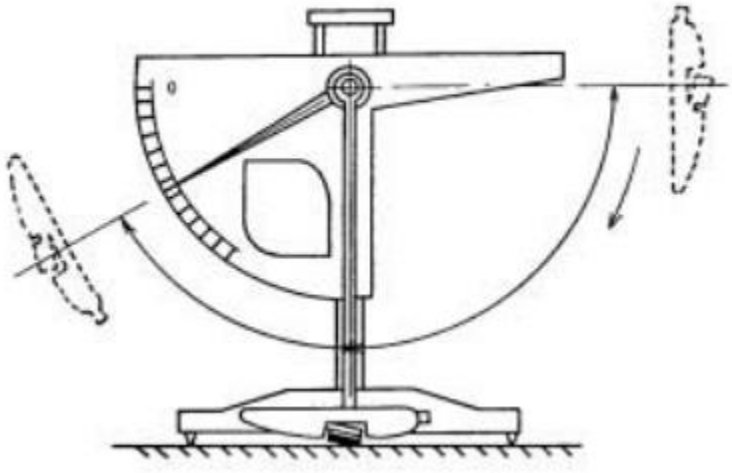

Figure 4-10: The Portable Skid Resistance Tester (SRT) (Wallman and Åström, 2001)

Blackburn et al. (1978) conducted a multi-year study on wet pavement crashes for various combinations of highway type, area type, and traffic volume over two one-year periods on 428 highway sections across 16 states to explore countermeasures that can either

increase the friction between tire and pavement, or reduce the friction demand required to safely operate the vehicle under wet pavement conditions. It was found that the wet-pavement accident rate decreases as skid number increases. The exact relationship dependents on the type of the environment and the highway facility, though reliable results for such relationship are only available for rural area, where sample sizes are largest.

Rizenbergs et al. (1976) performed a study in Kentucky to correlate crash with friction using friction, crash, and AADT data over 770 miles of rural, four-lane, limited access highways aggregated into 110 test sections. The researchers identified a negative correlation between skid number and wet crash rates, and the wet crash rate per 100 million vehicle-miles traveled (VMT) correlated best with ribbed tire. They also found a significant increase in crash rate when SN70 drops below 27. Burchett and Rizenbergs (1982) fitted a model representing how percentage of wet crashes vary with SN7R. The result is shown in Figure 4-11: Percentage of Wet Crashes Varying with SN70 (Kuttesch, 2004).

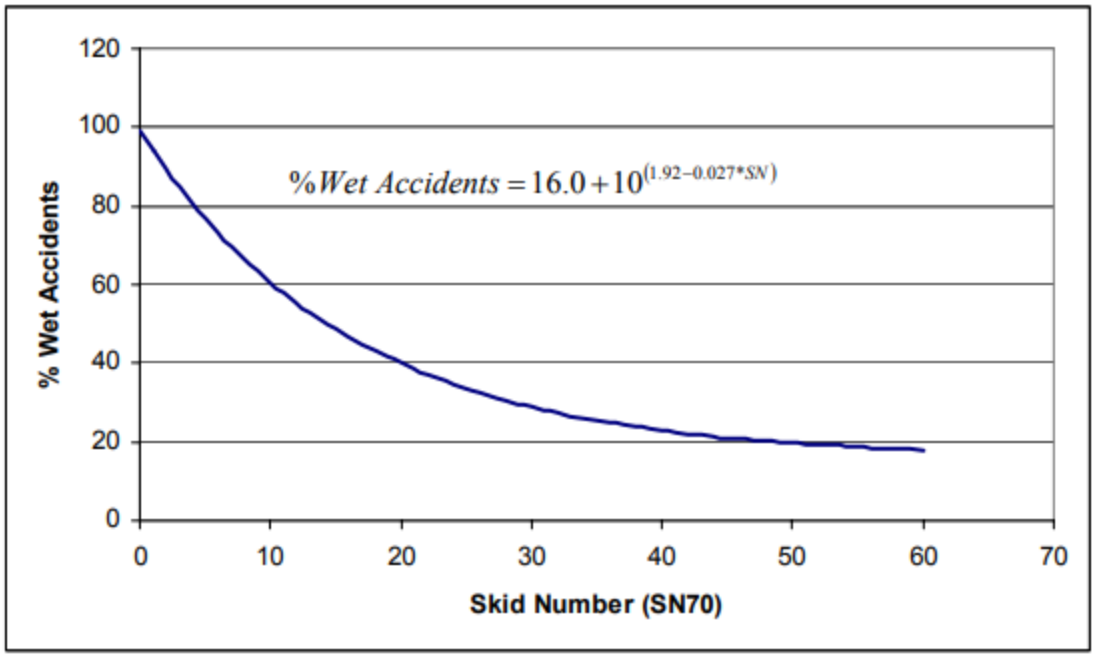

Figure 4-11: Percentage of Wet Crashes Varying with SN70 (Kuttesch, 2004)

Xiao et al. (2000) constructed and evaluated two fuzzy-logic models using crash data and the corresponding traffic data collected from 123 highway sections in Pennsylvania from 1984 to 1986. The input variables used in the model included skid number, posted speed, average daily traffic, percentage of wet time, and driving difficulty as input variables while the output variable was the number of wet-pavement crashes. Using a model based on Mamdani's fuzzy-inference method, the number of wet-pavement crashes was predicted to decrease by 60% as skid number increased from 33.4 to 48.

Kuttesch (2004) used crash and skid data both from the Virginia wet accident reduction program and from sections without pre-identified accident or skid problems to analyze the relationship between skid resistance, crashes, and traffic volume for the state of Virginia. Wet crash rates were calculated by dividing wet accident data aggregated in 1.6 km (1.0 mile) sections by the annual traffic to obtain wet accident rates. Wet skid resistance was measured with a locked-wheel trailer using a smooth tire, and the minimum skid number measured on each of section was added to the database. The study used regression analyses and concluded that wet crash rate increases as skid number decreases, and also as traffic volume increases. The author suggests a target skid number (SN64S) of 25 to 30.

Milton et al. (2008) used highway crash report injury data from Washington State to estimate a random parameters logit model to explore the effect that traffic highway and weather characteristics have on the distribution of highway crash severity among property damage only, possible injury, and injury. Pavement friction measured on a scale of 0-100 using a standardized test was used as one of the independent variables. And the authors considered a friction number over 30 as acceptable for roadways with design speeds over 40 mph. They found that increasing friction corresponds with a decrease in likelihood of

possible injury crashes, and thus an increase in likelihood of both property damage only and injury crashes. They hypothesized that this could be due to more aggressive driving behavior of some drivers when better friction is provided, but not all.

Friction Mechanisms

The two principal components of pavement friction are adhesion and hysteresis, as shown in Figure 4-12. Adhesion is the friction force developed from the small-scale bonding and interlocking as the tire rubber and the pavement surface come into contact with each other and is dependent on the interface shear strength and the area of the contact interface. The rest of the friction force develop as kinetic energy is converted and stored within the rubber as the vehicle tire compresses against the pavement surface. Part of the stored energy can be recovered when the tire relaxes, while the rest is converted into heat. As the conversion of kinetic energy to heat is an irreversible process, the net friction force developed from it is the hysteresis. Though there are also other components, such as tire rubber shear, their contribution to the overall friction force is negligible compared to the two aforementioned ones (Hall et al., 2009).

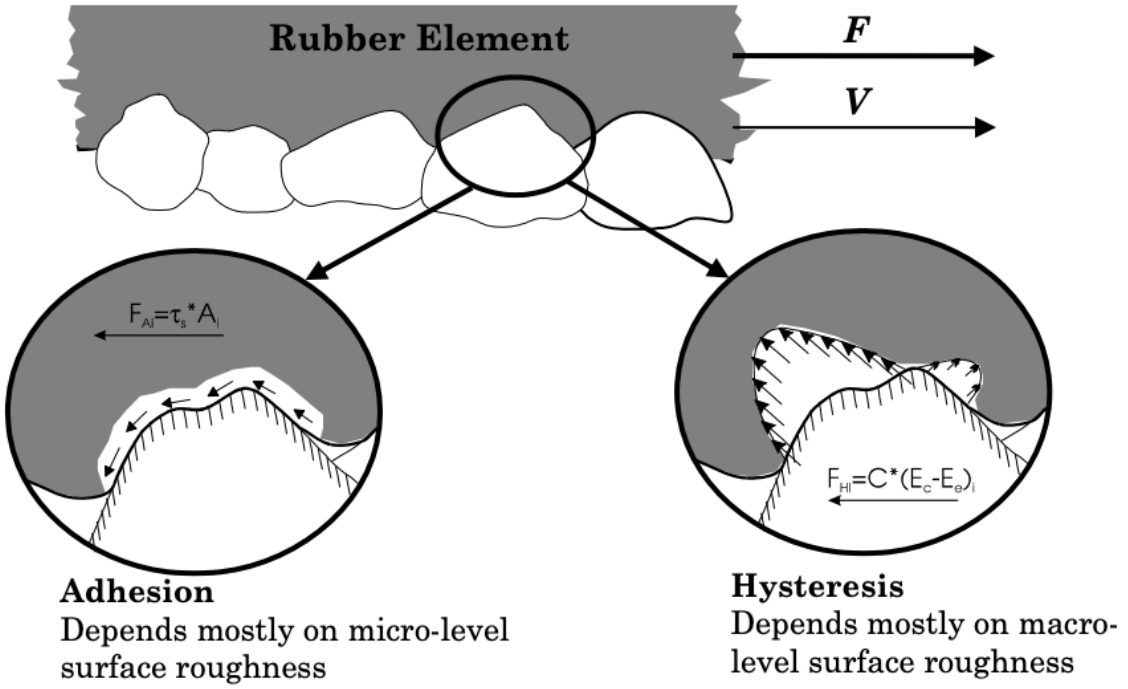

Figure 4-12: Mechanisms of Friction (Hall et al., 2009)

Factors Influencing Friction

According to Kummer (1966) and Sandberg (1998), among factors that influence pavement friction, those from roadway include macrotexture, microtexture, unevenness/megatexture, chemistry of materials, temperature, thermal conductivity, and specific heat. Factors from fluid contaminants include chemical structure, viscosity, density, temperature, thermal conductivity, specific heat, and film thickness. Factors from tire include tread pattern design, rubber composition, inflation pressure, rubber hardness, load, thermal conductivity, specific heat, and sliding velocity.

Surface Texture

Both adhesion and hysteresis depend upon pavement surface characteristics, tire properties, pavement/tire interaction, temperature, and sliding speed. Adhesion is more

sensitive to the microtexture of the aggregate particles contained in the pavement surface, while hysteresis is more sensitive to the macrotexture of the pavement surface through mix design. Thus, friction is determined by adhesion on smooth-textured, dry pavements, while hysteresis is dominant on rough-textured, dry pavements (Hall et al., 2009). However, with the presence of water, microtexture provides penetration through thin water films to produce more skid resistance, while macrotexture provides drainage channels for water, and thus allowing the tire to have better contact with the pavement, and preventing hydroplaning (Fontes et al., 2006).

Slip Speed

The coefficient of friction between tire and pavement varies with speed. As shown in Figure 4-13, it increases rapidly with increasing slip to a peak value typically between 10 and 20 percent slip, and then decreases to the coefficient of sliding friction, which happens when the wheel is fully locked, or, at full (100%) slip.

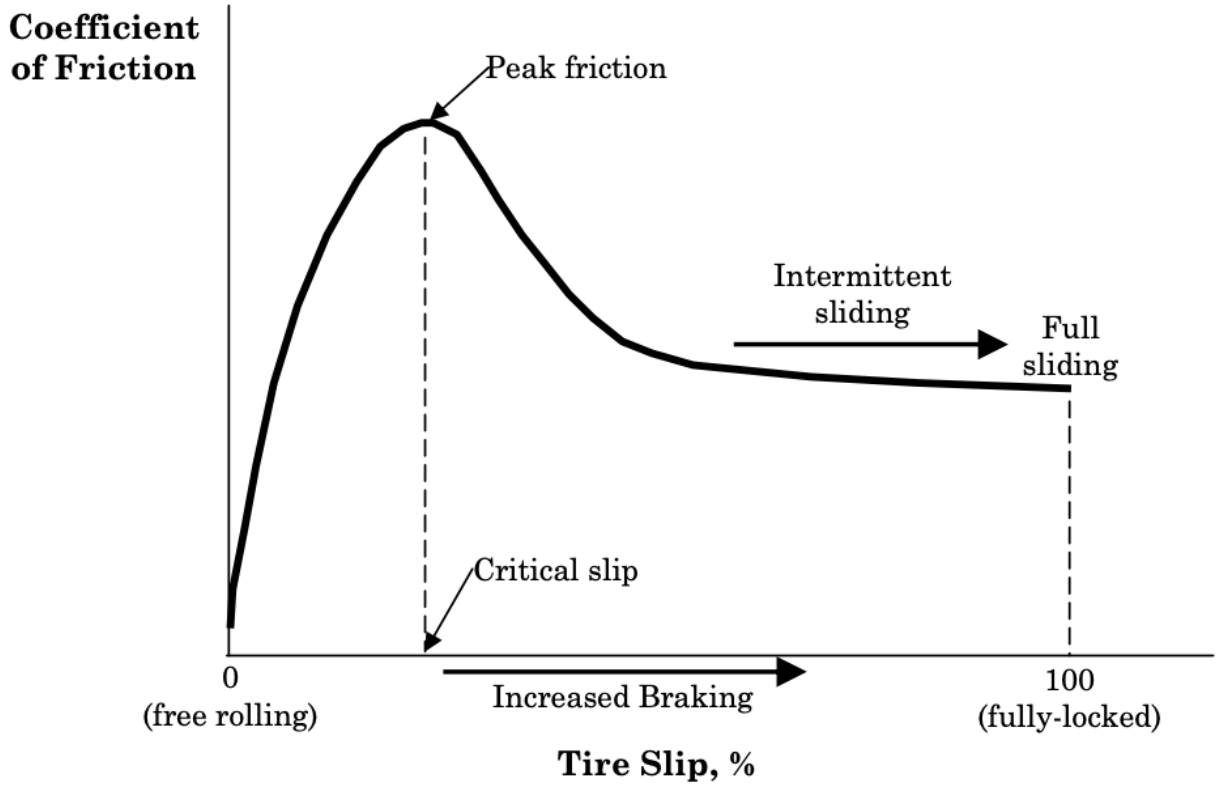

Figure 4-13: Coefficient Varying with Tire Slip (Hall et al., 2009)

Water

Fwa et al. (2003) identified skid resistance of roadway surface as one of the fundamental requirements for highway engineers to consider in order to ensure safety in the process of pavement design. It is important in directional control and stopping ability on a pavement (Msallam et al., 2017). The presence of water can significantly reduce the skid resistance between tire and pavement. The effect of water film thickness (WFT) on friction is minimal at speeds lower than 20 mph (32 km/h) and quite pronounced at speeds over 40 mph (64 km/h). Figure 4-14 plots the relationship between friction and WFT in inches for three different types of tires (Hall et al., 2009). It is shown that the coefficient of friction between the vehicle tire and the wet pavement surface decreases as WFT

increases. As WFT gets higher, friction does not reduce as drastically with each unit of WFT increase compared to when it is very thin. The friction on smooth tires are more responsive to WFT compared to both new and worn ribbed tires.

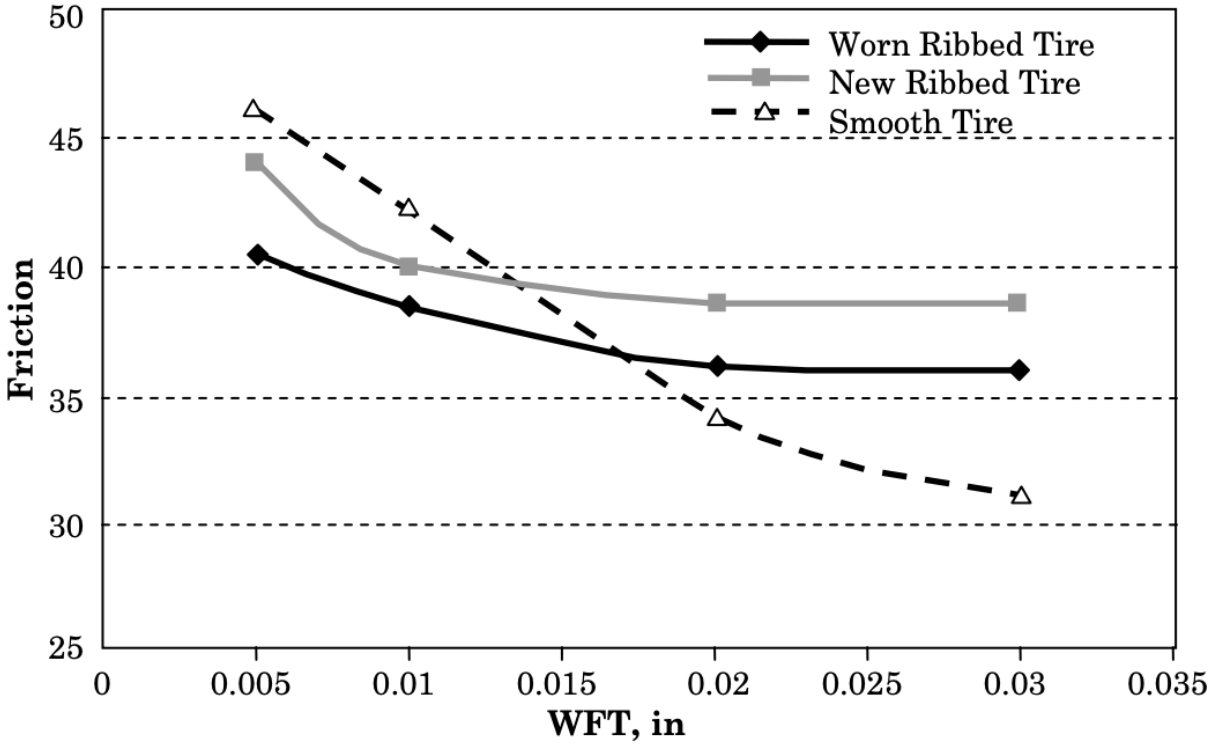

Figure 4-14: Friction Varying with Water Film Thickness (Hall et al., 2009)

Hydroplaning

Hydroplaning is defined as the phenomenon that takes place when a relatively water layer or film is present and as the vehicle is traveling at a higher speed, the water pressure accumulating at the pavement-tire interface separates the tire from the pavement surface (Horne and Buhlmann, 1983), resulting in a near-zero friction level. It can be affected by several factors including WFT, vehicle speed, pavement macrotexture, tire tread depth, tire inflation pressure, and tire contact area. When rainfall is heavy, macrotexture cannot provide sufficient drainage, a layer of water film is formed, or when puddles are created at

pavement distresses, hydroplaning are more likely to happen, especially when the traveling speed of the vehicle is high. Hayes et al. (1983) identified that on puddles around 1.0 inch (25 mm) deep and 30 ft (9 m) long, direct pavement-tire contact can be lost at even lower speeds of 40 to 45 mph (64 to 72 km/h).

Skid Resistance Measurement

Friction measuring devices take into account the main principle of a rubber sliding over the road surface and measure the applied and reaction forces. The three major operating principles of frictional measurement equipment are the slider, longitudinal friction coefficient (LFC) and side force coefficient (SFC).

Slider: British Pendulum Test (BPT)

The slide principle encompasses devices used for stationary testing. It entails the use of slider attached either to the foot of a pendulum arm or to a rotating head, which slows down on contact with the pavement surface. The rate of deceleration is used to derive a value representing the skid resistance of the road (Flintsch et al., 2012). Typically, slider operational devices are stationary, relatively inexpensive but require traffic control in order to be used safely out in the field.

The BPT is a manually operated test that provides an on-spot measurement of the surface friction. It evaluates skid resistance at low speeds by measuring the friction coefficient at a skidding speed of approximately 10 km/h (6 mph) (Henry, 2000). The test consists of using a pendulum-type tester with a standard rubber slider and a drag pointer. After calibration, the pendulum is raised to a locked position and then released to allow the slider to make contact with a pavement surface that has been manually wetted. A drag pointer swings along with the pendulum and indicate the British Pendulum Number (BPN)

once the pendulum reaches its highest point on the first swing. The more friction the pavement has, the more it will retard the swing of the pendulum, hence the higher the BPN reading. (ASTM E 303, 1998). Traditionally, BPN measurements were used as a surrogate of microtexture description given that it was assumed that microtexture plays a very significant role at low-speed friction. While this is true, it has been demonstrated that thin asphalt mixes made with crusher sands and lacking of macrotexture can offer significant friction at high speeds. Figure 4-15 illustrates the BPT equipment along with its field operation.

Figure 4-15: (left) British Pendulum Tester (BPT) and (right) field operation

Longitudinal Friction Coefficient (LFC): GripTester and Micro-GripTester

The LFC is represented as the ratio of vertical forces to drag forces and its principle consists of the application of a braking force to a test wheel so that it rotates more slowly than the forward speed of the vehicle. This makes the test wheel slip over the surface and allows for the development of frictional forces. LFC principle-based devices are divided into three modes: locked-wheel, fixed-slip and variable-slip. Each one having a different percentage of tire slip. All the test methods that are LFC based consist of pulled device methods that utilize one or two test tires to measure friction properties.

The GripTester and Micro-GripTester are two pieces of Continuous Friction Measuring Equipment (CMFE) capable of measuring continuously and dynamically the longitudinal skid resistance coefficient of the pavement in terms of Grip Number (GN), or the coefficient of friction. These devices use fixed slip mode for measuring friction experienced by vehicles without ABS braking system. They are characterized by maintaining a constant slip that is typically between 10 and 20 percent, as a vertical load is applied to the test tire (Henry, 2000). They have a single measuring wheel, fitted with a special smooth treat tire mounted on an axle designed to measure both the horizontal drag force and the vertical load force (Thomas, 2008). The difference between the GripTester and the Micro-GripTester is the scale of the device. The GripTester is towed behind a vehicle and uses measurement speeds that range from 5 to 100 km/h (3 to 62 mph) (Kogbara et al., 2016). The micro-GripTester is pushed manually by a technician at an average speed of 0.7 m/s (2.3 ft/s). Figure 4-16 and Figure 4-17 display the GripTester and Micro-GripTester devices, respectively, and their operation on the field.

Figure 4-16: (left) GripTester device and (right) field operation.

Figure 4-17: (left) Micro-GripTester device and (right) field operation.

The GripTester was selected as the primary method for measuring friction in this study because it has been shown to have good repeatability and reproducibility, adjustable water usage and it is commercially available (Kouchaki, 2018). The device uses the braked-wheel fixed-slip principle with a ratio of 15%. The test tire is dragged over the wetted pavement, product of the watering system, under a controlled speed by the vehicle towing the GripTester. The GripTester outputs the dynamic friction from measurements of horizontal and vertical forces, resulting in the Grip Number (GN), or coefficient of friction, in real-time (Thomas, 2008).

Locked-Wheel Skid Tester

Meyer et al. (1972) identify the usage of locked-wheel skid testers (shown in Figure 4-18) as the practice used by the majority of transportation departments in the United States among the several methods in use for skid resistance measurement. The standardized method is documented in ASTM E 274, with friction force measured as a locked test wheel equipped with a standard test tire, in accordance with ASTM E 249, is dragged over a pavement surface wetted with water film 0.02 in (0.5 mm) thick under constant speed (typically 40 mph (64 km/h)) and wheel load. The tire may either be a ribbed tire (ASTM

E 501) or a smooth tire (ASTM E 524), with the previous one more sensitive to the hysteresis component of friction, developed from macrotexture, while the latter one more sensitive to the adhesion component of friction, derived from microtexture.

The measurement system consists of a test vehicle with one or more test wheels incorporated or as part of a towed trailer, a standard tire used on the test wheel, a water container typically 200 to 500 gallons (750 to 1900 liters) and system to distribute water in front of the test wheel at test speed to wet the pavement, a transducer connected to the test wheel that senses the friction force developed between the test wheel and the pavement, an electronic signal conditioning equipment which receives and modifies the output signal from the transducer, and suitable readout equipment to record either the magnitude of the developed force or the resulting Skid Number (SN), as calculated by

$$SN = 100 \cdot \mu \qquad 4\text{-}4$$

Where μ = Friction coefficient as calculated in $Equation$ 2-3.

Figure 4-18: (left) Locked-Wheel Skid Tester and (right) Trailer.

When taking measurements, the braking system is enforced, and the resistive drag force is measured and averaged for one to three seconds after the test wheel is fully locked (Hall et al., 2009).

NOISE

According to World Health Organization (WHO) Guidelines for Community Noise (Berglund et al., 2000), road traffic is the largest source of community noise in most cities, especially where traffic volumes and speeds are high. Health effects resulting from environmental noise exposure includes increased risk of ischemic heart disease, sleep disturbance, cognitive impairment among children, annoyance, stress-related mental health risks, and tinnitus. The WHO estimates that people in high-income European countries lose a total of more than one million healthy years of life to these risks combined.

The European Union's Seventh Environment Action Programme (7th EAP) defines high noise levels in the 7th EAP as noise levels for L_{den} (annual average day, evening and night exposure to noise) above 55 dB and for L_{night} (averaged across the night period) above 50 dB (EEA, 2019). In the European Union (EU), about 40% of the population is exposed to traffic noise over 55 dB(A) during daytime, and 20% to levels over 65 dB(A). Even at night, more than 30% are exposed to noise levels exceeding 55 dB(A), a level that is disturbing to sleep. Though noise has not been paid as much attention in the United States compared to the EU nations, in a study conducted in Fulton County, Georgia, Seong et al. (2011) found that 48% of the total county population (870,166 residents) are potentially exposed to noise levels 55dB(A) or higher during daytime, while 32% are exposed to noise levels higher than 50dB(A) at nighttime, confirming that noise problems similar to those in the EU Nations exist in the United States as well.

Braun et al. (2013) classified the noise sources into engine noise, intake and exhaust system noise, and tire/road noise, and cited Zeller (2009) in support of the statement that unlike other noise sources, tire/road noise has not been effectively reduced over the years. Harland (1974) identified rolling noise as the dominant noise source for light vehicles traveling at high speeds and the one that makes a measurable contribution to the noise under many other conditions. Elsenaar et al. (1977) noted that rolling noise becomes the major part among all sources of traffic noise at speeds above 60 km/h for light vehicles (Elsenaar et al., 1977). Heckl (1986) cited Sandberg stating that for passenger cars traveling at speeds above 50 to 60 km/h and trucks at speeds above 80 to 90 km/h, tire noise tends to be the dominant source of traffic noise. Domenichini et al. (1999) pointed out that tire-road interaction contributes to 80 to 90% of the overall traffic noise at speeds higher than 70 to 80 km/h.

As the effort on noise reduction emitted by vehicle power units continue to make the engine, power train, and exhaust system quieter, tire/road noise, which may vary more than 15 dB under the same speed with different tire/road combinations, becomes a major contributor to overall traffic noise (Sandberg and Descornet, 1980, Chandler et al., 2003, Haider et al., 2007). Up to 2005, tire/road noise exceeded engine noise and became the dominant source at speeds of 22 and 31 mph (35 and 50 km/h) or higher for light vehicle and heavy vehicles, respectively (Keulen and Duskov, 2005).

Noise Generating Mechanisms

Elsenaar et al. (1977) identified aerodynamic effect, compression and expansion of cavity air, tire vibrations, and vehicle vibration as the four rolling noise generating mechanisms, with the last three being linked with surface asperity characteristics. These mechanisms were classified more specifically by later researchers into tread impact, air

pumping, slip-stick, and adhesion (Bernhard et al, 2005). The dominant noise frequency ranges related to each mechanism are as shown in Table 4-2.

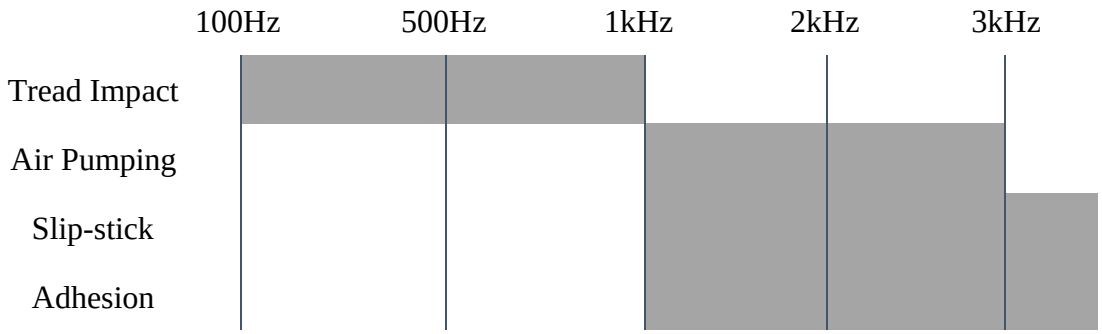

Table 4-2: Frequency Ranges for Noise Generating Mechanisms (Kuijpers and Van Blokland, 2001)

Factors Influencing Tire/Road Noise

Ongel and Harvey (2010) identified texture, roughness, air void content, thickness, stiffness, and age to be pavement surface characteristics that affect tire/road noise level. Because the main objective of this thesis is to correlate noise with texture, as the pavements sampled do not differ from one another by texture only, it is worth looking into other factors. Ideally, to analyze the effect of texture alone, the other factors should be controlled for and remain constant. As this approach is not viable, the other factors should be accounted for as much as possible so that their impacts can be isolated from the effects of texture.

The aforementioned authors conducted regression analyses to explore the effects of pavement characteristics on the noise levels at different frequencies. They separated the noise levels into 11 1/3 octave bands from 500 to 5000 Hz, with significant variables at a 5% significance level shown in Table 4-3 and Table 4-4, in a decreasing order in significance. A plus sign indicates a positive correlation, while a negative sign indicates a negative correlation.

500 Hz	630 Hz	800 Hz	1000 Hz	1250 Hz
MPD (+)	MPD (+)	Mix type (−)	Mix type (−)	AV (−)
RMS (+)	RMS (+)	FM (−)	AV (−)	Mix type (−)
AV (+)	AV (+)	C_u (+)	C_u (+)	C_u (+)
FM (+)	IRI (+)	AV (−)	FM (−)	Age (+)
Mix type (+)	Surface Thickness (−)	IRI (+)	Surface Thickness (+)	FM (−)
C_u (−)	C_u (−)	Rubber Inclusion (−)	NMAS (+)	NMAS (+)
IRI (+)	Mix type (+)		IRI (+)	Transverse Cracking (+)
Surface Thickness (−)	FM (+)			IRI (+)
				Fatigue Cracking (+)
				Surface Thickness (+)

Table 4-3: Influence of Pavement Characteristics on Noise Frequency 1250 Hz and Lower (Ongel and Harvey, 2010)

1600 Hz	2000 Hz	2500 Hz	3150 Hz	4000 Hz	5000 Hz
AV (−)	AV (−)	AV (−)	AV (−)	AV (−)	AV (−)
C_u (+)	Mix type (−)	Mix type (−)	RMS (−)	RMS (−)	RMS (−)
Mix type (−)	C_u (+)	RMS (−)	MPD (−)	MPD (−)	FM (−)
FM (−)	FM (−)	C_u (+)	FM (−)	FM (−)	MPD (−)

Surface Thickness (+)	RMS (−)	FM (−)	C_u (+)	C_u (+)	C_u (+)
RMS (−)	Surface Thickness (+)	MPD (−)	Mix type (−)	Mix type (−)	Mix type (−)
NMAS (+)	MPD (−)	Surface Thickness (+)	Surface Thickness (+)	Surface Thickness (+)	Surface Thickness (+)
MPD (−)	NMAS (+)	Transverse Cracking (+)	Transverse Cracking (+)	Transverse Cracking (+)	Transverse Cracking (+)
Age (+)	Transverse Cracking (+)	NMAS (+)		Age (+)	
Transverse Cracking (+)	Fatigue Cracking (+)				
Fatigue Cracking (+)					

Table 4-4: Influence of Pavement Characteristics on Noise Frequency 1600 Hz and Above (Ongel and Harvey, 2010)

Where:

AV = air void content (%)

C_u = coefficient of uniformity, $C_u = D_{60} / D_{10}$; D_{60} is the sieve size associated with 60% passing and D_{10} is the sieve size associated with 10% passing

Mix type is a Categorical Variable: Coded as 1 for open-graded mixes and 0 for gap- and dense-graded mixes

FM = fineness modulus, a larger value indicates coarser aggregate gradation

RMS = root mean square of profile deviation

NMAS = Nominal Maximum Aggregate Size in mm

MPD = mean profile depth in microns

Age = number of years since construction

Transverse Cracking is a Categorical Variable Coded as 1 if the total length of transverse cracks ≥ 5 m in 150 m section, and 0 otherwise

Fatigue Cracking is a Categorical Variable Coded as 1 if the total fatigue cracking ≥ 5% of the wheelpath area of the 150 m section, and 0 otherwise

IRI = roughness in m/km

Surface Thickness = surface thickness in mm

Pavement Type

As van Keulen and Duskov (2005) have identified, using low noise road surfacings is one of the most cost-effective and easy-to-implement approaches in terms of reducing traffic induced noise. Two examples listed by the authors were porous asphalt and thin surfacings. Kandhal (2004) cited several European studies conducted in the 1990s, confirming that open graded friction courses were about 3 to 5 dB quieter compared to dense graded hot-mix asphalt. While using dense graded hot-mix asphalt as the reference, he claimed Portland Cement Concrete (PCC) to be 3 dB louder (even more if with transverse grooves or tining), stone matrix asphalt 2 dB quieter, and open graded friction course 4 dB quieter.

Bernhard et al. (2005) identified surface texture with wavelengths greater than 20 mm to be a characteristic that correlates with noise positively, while surface texture with wavelengths less than 10 mm, porosity, elasticity, and negative texture tend to correlate

with noise negatively. There can be as much as 9 dBA difference in noise level for a single pavement type, and there can be as much as 14 dBA difference between different types of pavement under similar conditions.

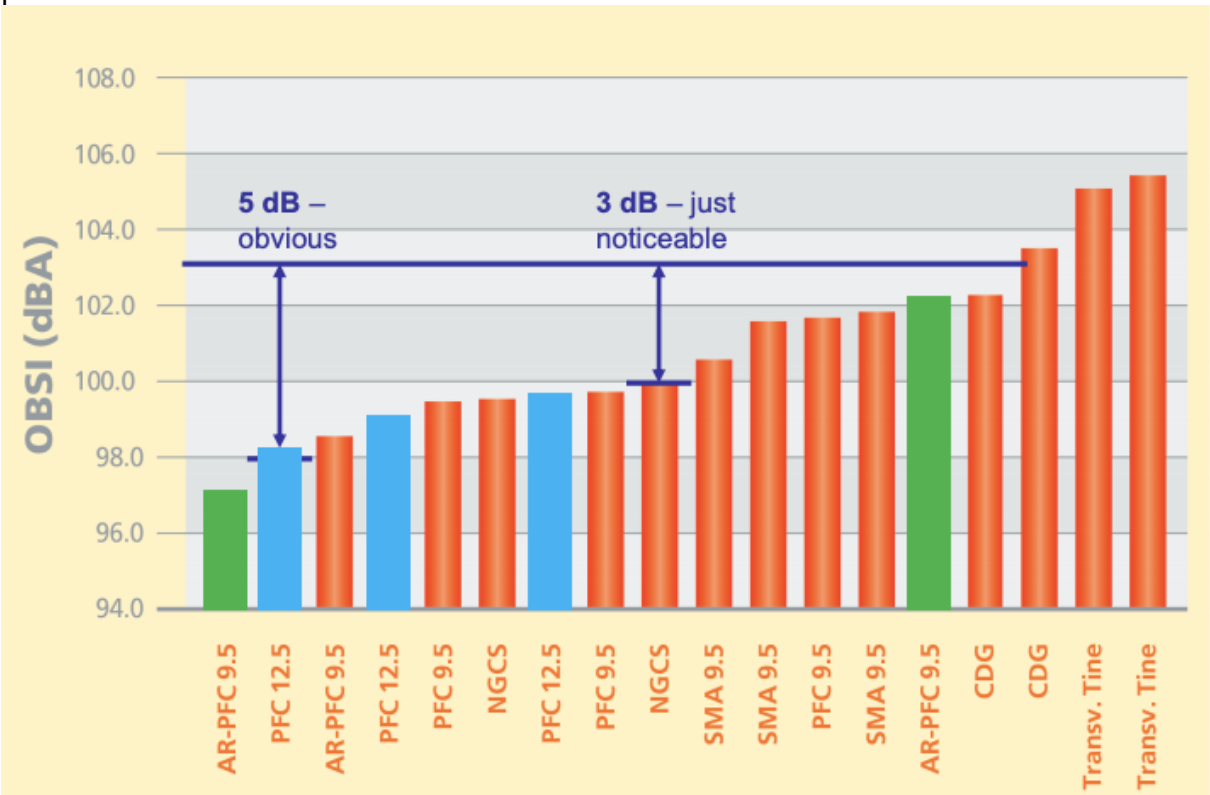

Figure 4-19 shows the sound intensity level in dBA measured along different types of pavement.

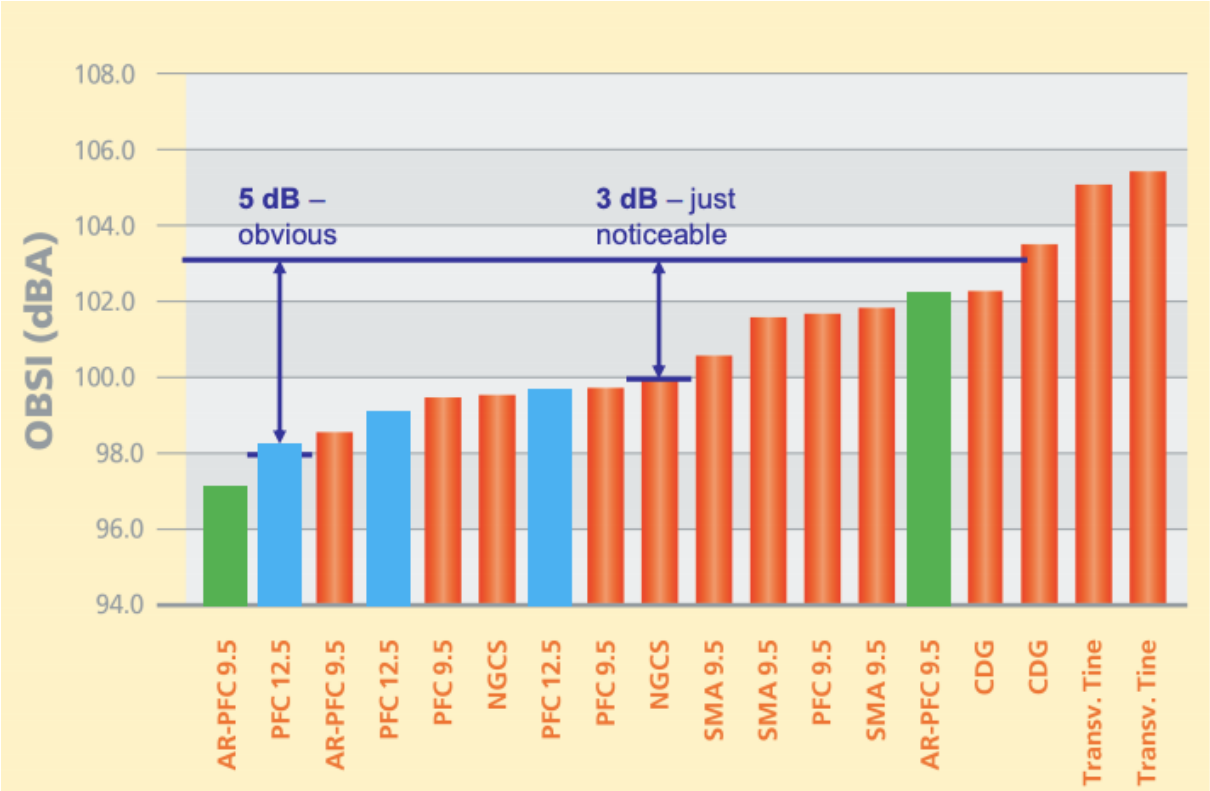

Figure 4-19: Noise Level Measured at Different Types of Pavements (McGhee, 2012)

Where AR-PFC 9.5 is Asphalt Rubber Porous Friction Course produced with a 3/8 in (9.5 mm) top size stone placed at 1.0 inch thickness, PFC 9.5 is polymer modified mix with 3/8 in top size stone placed at 1.0 inch thickness, PFC 12.5 is polymer modified mix with ½ in (12.5 mm) top size stone placed at 2.0 inches thickness, NGCS is Next Generation Concrete Surface, SMA is finer-gradation stone-matrix asphalt placed at 1.5 inches thickness, and CDG is conventional diamond ground.

Air Void Content

Porous asphalt mixture which was originally developed for the purpose of water drainage consists primarily of gap-graded aggregates held together by a polymer-modified binder to form a structure in which water can pass through the interconnected voids (Keulen and Duskov, 2005). They normally contain at least 20 % voids in comparison with

denser mixtures that contain 3 to 6 % of voids. Researchers have ascribed the noise reduction effect of porous asphalt to acoustical absorption, elimination of horn effect, and reduction of air-pumping. The authors claimed a 4 dBA reduction in noise at high speeds.

Thickness

Many researchers have agreed that when combined with air void content or porosity, a sufficiently thick layer of surface tends to provide better acoustic absorption for noise reduction (Van Keulen and Duškov, 2005, Haider et al., 2007). Haider et al. (2007) proposed a combination of air void content of 20% and surface thickness of 40 mm to be favorable for sound absorption.

Age

As Ongel and Harvey (2010) pointed out, pavement surface characteristics are time dependent. For example, asphalt pavement becomes stiffer, the air paths in the open-graded pavement surface can become clogged, and various types of pavement distresses may develop over the service life of the pavement. How these time-dependent characteristics impact noise generation can be complicated, as they may play a role in different noise generating mechanism, and the effect can be in either direction.

Noise Measurement

For noise measurements there are two main type of measurements from which many tests have been developed, they are: wayside and on-source measurements. Wayside measurements, also referred to as roadside measurements, are the most basic and common method of measuring traffic noise. They consist on sound pressure levels (SPL) measurements normally conducted by setting a sound meter mounted on a tripod either at a fixed distance from the road (typically 7.5 m (25 ft) or 15 m (50 ft)), or at a location

where human receivers would usually be, such as residential backyards or playgrounds (Smit et. al., 2014, Rasmussen et al., 2007). These measurements capture all the noise from all sources: tire-pavement, aerodynamic, powertrain, reflections, and even other sources of noise not related to traffic noise. It is important to consider the influence of the environment surrounding the road when analyzing noise levels and not only the noise created by vehicles since roadway features may increase road noise levels through reflection and propagation. Moreover, embankments and slopes on the road may serve to absorb and mitigate noise levels (Smit et. al., 2014).

Wayside Measurements

Wayside measurements can be categorized into two main method of testing: pass-by and time-averaged methods. Pass-by noise methods for noise testing refer to the procedures of measuring vehicle noise emission levels from the side of road. These type of noise testing methods are commonly used in Europe by highway agencies. The most common pass-by testing method is the statistical pass-by method (SPB). Statistical pass-by involves measuring the maximum noise levels at the roadside from a statistical significant number of vehicles. As described in ISO 11819-1: *Measurement of the Influence of Road Surfaces on Traffic Noise*, SPB is a technique designed to evaluate the total traffic noise generated on a given section of road surface under specific traffic and weather conditions. The standard specifies that a microphone is mounted on a tripod and placed 7.5 m (25 ft.) from the center of the lane of traffic to be tested and 1.2 m (4 ft.) above the plane of the roadway. Once the microphone is set up, technicians proceed to measure vehicle speeds and SPL for at least 100 passenger cars and 80 dual axle or multi-axle heavy vehicle pass-bys. Each individual pass-by is recorded with its corresponding vehicle speed and a regression line of the maximum A-weighted SPL versus the logarithm of speed is

calculated for each vehicle category. Then, the average maximum A-weighted SPL is determined at the reference speed using the regression lines. This level is also known as the vehicle sound level.

The other two most common pass-by measurements are controlled pass-by and coast-by method. Controlled pass-by method (CPB) makes use of a similar microphone set up as the SPB method but instead of measuring noise from the existing traffic stream, this method employs a single test vehicle while no other vehicles are on the road (Smit et al., 2014). In this method, several passes of the test vehicle are made and from those passes the maximum pass-by SPL is recorded. Coast-by method (CB) can be considered a variation of the CPB method that is oriented towards isolating and recording mostly noise created due to tire pavement interaction. In the CB method, the driver of the test vehicle shuts off the engine as the vehicle approaches the testing location in order to drastically reduce the contribution of noise from the powertrain of the vehicle.

The second type of wayside measurement are time averaged methods. On occasion, the conditions required to conduct a pass-by test are too difficult to be satisfied. Whenever this situation occurs, transportation agencies resort to time-averaged methods. The most commonly used time-average test in the continuous flow traffic time-integrated model (CTIM). Based on AASHTO TP 99-12: *Standard Method of Test for Determining the Influence of Road Surfaces on Traffic Noise Using the Continuous Flow of Traffic Time Integrated Method (CTIM)*, the CTIM is a procedure for measuring the influence of road surfaces on highway traffic noise at a specific site. In this method, a sound pressure meter measures all traffic noise over a specified time period which is typically 5 to 30 minutes (Rasmussen, et al. 2017). In addition, traffic volumes, speeds, vehicle categories and meteorological data are measured continuously for a long enough period of time to properly represent these conditions on a typical day on the site (Smit et al., 2014). An equivalent

continuous sound level (L_{eq}) over the specified time period is later calculated and reported as the arithmetic mean of repeat measurements. The parameter L_{eq} is used for all traffic noise analyses for TxDOT highway projects, and it is defined as the equivalent steady-state sound level at a given time period that contains the same acoustic energy as a time-varying sound level during the same period. (Smit et al., 2014).

On-Source Measurements

Alternatively, transportations agencies may prefer to run on-source measurements, as opposed to wayside measurements. On-source testing provides isolated noise measurements from a specific source, such as at the tire-pavement interface. However, a limitation shared by these methods is that they cannot provide an indication of the influence of roadway features such as geometry and cross section on noise generation, mitigation or propagation. The two most typically used on-source test methods used in the U.S. and Europe are on-board sound intensity (OBSI) and the close proximity method (CPX), respectively. The OBSI method is a measurement procedure used to evaluate the tire-pavement noise component resulting from the interaction of an ASTM F2493, Standard Reference Test Tire (SRTT) on a pavement surface by installing a dual or single configuration of microphone probes at the trailing and leading edges of the tire, as shown in Figure 4-20. The vehicle is later driven at a reference speed 96 km/h (60 mph) for 134 m (440 ft) on three selected sites within a section of road, with minimum elevation grades or curves, to measure the sound intensity created as the vehicle moves along the pavement (AASHTO TP 76-15). The main advantage of this method is that it is relatively fast compared to wayside measurements and it isolates the tire-pavement noise from all other traffic noise making it simpler to analyze sound intensity levels on different frequencies by means of correlation. However, the main drawbacks of this method is that it requires a

vehicle with a specific reference tire to rule out variations in tire geometry, it must be conducted under specific environmental conditions such as: dry pavement and low wind speeds, and it does not take into account other features in the road that might influence the sound propagation of the noise generated at the tire-pavement interface.

Figure 4-20: OBSI dual probe configuration set up

The CPX method was developed in Europe and is defined by ISO 11819-2: *Acoustics-Measurement of the Influence of Road Surfaces on Traffic Noise. Part 2: Close-Proximity Method,* to measure the tire-pavement noise at the source. In this method, a test tire is mounted along with an array of microphones within a specially designed trailer that is to be towed behind a test vehicle at highway speeds (Ohiduzzaman et al, 2016). The tire is enclosed in a box of sound-absorbing material to minimize the variation in noise levels due to environmental variations and only measure tire-pavement noise (Smit et al., 2014). The primary disadvantage of CPX testing is that a larger investment must be made to purchase microphones, data processing equipment, and the trailer. Furthermore, it has

similar limitations to the OBSI method, however wind speeds do not have to be low given that the set of microphones are isolated by the trailer.

Chapter 3: Literature Review

FRICTION-TEXTURE MODELS

Many researchers have identified a positive correlation between friction and pavement texture, which means that a rougher pavement surface tends to provide better skid resistance. The Federal Highway Administration (FHWA)'s technical advisory on pavement texture (2005) identified the characteristics of pavement texture that provide wet weather friction to be microtexture and macrotexture. Both are necessary to provide sufficient skid resistance, especially under wet pavement conditions, and at low and high vehicle speeds. Roe et al. (1998) found that friction drops more rapidly with speed on surfaces with a lower texture depth compared to the high-textured ones, especially at lower speeds. The effect of texture depth on loss of friction was similar for all impermeable materials. This effect is at its highest at texture depths less than 0.7 mm. Skid resistance of a pavement surface is largely affected by both microtexure and macrotexture (Flinsch et al., 2003). Macrotexture provides the hysteresis component of the friction and contributes to water drainage from the pavement, thus preventing hydroplaning. Microtexture contributes to the tire-pavement contact and the adhesion component of friction, with impact on both wet and dry surfaces at all speeds (Chandler et al, 2003).

Kogbara et al. (2016) conducted a state-of-the-art review of key parameters influencing the measurement and modeling of asphalt pavement skid resistance, with a focus on texture parameters. Texture is classified into microtexture, with wavelengths ranging from 0 mm to 0.5 mm, macrotexture, with wavelengths ranging from 0.5 mm to 50 mm, megatexture, with wavelengths ranging from 50 mm to 500 mm, and unevenness, with wavelengths ranging from 500 mm to 50 m. Out of these classifications of texture, micro- and macro- are the two components primarily contributing to tire-pavement friction,

though via different mechanisms. Microtexture is important regardless of whether the pavement surface is in dry or wet conditions, and it plays a key role when the pavement is wet as it helps cutting through the water film between the pavement surface and the tire. Macrotexture is the determining factor for skid resistance along wet pavements, especially when the vehicle travels at speeds above 90 km/h. As it affects water drainage from the tire pattern, it is considered to be responsible for the hysteresis component of friction at high speeds. Pavement texture is dependent on the pavement material, out of which maximum aggregate size, course and fine aggregate types, mix binder content and viscosity, mix gradation and mix air content are the ones affecting macrotexture, and the coarse aggregate type mainly affects microtexture.

Among the standard characterizing parameters for surface macrotexture, the most common ones used are mean texture depth (MTD), mean profile depth (MPD), and sensor measured texture depth (SMTD). Apart from these, there are many other parameters as potential outputs of laser system software, including the arithmetic mean and root-mean-square (RMS) deviation, which are vertical extension parameters, and the average and RMS wavelength of the profile, which are horizontal extension parameters. In spite of the absence of a standardized method for microtexture characterization, many parameters based on non-contact measurements have been proposed in the literature, such as average asperity height, average asperity density, average shape factor, MPD, estimated texture depth (ETD), slope variance, and the RMS of the microtexture profile.

Li et al. (2016) classified texture parameters into scale-dependent and scale-independent, as shown in Figure 5-1. Scale independent parameters are parameters that are not affected by the measurement scale and data resolution, such as fractal dimension; while scale dependent parameter measurements are affected by the scale.

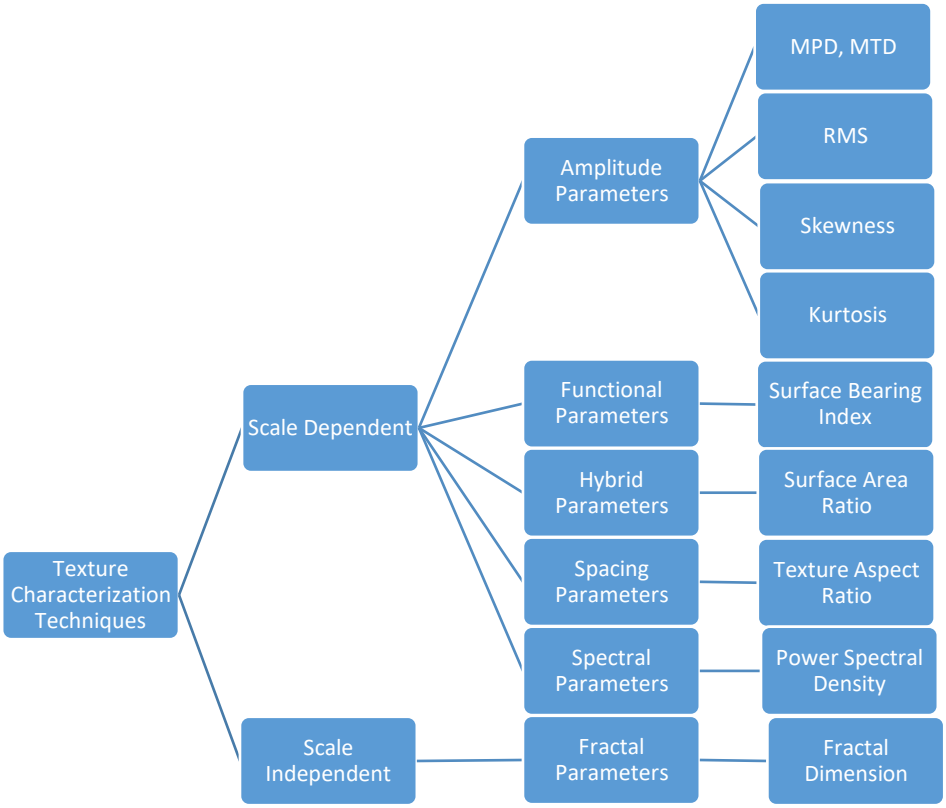

Figure 5-1. Schematic Diagram of Pavement Surface Characterization Techniques (Li et al., 2016)

Fractal Parameters

Two major fractal parameters are fractal dimension and topothesy (Petropoulos, 2007). As a scale independent parameter, fractal dimension describes the complexity of surface, calculated by the enclosing boxes method. Each section of a surface is enclosed by a box of width ε, and the volume of all the boxes enclosing the whole surface V_ε is calculated. The fractal dimension D is the slope

$$D = \frac{\ln(V_\varepsilon)}{\ln(\varepsilon)} \qquad 5\text{-}1$$

Topothesy is a characteristic length that typically takes very small values, as it represents the horizontal separation of profile heights corresponding to an average slope of one radian.

Height Parameters

Apart from MPD and MTD, some commonly used height parameters include arithmetic mean height (S_a), the average height evaluated over the defined area, root-mean-square height (S_q), the standard deviation of heights within a defined area, representing the root-mean-square of ordinate values in the area, skewness (S_{sk}), reflecting the height distribution asymmetry, and height distribution kurtosis (S_{ku}). The equations for calculating these height parameters have been listed in Table 4-1.

Spatial Parameter

Texture Aspect Ratio (TAR), as a spatial parameter, characterizes the isotropy of the pavement surface texture (Li et al., 2016). Autocorrelation Function (ACF), defined as the mathematical multiplication product of the measured surface Z(x, y) and its duplicate surface with a relative lateral displacement (∇x, ∇y), Z((x-∇x),(y-∇y)), can be applied for texture pattern recognition, as it represents how similar the texture is at a certain distance from the original location. Anisotropic pavement surface typically has ACF that decays the slowest along the predominant texture direction, while fastest along the direction perpendicular to this direction. Due to its similar texture aspects in all directions, in an isotropic pavement surface, however, is difficult to distinguish between a fastest and a slowest decaying direction.

For TAR calculation, two lengths are of concern: the length of fastest decay, which measures the distance over the surface along the direction of minimal correlation with the

original location, and the length of slowest decay, which measures the distance over the surface along the direction of maximum correlation. The parameter is then calculated as the ratio between the two lengths, namely:

$$TAR = \frac{distance\ the\ normalized\ ACF\ decays\ fastest\ to\ 0.2\ in\ any\ possible\ direction}{distance\ the\ normalized\ ACF\ decays\ slowest\ to\ 0.2\ in\ any\ possible\ direction}$$

TAR has values within the range between 0.0 and 1.0. Typically, a TAR value > 0.5 indicates stronger isotropic or uniform texture distribution in all direction, while a TAR value < 0.3 indicates a stronger periodic texture property.

Hybrid Parameters

Hybrid parameters, as suggested by the name, are affected by both amplitude and spacing properties of the surface texture. Some examples are root-mean-square slope (S_{dq}), developed interfacial area ratio (S_{dr}), and surface area ratio (SAR) (Li et al., 2016).

$$S_{dq} = \sqrt{\frac{1}{A}\sum_{A}\left[\frac{\partial^2 z(x,y)}{\partial x} + \frac{\partial^2 z(x,y)}{\partial y}\right]} \qquad 5\text{-}2$$

$$S_{dr} = \frac{1}{A}\left\{\sum_{A}\left[\sqrt{1 + \left(\frac{\partial z(x,y)}{\partial x}\right)^2 + \left(\frac{\partial z(x,y)}{\partial y}\right)^2} - 1\right]\right\} \qquad 5\text{-}3$$

To characterize the SAR, the interfacial area of a smallest sampling quadrilateral ABCD is first calculated by

$$A_{ij} = \frac{1}{4}\left(\overrightarrow{|AB|} + \overrightarrow{|CD|}\right)\left(\overrightarrow{|AD|} + \overrightarrow{|BC|}\right)$$
$$= \frac{1}{4}\left\{\left(\left[\Delta y^2 + \left(f(x_i, y_j) - f(x_i, y_{j+1})\right)^2\right]^{\frac{1}{2}}\right.\right.$$
$$+ \left[\Delta y^2 + \left(f(x_{i+1}, y_j) - f(x_{i+1}, y_{j+1})\right)^2\right]^{\frac{1}{2}}$$
$$+ \left[\Delta x^2 + \left(f(x_i, y_j) - f(x_{i+1}, y_j)\right)^2\right]^{\frac{1}{2}}$$
$$\left.\left. + \left[\Delta y^2 + \left(f(x_i, y_{j+1}) - f(x_{i+1}, y_{j+1})\right)^2\right]^{\frac{1}{2}}\right)\right\}$$

The total interfacial area is

$$A = \sum_{j=1}^{N-1}\sum_{i=1}^{M-1} A_{ij} \qquad 5\text{-}4$$

And SAR is calculated by

$$SAR = \frac{A - (M-1)(N-1)\Delta x \Delta y}{(M-1)(N-1)\Delta x \Delta y} \qquad 5\text{-}5$$

Feature Parameters

Feature parameters include peak density (S_{pd}), the number of peaks per unit area making up the surface, and arithmetic mean peak curvature (S_{pc}), the mean peak curvature for the peak structures (Hu et al., 2016, Kogbara et al., 2018). The two parameters are as calculated in the equations

$$S_{pd} = \frac{n}{A} \qquad 5\text{-}6$$

$$S_{pc} = -\frac{1}{2n}\sum_{k=1}^{n}\left(\frac{\partial^2 z(x,y)}{\partial x^2} + \frac{\partial^2 z(x,y)}{\partial y^2}\right) \qquad 5\text{-}7$$

Where *n* is the number of peaks, and a peak is defined as a point on the surface higher than all other points within a neighborhood of it.

Volume Parameters

Peak material volume (V_{mp}) is the volume of material from the surface of height corresponding to a 10 % material ratio (MR) level to the highest peak, representing the volume of material that's potentially worn away and characterizes the contact zone. Core material volume (V_{mc}) is the volume of material between the surface of heights corresponding to 10 and 80 % MR, representing the volume of material remained to support load after the top of the surface wears away. MR is defined as the ratio between the intersecting area of a plane parallel to the mean plane passing through the surface at a given height and the cross-sectional area of the evaluation region (Kogbara et al., 2018). The material volume (V_m) at a certain MR p is defined as

$$V_m(p) = \frac{K}{100\%}\int_0^p S_{mc}(q) - S_{mc}(p)\,dq \qquad 5\text{-}8$$

S_{mc} is the inverse areal material ratio, representing the height which gives the specified material ratio, and K is a constant to convert to milliliters per meter squared. The two volume parameters are thus calculated as

$$V_{mp} = V_m(10\%) \qquad 5\text{-}9$$

$$V_{mc} = V_m(80\%) - V_m(10\%) \qquad 5\text{-}10$$

Functional Parameters

Functional parameters relate closely to the wearing and friction of a pavement surface (Li et al., 2016). Surface bearing index (SBI), a functional parameter found to correlate with the wearing properties of the surface, is calculated as

$$SBI = \frac{S_q}{H_{5\%}} \qquad 5\text{-}11$$

where S_q is the RMS height, and $H_{5\%}$ is the surface height at 5% bearing area, equivalent to a 5% MR described per the volume parameters.

Spectral Parameters

Spectral analysis, conducted in accordance with ISO/TS 13473-4, characterizes texture level by wavelengths or wavelength bands. It manages to quantify surface properties by capturing the range and distribution of surface asperities (Miller et al., 2012, Yan et al., 2020, Chen, 2020). $L_{tx,m}$, texture level in decibels along a surface at the octave band m is calculated per

$$L_{tx,m} = 10\log_{10}\left(\frac{Z_{p,m}}{a_{ref}^2}\right) \quad \text{5-12}$$

Where:

a_{ref} = reference value of mixture surface profile amplitude in 10^{-6} m

$Z_{p,m}$ = power within the fractional octave band m

And the combination of the fractional octave bands is calculated by

$$L_{tx,i-j} = 10\log_{10}\left(\sum_{m=i}^{j} 10^{\frac{L_{tx,m}}{10}}\right) \quad \text{5-13}$$

Where:

$L_{tx,i-j}$ = average texture level from wavelength i to j mm (dB)

$L_{tx,m}$ = texture level at wavelength = m mm (dB)

Hu et al. (2016) used a handy laser scanner to collect 3D macrotexture data of asphalt pavement surface to calculate texture parameters that correlate to dynamic friction coefficient measured by a dynamic friction tester. A water film of 1.0 mm (0.04 in) thickness was sprayed on the test surface using a special water distribution system and the dynamic friction coefficient was measured at different testing speeds: 30, 40, 50 and 60 km/h. The surface temperature was held constant at 20˚C throughout the testing procedure. A 3D scanner (HandySCAN 300 produced by CREAFORM Inc, Canada) was used to collect 3D pavement surface data. The device has a resolution of 0.1 mm and precision of

0.04 mm. To process the original surface texture data, transverse and longitudinal slopes were first eliminated. Then, a Gaussian filter with wavelength of 0.5 mm was applied to separate the micro- and macro- components of texture and only the macrotexture was kept. The MATLAB software was used to reconstruct the 3D macrotexture images.

The highest correlation was found between dynamic friction coefficient and the two feature parameters, with different regression equations and R^2 at different speeds

$$\mu_{30} = 0.132 + 4.337S_{pd} + 0.037S_{pc}, R^2 = 0.825$$

$$\mu_{40} = 0.129 + 4.285S_{pd} + 0.038S_{pc}, R^2 = 0.832$$

$$\mu_{50} = 0.131 + 4.112S_{pd} + 0.042S_{pc}, R^2 = 0.818$$

$$\mu_{60} = 0.147 + 3.501S_{pd} + 0.047S_{pc}, R^2 = 0.756$$

Where μ_v represents the dynamic friction coefficient at speed = v km/h. The correlation was found to be high with either of the feature parameters being used alone as a single independent variable. The R^2 value decreases with speed for S_{pd} and increases with speed for S_{pc}, as shown in Table 3-1.

Measuring Speed	30 km/h	40 km/h	50 km/h	60 km/h
S_{pd}	0.803	0.791	0.764	0.733
S_{pc}	0.662	0.688	0.699	0.707

Table 5-1. R^2 with Each of the Feature Parameters as Single Independent Variable and Dynamic Friction Coefficient as Dependent Variable

Li et al. (2016) used friction data collected with Dynatest 6875 Highway Friction Tester and full-lane 3D pavement surface texture data with sub-millimeter resolution acquired using Digital Highway Data Vehicle (DHDV) equipped with PaveVision3D Ultra to explore relationships between friction and four types of texture parameters: amplitude, spacing, hybrid, and functional. The texture data collection system was capable of

conducting full-lane data at highway speeds up to 100 km/h, with resolutions of 0.3 mm in the vertical direction and 1.0 mm in the longitudinal direction. Texture and friction data were collected along the ramp from NB IH-65 to EB SH-152, a section consisting of two surface types: high friction surface treatment (HFST) approximately 206 m in length and regular asphalt concrete (AC) surface approximately 187 m. The entire section was sampled into 84 segments, each being 4.57 m (two 3D image length) long. Apart from amplitude (height) parameters such as MPD, MTD, RMS, Skewness, and Kurtosis, the authors calculated a spatial parameter (Texture Aspect Ratio, TAR), a hybrid parameter (Surface Area Ratio, SAR), and a functional parameter (Surface Bearing Index, SBI). They then explored correlations among geometric texture indicators and found that MPD does not have a strong correlation with other texture indicator except for SMTD, while RMS and SAR are highly correlated with R^2 of 0.9. No strong correlation was found among skewness, kurtosis, TAR, SAR, or SBI. Based on the correlations, MPD, skewness, kurtosis, TAR, SAR, and SBI were selected for model development. Assuming a linear relationship between the independent and dependent variables, the authors arrived to the following model specification:

$$FN_p = 48.27MPD + 7.38Skewness + 12.34TAR + 59.42SBI - 105.58$$

Finally, based on the residual plot, they proposed a non-linear model, that followed the following specification:

$$FN_p = -714.15MPD^3 + 2256.43MPD^2 - 2264.432MPD + 7.04Skewness + 13.43TAR + 5.89e^{0.94SBI} + 743.93$$

With the final specification, an $R^2 = 0.895$ was achieved, even with the presence of outliers. However, using a third degree polynomial for MPD had not real meaning and the model was a data fitting exercise.

Kogbara et al. (2018) attempted to use asphalt pavement surface texture parameters of both micro- and macro- scales for explaining friction. The study collected texture data using close range photogrammetry (CRP) and measured friction using the GripTester. Measurements were conducted along a 900-m long pavement section constructed in 2010 with lanes going both North-South (NS) and South-North (SN) directions. It consisted of six sections with different asphalt binder types and mix designs each being 150 m in length, with a consistent 50-mm thick wearing course layer using dense graded asphalt concrete with gabbro aggregate, an intrusive igneous rock equivalent in composition to basalt. The detail of asphalt binder types and mix designs of the six sections are as shown in Table 3-2.

Section 1	Section 2	Section 3A	Section 3B	Section 4	Section 5	Section 6
Marshall/ Percentage refusal density, 40-50 PEN	Marshall/ Percentage refusal density, 60-70 PEN	Marshall/ Percentage refusal density, 60-70 PEN	Marshall/ Qatar Construction Specs, 60-70 PEN	Marshall/ Qatar Construction Specs, 60-70 PEN	Marshall/ Percentage refusal density, polymer-modified bitumen	Marshall/ Percentage refusal density, polymer-modified bitumen

Table 5-2. Material Description of the Pavement Test Sections

Grip Number was evaluated at 5-m intervals along the outer wheel path of each lane at 50 km/h with a water flow rate of approximately 10 L/min, yielding a water film thickness of 0.5 mm.

For processing the texture data collected with the CRP, a leveling step with respect to a least squares plane was first carried out to remove the effect from the artificial gradient on the height parameters. Then, they extracted the area of interest to eliminate redundant data. The general form, which reflects the surface rippling, is then removed using a second

order polynomial. A Robust Gaussian filter operator was applied to separate the high-frequency and low-frequency texture based on a 0.8-mm cut-off wavelength. Using the processed data, they evaluated height (root-mean-square height (S_q) and arithmetic mean height (S_a)), volume (peak material volume (V_{mp}) and core material volume (V_{mc})), and feature parameters (peak density (S_{pd}) and arithmetic mean peak curvature (S_{pc})).

The study also considered analyzing the top 1.0 to 2.0 mm of the surface only rather than using the entire profile texture, based on the hypothesis that the tire of the GripTester envelops only pavement surface asperities up to 2.0 mm in depth. The four scenarios considered were after form removal, and each represent surface, roughness and waviness surfaces separated, top 1.0 mm after 0.5 % MR removal, and top 2.0 mm after 0.5 % MR removal.

Conducting a stepwise regression, they obtained an R^2 = 0.76 with Grip Number using density of peaks and the peak material volume based on the top 2.0 mm of texture after removing the data points above the 0.5 % MR surface. The regression equation for the NS lanes was:

$$GN = 0.187 + 2.656V_{mp} + 1.834S_{pd}$$

While the equation for the SN lanes was:

$$GN = 0.155 + 1.404V_{mp} + 1.092S_{pd}$$

No indication was given as these two equations were significantly different. In the conclusion, the authors suggested the potential of investigating pavement sections with different aggregate types and asphalt mixtures, as well as at testing friction at various GripTester speeds for future studies.

Yan et al. (2020) conducted a spectral analysis to identify the wavelength range in texture that best correlates with friction using friction data collected with mu-meter complemented by a British Pendulum Tester and texture data collected with a stationary

laser profilometer equipped with two laser sensors: Selcom 2005 with laser spot diameter of approximately 1.0 mm for covering texture wavelengths 2 to 500 mm, and Remplir SD65-R12 with a laser spot diameter of approximately 0.1 mm for covering texture wavelengths 0.2 to 5 mm.

One of the reasonings behind spectral analysis is that it provides a more detailed statistical description of the pavement texture profile compared to texture amplitude values. Tests were conducted along 21 different in-service roadway sections in New Zealand representing different texture features, with MTD measured with the sand patch test varying from 0.57 to 4.34 mm. Pavement surface types included dense asphalt concrete, porous asphalt concrete, cement concrete, interlocking cement blocks, surface dressings (chip seals) and slurry seals, with pavement age ranging from new to 25 years. At each site, 10 profiles each being 1.0 m in length were evenly spaced over approximately 100 m in the mu-meter wheelpath. It should be noticed that a profile length of 1.0 m lead to relatively higher uncertainty in texture level calculation at wavelengths longer than 0.08 m (ISO 13473-4). Side force coefficient (SFC) was measured every 1.0 m and averaged over 100 m for each test section with the mu-meter at speeds 40, 60, and 80 km/h with a water depth of 1.0 mm. British Pendulum Number (BPN) was recorded for at least 10 locations per site.

To identify texture internal relations, the authors mapped the correlation among texture levels measured at different wavelengths and identified two areas with high intercorrelation: one in the range of 16 to 160 mm, and another in the range of 0.5 to 15 mm in wavelength. They then correlated five friction measures including SFC at 10, 40, 60, 80 km/h, the inverted SFC slope with speed, and BPN, with texture level of different wavelengths. Overall, the correlation coefficient increases with speed. The peak correlation coefficients of 0.38, 0.47, 0.66, and 0.73 were found between SFC at speeds 10, 40, 60, and 80 km/h with texture levels 2, 2.5, 6.3, and 6.3 mm in wavelength, respectively. A key

wavelength band, wavelengths where texture level and friction data correlation is higher than 95 percent of the peak correlation coefficient, was identified for each speed and combines to $L_{tx,\ 1.25\ -\ 12.5.}$ While a correlation coefficient of 0.9 was found between the inverted slope of SFC vs. speed with texture wavelengths at 8 to 25 mm.

Chen (2020) collected friction data with a hand-push friction tester (HFT) and texture data both based on the sand patch test and with a 3-dimensional image-based texture analysis method (3D-ITAM) along pavements with different mixture types, aggregate sizes and types, asphalt-aggregate ratio, compaction effort levels and compaction temperatures to correlate low-speed tire-pavement friction coefficient with texture. For data processing, the author removed the highest and lowest 2.5% of pixel values, applied a Gaussian smoothing filter on the recognized defect areas, and used the photometric stereo method to recover the 3D asphalt mixture surface. He concluded that $Ltx_{,0.13-0.5}$ displays good correlation with both MTD based on sand patch method (R^2_{adj} = 0.81) and with HFT-measured friction coefficient (R^2_{adj} = 0.88).

NOISE-TEXTURE MODELS

Four types of models have been used to predict tire/pavement noise, namely statistical, physical, hybrid statistical, and hybrid theoretical (Keulen and Duskov, 2005). Kujipers and Van Blokland (2001) evaluated a list of existing models and distinguished them by their focus and objectives. They found that physical models tend to focus on tire properties, while statistical models tend to focus on pavement properties. As the major focus of this project is on pavement, and more specifically, pavement texture, a heavier emphasis will be placed on statistical models.

Sandberg and Descornet (1980) identified tire/pavement noise as a major component of passenger car noise from moderate speeds up, and a significant component

of truck noise at high speeds. Surface characteristics are identified to be the main factors influencing tire/road noise. The researchers used four types of tires: PIARC reference tire, smooth tread, Firestone S1 Cavallino, "summer" type tread, Firestone TC Assym., "winter" type tread, and Michelin XZX, "summer" type tread, on asphaltic concrete, rubber bitumen (3 to 6 % rubber), open-graded asphalt concrete, resinous slurry, surface dressing, cement concrete (grooved and non-grooved), and paving blocks pavement types, with sand patch measured texture depth varying over a range of 0.4 to 4.6 mm. They measured macrotexture profile curve with profilometers, taking samples by steps of 1.0 mm in the longitudinal direction and 2.0 mm in the transverse direction. Skid resistance measurements were taken either SFC at 20, 50 and 80 km/h or friction coefficient at 15% slip at 50 and 70 km/h. The macrotexture profile was represented but its spatial frequency in m^{-1} and its inverse, wavelength in meters. The bandwidth used were 1/3 octave bands. Noise was presented in 1/3 octave band power in dB with a reference scale of 0 dB defined as 10^{-12} W/m^2. The researchers explored noise/texture correlations between every couple of noise and texture 1/3 octave band levels. The correlation coefficient is a function of sound frequency and profile wavelength. It was found that highly significant correlations appeared in two separate frequency and wavelength domains: noise with low frequency ($f \leq 1500$ Hz) was positively correlated with profile components with large wavelength ($\lambda \geq 10$ mm), while high frequency noise was negatively correlated with profile components with shorter wavelengths. Critical frequencies and wavelengths were defined as those corresponding to the maximum and minimum correlation coefficients, respectively. These critical values identified are listed in Table 5-3.

Tire	PIARC Reference Tire	Firestone S1 Cavallino	Firestone TC Assym.	Michelin XZX	Michelin XZX	Michelin XZX	Michelin XZX	Michelin XZX

Speed (km/h)	80	80	80	40	60	80	100	120
Critical Wavelength for Low Frequency (mm)	80	80	63	63	80	80	80	80
Critical Low Frequency (Hz)	400	400	400	400	500	500	500	500
Critical Wavelength for High Frequency (mm)	2.5	2.5	2.0	3.2	3.2	3.2	3.2	3.2
Critical High Frequency (Hz)	8000	3150	2500	3150	3150	3150	3150	3150

Table 5-3: Critical Frequencies and Wavelengths (Sandberg and Descornet, 1980).

From the two domains, the researchers hypothesized that two different noise generating mechanisms were acting. The first mechanism takes place with larger scale texture and contributes to lower frequency noise. Under this mechanism, the more texture there is along the pavement, the more noise is expected to be generated. The second is identified with smaller scale texture and related to the generation of high frequency noise. Under this mechanism, however, the more texture is observed along the pavement, the lower the noise level is expected. Then, the tire/road noise is the superposition of two independently generated spectra. The assumptions were that the slope of how each spectrum of noise varies with pavement properties does not change but only the intercept, and that the critical frequencies of the high and low spectra do not overlap.

They further identified the two noise generating mechanisms to be radially excited tire vibrations and pumping of the air entrapped between tire and surface. The first one is identified in the low-frequency range (below 1 kHz), and generates more noise with deeper texture; while the latter one is identified in the high-frequency range and generates less noise with deeper texture.

A similar procedure was carried out by Anfosso-Lédée and Do (2002) across 12 pavements, out of which two were dense asphalt concrete with maximum aggregate size of 10 mm, four were surface dressing with maximum aggregate size of 1.5 mm, 4 mm, 10 mm and 14 mm, respectively, two were porous asphalt concrete with maximum aggregate size of 10 mm, one was porous cement concrete with maximum aggregate size of 10 mm, another one was very thin asphalt concrete with maximum aggregate size of 10 mm, one was cement concrete, and the last one was smooth epoxy surface. Texture was expressed in texture level, with center wavelength ranging from 2.5 to 250 mm, divided into 21 1/3 octave bands, and noise measured at 90 km/h was expressed in sound pressure level, with frequency ranging from 100 to 5000 Hz, divided into 18 1/3 octave bands. Correlation coefficients between 18 sets of noise level and 21 sets of texture level were calculated across the twelve pavements. While similar patterns were discovered, the authors also noticed that the correlation was stronger when porous pavements were excluded. They ascribed this finding to two reasons: overestimation of texture when negative texture is evaluated as a positive one, and sound attenuation along the propagating path due to acoustic absorption by the pores.

Another feature proposed by Anfosso-Lédée and Do (2002) was a profile indenter, composed of a profile peak and its neighboring valleys to the left and to the right and characterized by its shape and relief. The indenter shape is defined by the cotangent of its summit semi-angle calculated by:

$$\alpha = \frac{1}{2}[\tan^{-1}\left|\frac{x_e - x_{e-1}}{z_e - z_{e-1}}\right| + \tan^{-1}\left|\frac{x_{e+1} - x_e}{z_{e+1} - z_e}\right|] \quad 5\text{-}14$$

Where z_e and x_e are the height and abscissa of the e_{th} extremum, and its relief, defined by the angle between the horizontal line and the segment connecting the summits of two consecutive indenters, calculated by:

$$\theta = \tan^{-1}\left|\frac{z_{p+1} - z_p}{x_{p+1} - x_p}\right| \quad 5\text{-}15$$

Where z_p and x_p are the height and abscissa of the p_{th} peak. Another parameter that can be used to characterize indenters is density, defined as the number of indenters per unit length.

It was found that rolling noise increased when cotangent (α) or (θ) increased, or when the density decreased, and the three geometric parameters were strongly intercorrelated. The authors pointed out that when cotangent (α) increased, both the drainage capacity and vibration excitation decreasd too. As drainage capacity was reduced, more high-frequency noise was generated through air pumping, as the amount of asperities enveloped by the tire rubber increased; while as vibration excitation decreased, low-frequency noise was reduced due to decreased rubber deformation. As these two effects counteract each other's impact on total noise, how an increased cotangent (α) or (θ) affects the overall noise level varies depending on the specific tire and pavement. Meanwhile, when the indenter density increased, smaller spacing was found in between two consecutive ones, causing lower vibration excitation as well as higher drainage capacity for air. As discussed earlier, lower vibration excitation reduced low-frequency noise from tread impact, and higher drainage capacity reduced high-frequency noise from air pumping.

Domenichini et al. (1999) agrees with the concept that texture wavelength in the range 10 to 500 mm increases the noise in the low frequency range (<1000 Hz for light vehicles and <500 Hz for heavy vehicles) originating from tire vibration, and texture

wavelengths in the range 0.5 to 10 mm decreases the noise at high frequencies (>1000 Hz) originating from air pumping. This was consistent with what Sandberg and Descornet (1980) identified earlier. The researchers identified three pavement surface characteristics relevant to tire-road noise: pavement texture, wearing course porosity, and thickness of the porous surface layer. The study evaluated the MPD based on pavement profiles using the TINO 3D profilometer according to ISO 13473-1 and MTD based on the sand patch test according to ASTM E965, calculated power spectral density (PSD) and of the texture level of the pavement profiles, classified unevenness with respect to traffic induced vibrations according to ISO 8608, and with respect to comfort according to the World Bank Index IRI (WB TP 46), and evaluated the skid resistance properties at different speeds as a function of MTD and British Pendulum Numbers. Noise measurements were made with a smooth tire and a normal production tire at 50 and 80 km/h. The correlation between texture and noise was analyzed each at a certain spatial frequency of texture level with a noise level at a certain temporal frequency, called "texture-noise gradient."

Friction properties were estimated from the results of the British Pendulum Test and MTD measurements based on the relationship identified by Leu and Henry (1978):

$$SN_0 = -31 + 1.38 \cdot BPN \qquad 5\text{-}16$$

$$PSNG = 4.1 \cdot \left(\frac{MTD}{0.0254}\right)^{-0.47} \qquad 5\text{-}17$$

$$SN_V = SN_0 \cdot \exp\left(\frac{-PSNG \cdot V}{100}\right) \qquad 5\text{-}18$$

For noise-texture analysis, the researchers correlated the sound pressure level (SPL) values measured by the rear lateral microphone (near field measurement) with a normal production tire, as texture index was calculated as follows:

$$TI = 2.5 \cdot PSP + L_{UNE} \quad (5\text{-}19)$$

$$PSP = \frac{L_{PEAK} \cdot i}{100} \quad (5\text{-}20)$$

Where PSP refers to the "peak-slope parameter" and L_{PEAK} is the first relative maximum value of the texture level longer than the wavelength of 2.0 mm (lower than the spatial frequency of 500 m^{-1}), smoothed over the nearest three frequencies

$$L_{PEAK} = \frac{l_{fPEAK^-} + l_{fPEAK} + l_{fPEAK^+}}{3} \quad (5\text{-}21)$$

f_{PEAK} is the spatial frequency corresponding to the wavelength λ_{PEAK} at which the relative maximum occurs, and f_{PEAK-} and f_{PEAK+} the previous and following spatial frequencies respectively.

i represents the slope of the descending portion of a pavement texture between the maximum texture level and the texture level at 500 m^{-1}

$$i = \frac{L_{PEAK} - L_{500}}{\log(\lambda_{PEAK}) - \log(2)} \quad (5\text{-}22)$$

L_{500} is the texture level smoothed over the three nearest wavelengths for a spatial frequency of 500 m^{-1} (wavelength of 2.0 mm)

$$L_{500} = \frac{L_{500^-} + L_{500} + L_{500^+}}{3} \quad (5\text{-}23)$$

L_{UNE} is the unevenness level and is the average level of texture centered around the frequency of 1.58 m^{-1}

$$L_{UNE} = \frac{L_{1.26} + L_{1.58} + L_{2.00}}{3} \quad (5\text{-}24)$$

The SPL is then calculated from texture index:

When V = 50 km/h,

$$SPL = 0.47\ TI + 49.39$$

When V = 80 km/h,

$$SPL = 0.47\ TI + 42.94$$

The authors claimed $R_2 = 0.91$ based on measurement data collected along eleven pavements.

Liu and Shalaby (2015) stated that pavement texture is a factor that influences tire-pavement interactions such as noise and friction. The authors cited Flinsch et al. (2003) as the argument to use three-dimensional (3D) texture descriptors instead of mean profile depth (MPD), which is a 2D approximation of the 3D mean texture depth (MTD). Vehicle-mounted laser devices could measure macrotexture of pavement without disrupting traffic flow. However, studies showed that two-dimensional (2D) texture measurement and indicators are insufficient especially when analyzing friction and noise (Liu and Shalaby, 2015, El Gendy and Shalaby, 2007, El Gendy et al., 2011). Texture size, spacing, and distribution are factors to be considered as well.

The authors' goal was to develop several 3D texture parameters to describe texture and to correlate with friction and noise. They used a section of the South Extension of the I-355 North-South Tollway between I-55 and I-80 near Joliet, Illinois, as the test site, and selected for testing Portland cement concrete (PCC) surface texture. The test section was divided into 13 segments, each about 160 m long, and representing a different type of PCC pavement texture. Texture was measured using a photometric stereo device, CTM, and high-speed texture profiler (HSTP). Friction was measured using Dynamic Friction Tester (DFT) (ASTM E1911 2009), and sound intensity was measured in accordance with AASHTO Provisional Standard TP076 (AASHTO TP076 2008).

The first 3D macrotexture indicator was simulated mean texture depth (SMTD) and was calculated as follows:

$$SMTD = h_{max} - \frac{1}{A}\sum_{i=1}^{M}\sum_{j=1}^{N}\frac{1}{3}ah_{ij} \quad (5\text{-}25)$$

Where:

SMTD = simulated mean texture depth,

h_{max} = highest elevation of the recovered surface texture,

h_{ij} = elevation of any pixel of the recovered texture,

A = area of the recovered surface,

a = area of each pixel of the recovered texture, and

M, N = number of pixels in each direction of the recovered texture

Root-mean-square roughness, calculated by

$$S_q = \sqrt{\frac{1}{A}\sum_{i=1}^{M}\sum_{j=1}^{N}ah_{ij}^2} \quad (5\text{-}26)$$

S_q = root-mean-square roughness of the recovered texture

Skewness of the recovered surface, calculated by

$$S_{sk} = \frac{1}{AS_q^3}\sum_{i=1}^{M}\sum_{j=1}^{N}ah_{ij}^3 \quad (5\text{-}27)$$

S_{sk} = skewness of the recovered texture

Kurtosis of the recovered surface, calculated by

$$S_{ku} = \frac{1}{AS_q^4}\sum_{i=1}^{M}\sum_{j=1}^{N}ah_{ij}^4 \quad (5\text{-}28)$$

S_{ku} = kurtosis of the recovered texture

It was found that skewness and kurtosis, which are based on third and fourth moment of surface texture heights, respectively, were highly correlated, so only one of them would be sufficient to describe the shape and distribution of the surface texture. The regression conducted among sound intensity noise, SMTD, and skewness was found to be:

$$\text{Noise} = 105.87 + 2.06\ \text{SMTD} + 3.88\ S_{sk}$$

$$R_2 = 0.71;\ \text{SEE} = 0.56$$

And the friction number F(60) was found to be:

$$F(60) = 14.64 + 11.54\text{SMTD} - 0.45\ S_{sk}$$

$$R_2 = 0.53,\ \text{SEE} = 2.45$$

The authors concluded that both texture heights and texture distribution (skewness and kurtosis) were important factors in pavement noise/friction. Negatively skewed surface textures tend to provide better friction and generate less noise (Liu and Shalaby, 2015). They also cited Do et al., (2000) and Flintsch et al. (2003) to support the argument that information on macrotexture alone is not sufficient to predict pavement friction, and that both microtexture and macrotexture are needed in order to obtain higher accuracy in friction prediction. Serigos and Zuniga agreed that when microtexture and macrotexture were taken into consideration on skid resistance correlation models, together they can account for at least 70% of the total variance in skid resistance on the road (Serigos et al., 2016; Zuniga, 2018). Furthermore, most traffic noise analysis research indicates that the peak of traffic noise occurs within the macrotexture wavelength spectrum, nevertheless, while there seems to be a correlation between texture and noise, it is still not fully understood how those two parameters interact (Smit et al., 2016).

INTERCORRELATION

Past researchers have also attempted to correlate friction with texture and noise. Baran and Henry (1983) measured friction with the British Pendulum Tester and full-scale locked-wheel tester using both smooth and ribbed tires, near-field tire/pavement noise with an on-board microphone mounted near the tire, and far-field tire/pavement noise while the vehicle is coasting through the testing sites with a microphone 15 m from the edge of the

pavement along six pavements covering a wide range of textures. Though spectral characteristics of near-field noise data obtained from the study correlated well with friction for Portland Cement Concrete (PCC), and far-field noise data at 64 and 80 km/h correlated well with friction for all pavements, no strong relationship was discovered between near-field noise and friction for asphalt concrete surfaces.

In 2008, Caltrans conducted a study on pavements with longitudinally tined Portland Cement Concrete (LT PCC), burlap drag Portland Cement Concrete (PD PCC), dense graded asphalt concrete (DGAC), and open graded asphalt concrete (OGAC) surfaces (Rymer et al., 2010). OBSI was measured in accordance with the AASHTO standard, dividing the measured pavement into three 440-ft sections, while measuring the A-weighted noise at 60 mph. Friction was measured with a dynamic locked wheel friction trailer and a stationary Dynamic Friction Tester (DFT). Pavement macrotexture was measured in Mean Profile Depth (MPD) with the Circular Track Meter (CTM). Compared to dense-graded, the open-graded pavements tested exhibited a much higher texture level, generally comparable friction, higher noise level at lower frequencies (< 1000 Hz), and lower noise level at higher frequencies. McDaniel et al. (2014) developed a one-parameter model using MPD as the input parameter, with best-fit coefficients of 3.46, 7.35, and -1.44 dB/mm for the low-, mid- and high-frequency constituent spectra, respectively. With the variations in MPD measured along the test pavements, a predicting range of 13.8, 58.8, and 2.88 dB can be expected with the model. Skewness was also attempted as an independent variable, but the effect was not found to be significant. The single parameter model using friction, however, did not have as strong a predicting power compared to the model based on texture, with only 4, 3, and 0.05 dB maximum effect for the three spectra, respectively. Thus, it is expected that noise does not correlate as well with friction as it does with texture.

Chapter 4: Methodology

DATA COLLECTION

Data collection was conducted along a total of eight in-service flexible pavements in Texas. The sites were chosen from four different districts with different types of asphalt mixes, two thin overlay mix (TOM), two seal coat, three open-graded, and one dense-graded. More detailed identification of the location and types of mixes of the sites are as shown in Table 6-1.

District	Number of Sites	Type of Mix
Austin	4	2 PFCs and 2 TOMs
San Antonio	1	NovaChip
Bryan	1	Seal Coat
Brownwood	2	1 Type C and 1 Seal Coat

Table 6-1: Sites and mix design distribution

Texture Data Collection

For each site, texture measurements were taken at three locations over a span of 30 meters (98.5 ft) with a 15 m (49.2 ft) spacing in between two consecutive testing locations in the longitudinal direction. The selection of the locations was based on homogeneous areas representative of the pavement type. The right wheel path of the outside lane was measured for all three sections, in a single direction. Traffic control was required because some of the tests were stationary. Figure 4-1 illustrates the sampling method used to collect texture data.

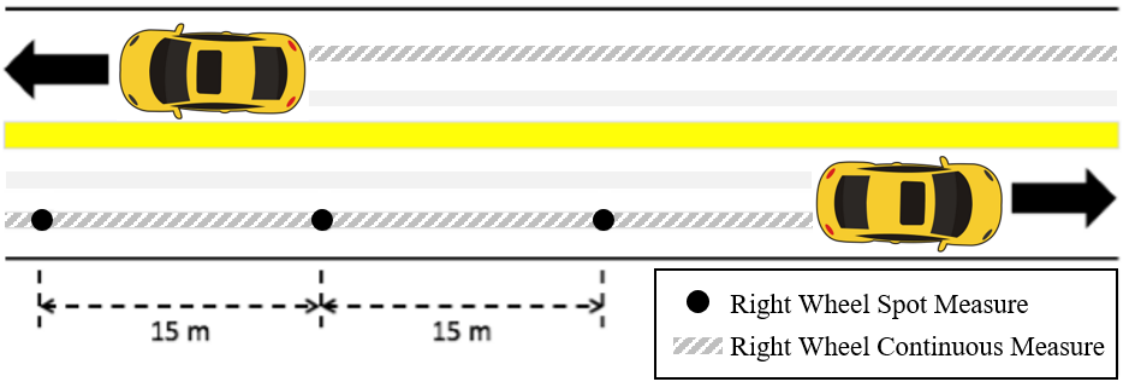

Figure 6-1: Field test sampling method

The Line Laser Scanner (LLS) was used to collect 3D data of the pavement texture utilizing a laser which moved in the longitudinal direction (direction of traffic). The LLS covered a longitudinal distance of 600 mm with a laser line width of 200 mm. The Circular Track Meter (CTM) measurements were made in the same area covered by the LLS. Figure 6-2, the LLS and CTM being used in the field. The sand patch test (SPT) was also performed adjacent to the area where the LLS and CTM were performed to avoid contamination from the SPT's sand.

Figure 6-2: LLS in operation (left), CTM placement (center) and Sand Patch Test (right)

Noise Data Collection

The tire/pavement noise of the road was evaluated using the on-board sound intensity (OBSI) method. All measurements were taken alongside both the leading and trailing edge of the Standard Reference Test Tire (SRTT) contact patch on the side of the vehicle opposite of the driver using a dual probe configuration of microphones as shown in Figure 6-3. Test were carried out at a constant speed of 96 km/h (60 mph), as per AASHTO standard TP 76-15. To ensure consistency throughout the testing, a single driver used the same testing vehicle and SRTT on all eight sites. It was also ensured that the vehicle only had necessary equipment on board, to avoid variations in total vehicle weight.

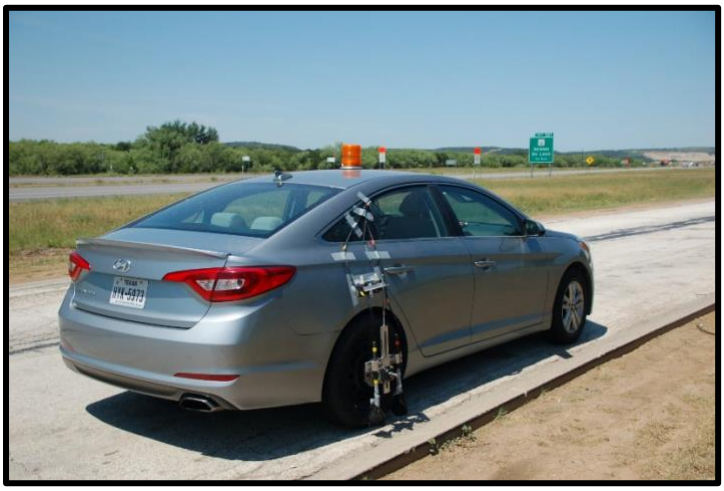

Figure 6-3: OBSI setup on passenger side rear wheel

Friction Data Collection

The friction characterization consisted of three different friction tests. The British Pendulum Tester (BPT) was applied in each of the sampling sites following the traffic direction. The micro-GripTester collected a continuous measure of friction at a walking speed of 0.7 m/s (2.3 ft/s). The result consists of an averaged value of friction measures,

expressed as the Grip Number (GN), for the three locations at each section. For the Grip-Tester, the output was given as GN with the test performed at 70 km/h (43.5 mph) target speed. Previous studies indicated Grip-Tester at higher speeds correlates better when observing texture-friction (Kouchaki, 2018). The speed was maintained within 5% of the target speed. The pavement was wetted with a constant water thickness of 0.5 mm with an automatic water tank system. The GN for each section was obtained as the average of the GN measures along the total evaluated distance (approximately 30 m).

Figure 6-4: BPT (left), micro-GripTester (cebter) and GripTester (right)

DATA PROCESSING

As described by Sabillon et al. (2020), the noise data collected using the OBSI system was processed as per AASHTO TP-76. The intensity levels (ILs) collected from the trailing and leading-edge probes were averaged to yield an average IL, using Equation 4-1. The individual test run average levels were then arithmetically averaged to calculate the average noise ILs for the three test runs at each 1/3 octave band frequency between 400 and 5,000 Hz.

$$L_{E-avg} = 10\log_{10}\left(\frac{1}{N}\sum_{i=1}^{N}\left(10^{\left(\frac{L_i}{10}\right)}\right)\right) \qquad 6\text{-}1$$

Where:

L_{E-avg}: Average energy level (dBA)

L_i: Levels (dBA)

N: Number of sets of data

Texture data collected using the LLS setup was processed as per ISO/TS 13473 which involves applying multiple transformations algorithms. First, invalid points were located within the dataset by using numerical thresholds and computed as a percentage of all points. This percentage is known as the drop-out rate and it must never exceed 10%. Once all sections were confirmed to have a drop-out rate below 10%, all invalid points were replaced by using one-dimensional linear interpolation as per Equation 4-2.

$$z_i = \frac{z_n - z_m}{n - m}(i - m) + z_m \qquad 6\text{-}2$$

Where:

i: Sample number where the value is invalid

m_i: Sample number of the nearest valid value before i

n: Sample number of the nearest valid value after i

z_i: Interpolated value for sample i

z_{m_i}: Value for sample m

z_n: Value for sample n

A least-square fitting algorithm was then used to achieve a slope of zero in the profile in a process called slope suppression. The mean amplitude of the profile was later set to zero in a process referred to as offset suppression. This yielded a profile with a base height of 0.0 mm, where peaks and valleys can be easily distinguished. In addition, the profile was subjected to a windowing algorithm to reduce the signal amplitude to zero at the edges of the profile and avoid leakage. Given that the length of the measured profile was less than one meter, a Split Cosine Bell Window (SCBW) was applied as per Equation 4-3.

$$w_{i,C} \coloneqq \begin{cases} cos^2\left(\frac{5\pi i}{N} - \frac{\pi}{2}\right) \text{ for } & 0 \le i < \frac{N}{10} \\ 1 \text{ for } & \frac{N}{10} \le i < \frac{9N}{10} \\ cos^2\left(\frac{5\pi i}{N} - \frac{9\pi}{2}\right) \text{ for } & \frac{9N}{10} \le i < N \end{cases} \quad \text{6-3}$$

Where:

$w_{i,C}$: Window coefficient,

i: Sample number, and

N: Number of data points.

The window coefficient was multiplied by the signal and later normalized by the integral of the window to prevent attenuation of the signal as per Equation 4-4.

$$Z_{i,win} \coloneqq \frac{w_{i,C} * z_i}{0.9354} \quad \text{for } i = 0, \dots, N-1 \quad \text{6-4}$$

Where $Z_{i,win}$ is the windowed profile height at point i (mm).

A Discrete Fourier Transform (DFT) is applied to the windowed profile as defined by Equation 4-5 to transform the texture data from the spatial time domain into the spatial frequency domain.

$$Z_k \coloneqq \frac{1}{N} \sum_{i=0}^{N-1} Z_{i,win} * e^{-j\left(\frac{2\pi k}{N}\right)i} \quad \text{for } k = 0, \dots, N-1 \quad \text{6-5}$$

Where:

Z_k: DFT of the windowed profile, and

j: imaginary unit ($j^2 = -1$)

The result of the DFT is a constant bandwidth narrow band spectrum with complex values. The bandwidth is a function of the evaluation length defined by Equation 4-6.

$$\Delta f_{sp} = \frac{1}{l} \quad \text{6-6}$$

Where:

Δf_{sp}: Bandwidth intervals (cycle/meter), and

l: Evaluation length (m)

An important property of the DFT is that it obeys the Nyquist Sampling Theorem, which states that the sampling frequency should be at least twice the highest frequency contained in the original signal. An alternate way to interpret this statement is that the shortest wavelength that can be obtained from a discrete signal is twice the sample spacing. Given that the LLS is capable of sampling two points with a spacing of 8 microns in the longitudinal direction, the shortest wavelength that can be analyzed using the DFT is 16 microns. This implies the DFT can capture all the information down to the shortest wavelength of the first decade of microtexture, which is 50 microns.

The results of the DFT are later converted into a power spectral density (PSD) by means of Equation 4-7.

$$Z_{PSD} = \frac{2|Z_k|^2}{\Delta f_{sp}} \quad \text{for } k = 0, \dots, \left(\frac{N}{2} - 1\right) \tag{6-7}$$

Where Z_{PSD} is the Power Spectral Density (PSD).

Given that the results of a PSD are in the form of constant bandwidth spectral data, it was later transformed into constant-percentage bandwidth spectral data such that it could be represented in the form of fractional octave bands. The power within the fractional octave band, m, can be calculated from the narrow band PSD according to Equation 4-8.

$$\begin{aligned} Z_{P,m} = {} & Z_{PSD,low} * \left(f_{sp,low} + \frac{1}{2}\Delta f_{sp} - \left(10^{\left(-\frac{1.5}{10n}\right)}\right) * f_{sp,m}\right) \\ & + \sum_{k=low+1}^{up-1} Z_{PSD,k} * \Delta f_{sp} + Z_{PSD,up} \\ & * \left(f_{sp,m} * \left(10^{\left(-\frac{1.5}{10n}\right)}\right) - f_{sp,up} + \frac{1}{2}\Delta f_{sp}\right) \end{aligned} \tag{6-8}$$

Where:

$Z_{PSD,low}$: PSD of the narrow band that coincides with the lower boundary of the fractional-octave band,

$f_{sp,low}$: Center frequency of the narrow band that coincides with the lower boundary of the fractional-octave band,

$f_{sp,m}$: Center frequency of the fractional-octave band m,

$Z_{PSD,up}$: PSD of the narrow band that coincides with the upper boundary of the fractional-octave band,

$f_{sp,up}$: Center frequency of the narrow band that coincides with the lower boundary of the fractional-octave band, and

n: Integer whose value can be freely chosen to obtain a desired speed, for this study is was chosen to be one.

Finally, a texture level distribution (TLD) was computed. The TLD provides a more detailed metric by which to evaluate texture and can be related to mixture properties. The TLD estimates the proportion of particular wavelengths in the profile that can be attributed to aggregate and mixture properties (Miller et al., 2011). These wavelengths are captured in the form of fractional one 1/3 octave bands. The texture profile level (L_{tx}) was measured in decibels (dB) and computed using Equation 3-12.

Once the texture data were converted to a TLD at different 1/3 octave band wavelengths, it was further trimmed to wavelengths for which there was enough texture data to compute a texture level. The final distribution of wavelengths covered 36 different 1/3 octave band wavelengths ranging from 80 mm down to 0.025 mm.

DATA DESCRIPTION

The noise level distribution by 1/3 octave band frequency across the eight pavements are as shown in Figure 6-5, texture level distribution shown in Figure 6-6, and friction measurement results in Figure 6-7 through Figure 6-9. Since texture was measured

at three point-locations, each noise or friction measurement should correspond to three texture measurements, as shown in the three panels (a) through (c) in Figure 6-6.

In Figures 4-5 and 4-6, the blue line represents permeable friction course, orange for Type C dense graded, green for thin overlay mix (TOM), grey for NovaChip, and purple for seal coat. It can be seen that the pavements with TOM have both lower noise and texture level. The peak of their noise also occurs at a higher frequency compared to other pavements. It is worth noticing that US 84 has a relatively lower level of texture, especially in the range of 1 to 10 mm, while it also has a higher level of noise at frequencies greater than 1000 Hz. However, as many researchers have pointed out, that the generation of tire/pavement noise could be a superposition of multiple spectra of noise generated from different mechanisms, and the long wavelength texture might not be strongly correlated with high frequency noise.

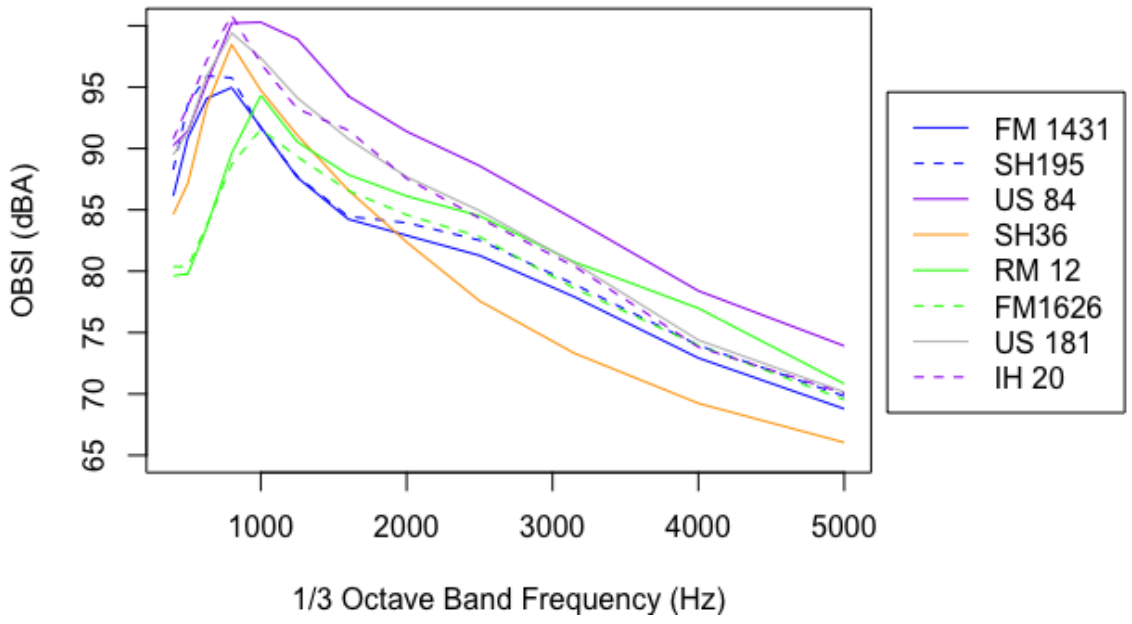

Figure 6-5: OBSI Noise Level Distribution by Frequency

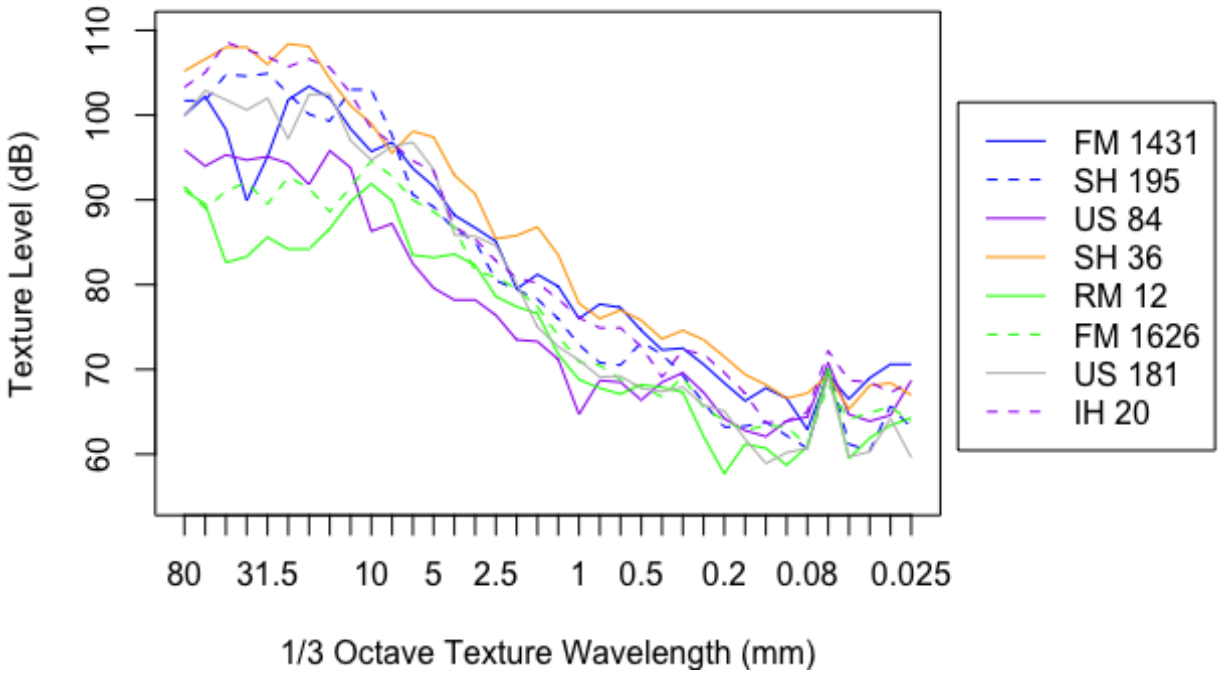

(a) Sample 1

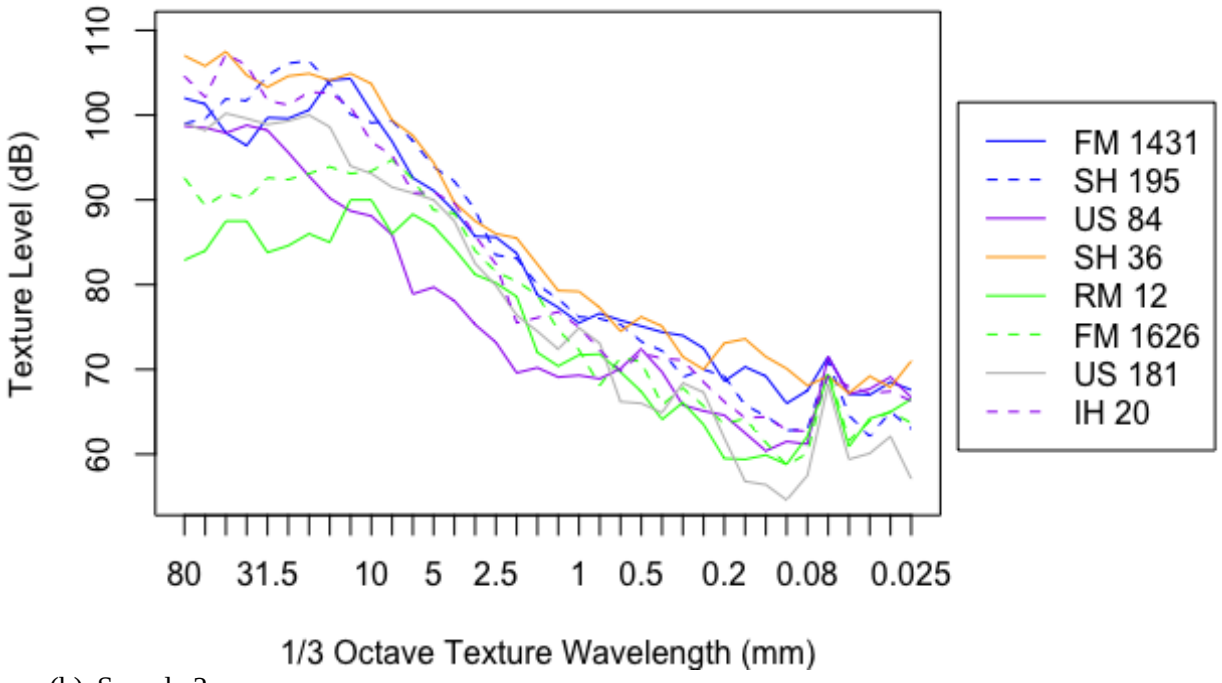

(b) Sample 2

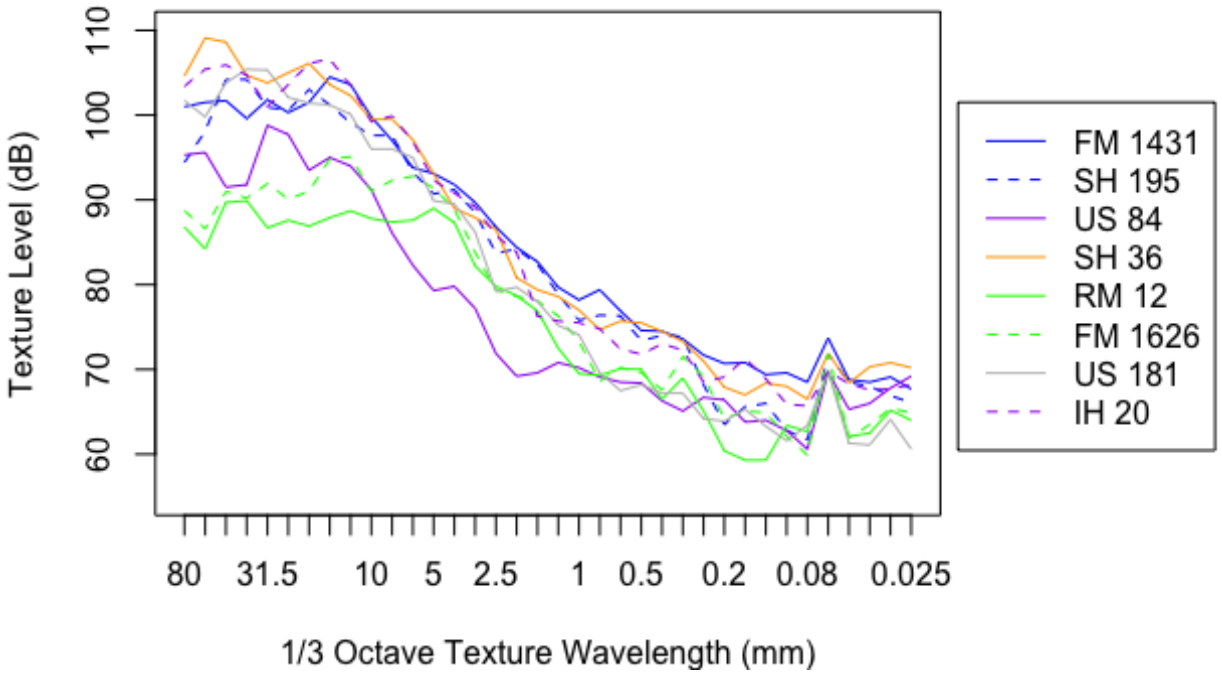

(c) Sample 3

Figure 6-6: Texture Level Distribution by Wavelength

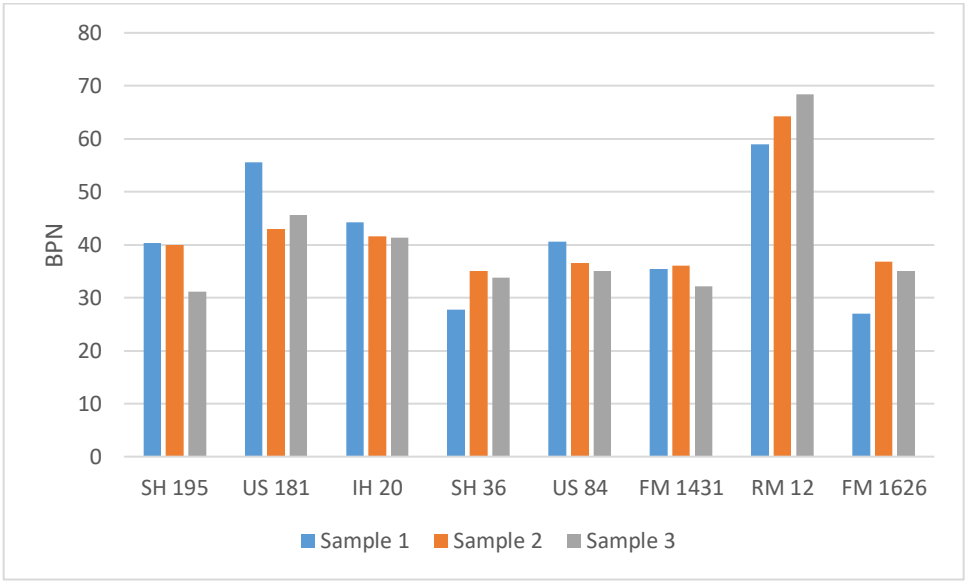

Figure 6-7: Friction Measurements from British Pendulum Tester

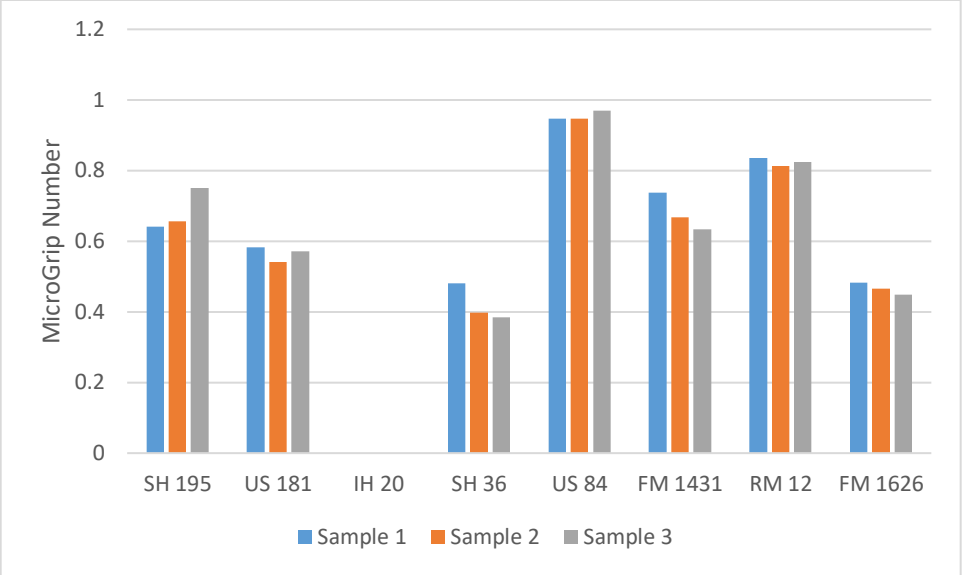

Figure 6-8: Friction Measurements from MicroGrip Tester

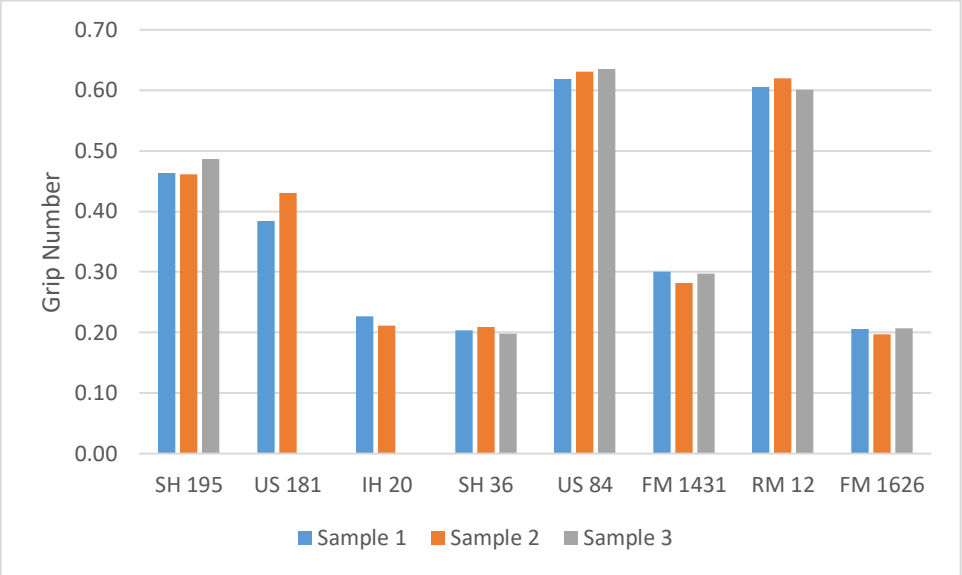

Figure 6-9: Friction Measurements from Grip Tester

DATA ANALYSIS

Noise-Texture Correlation

Wavelength Set Approach

In the frequency range from 400 to 5000 Hz, there are 12 1/3 octave bands in noise measurements, while there are 36 1/3 octave bands in texture measurements, from wavelength of 0.025 to 80 mm. The approach utilized in this study consisted on disaggregating the texture measurements into wavelength sets, as shown in Table 6-2.

Wavelength Set	Start		End	
	Wavelength (mm)	Frequency (m^{-1})	Wavelength (mm)	Frequency (m^{-1})
1	80	12.5	6.3	160
2	63	16	5	200
3	50	20	4	250
4	40	25	3.15	315
5	31.5	31.5	2.5	400
6	25	40	2	500
7	20	50	1.6	625
8	16	62.5	1.3	800
9	12.5	80	1	1000
10	10	100	0.8	1250
11	8	125	0.63	1600
12	6.3	160	0.5	2000
13	5	200	0.4	2500

14	4	250	0.315	3150
15	3.15	315	0.25	4000
16	2.5	400	0.2	5000
17	2	500	0.16	6250
18	1.6	625	0.13	8000
19	1.25	800	0.1	10000
20	1	1000	0.08	12500
21	0.8	1250	0.063	16000
22	0.63	1600	0.05	20000
23	0.5	2000	0.04	25000
24	0.4	2500	0.0313	32000
25	0.315	3150	0.025	40000

Table 6-2: Wavelength Sets and Corresponding Wavelengths

A total of 600 single variable ordinary least-square (OLS) regressions (noise vs. 25 sets of wavelengths, 8 roadways, 3 samples each) were conducted, with the best fitted set shown in Table 6-3. Most of the samples reached the best fit around the fifth wavelength set (31.5 mm to 2.5 mm).

	Best Fit Set	Highest Adjusted R_2
FM 1431	6	0.94
FM 1626	5	0.82
IH 20	5	0.94
RM 12	5	0.78

SH 36	5	0.89
SH 195	4	0.99
US 84	2	0.86
US 181	1	0.90

Table 6-3: The Best Fit Result by Roadway

One interesting aspect for the linear goodness-of-fit between noise and texture was their distribution across frequencies, more specifically, the overall trend and the critical point. It is not necessarily true that each 1/3 octave band of noise would correspond to one 1/3 octave band of texture. One of the samples with higher linear fit, for example, the distribution of the fifth wavelength set in the second texture measurement of FM 1431 and its noise level distribution is as shown in Figure 6-10 and Figure 6-11. It can be seen that the two distributions have a similar overall trend and location of the critical point. However, there was not enough evidence to claim that this similar pattern in distribution directly results from the fact that noise level relies the heaviest on this wavelength set. Actually, it is not necessarily true that each 1/3 octave band in noise frequency correspond to exactly one 1/3 octave band in texture wavelength.

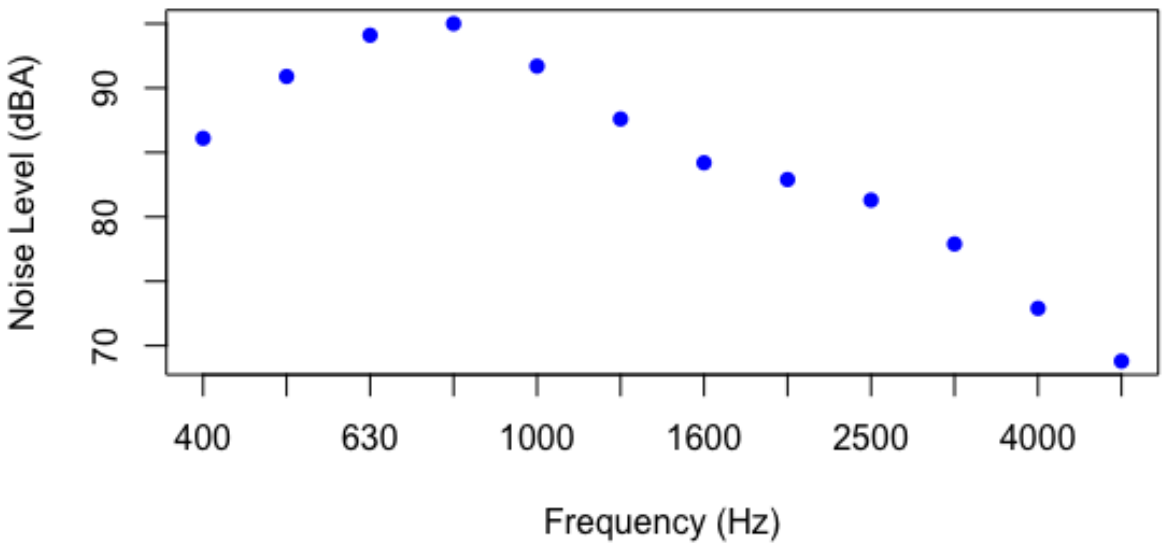

Figure 6-10: Distribution of Noise Level over Frequencies 400 to 5000 Hz

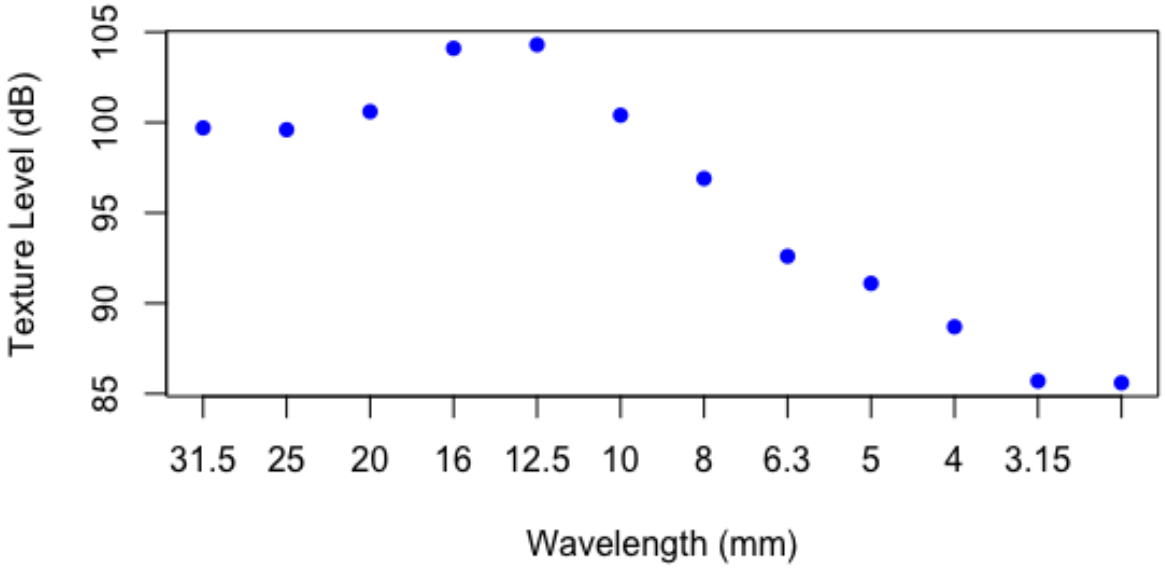

Figure 6-11: Distribution of Texture Level over Wavelengths 31.5 mm to 2.5 mm

Critical High/Low Wavelength and Frequency Approach

Correlation mapping following the procedure described by Sandberg and Descornet (1980) and Anfosso-Lédée and Do (2002) was conducted with the collected data, with

texture level over the range of 0.025 to 80 mm and noise level over the range of 400 to 5000 Hz for the eight pavements, with correlation coefficients mapped in Figure 6-12.

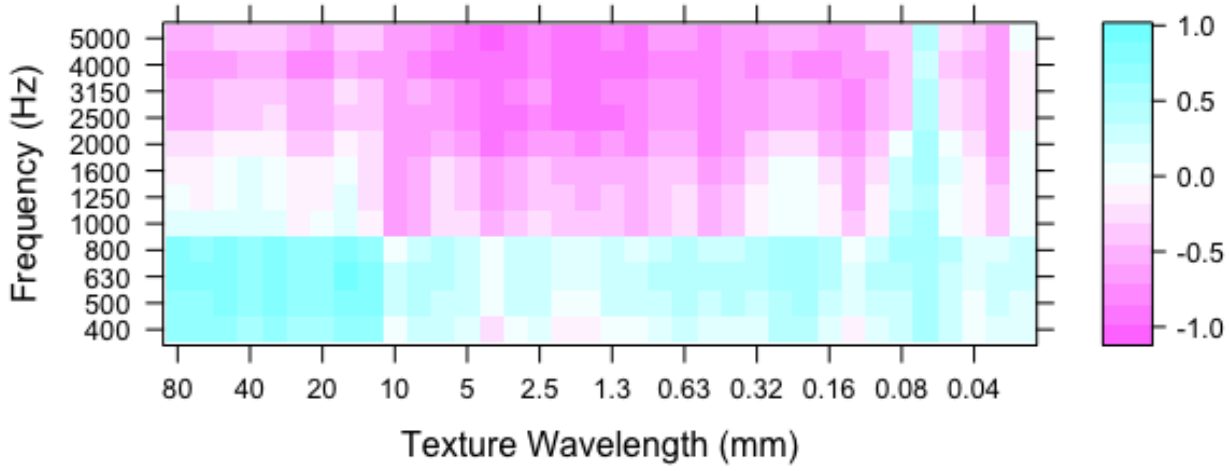

(a) Noise vs. Sample 1 Texture

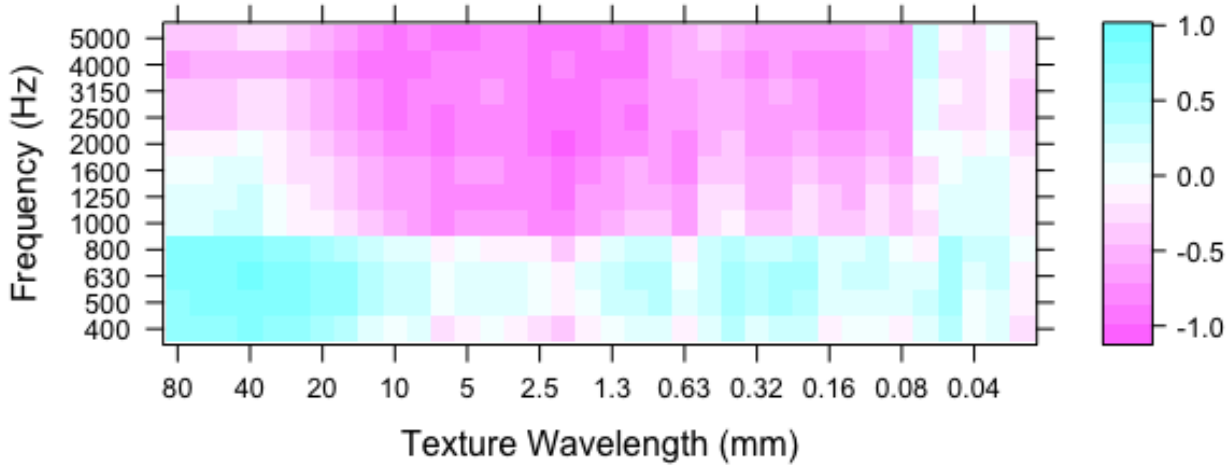

(b) Noise vs. Sample 2 Texture

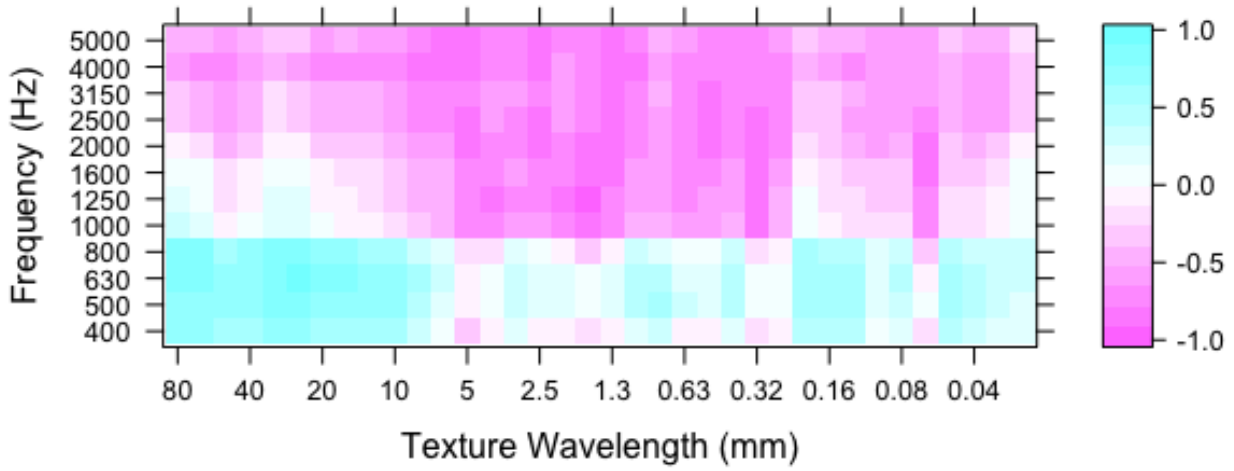

(c) Noise vs. Sample 3 Texture

Figure 6-12: Correlation Coefficient between Sound Pressure Level and Texture Level

The overall pattern was consistent with what previous researchers have found, that low frequency noise (< 1000 Hz) correlates positively with large scale texture (> 10 mm), and high frequency noise correlates negatively with small scale texture. However, from the plots, it can be observed that a high level of randomness was found between noise and

microtexture around the wavelength of 0.05 mm. One reason is that, as shown in

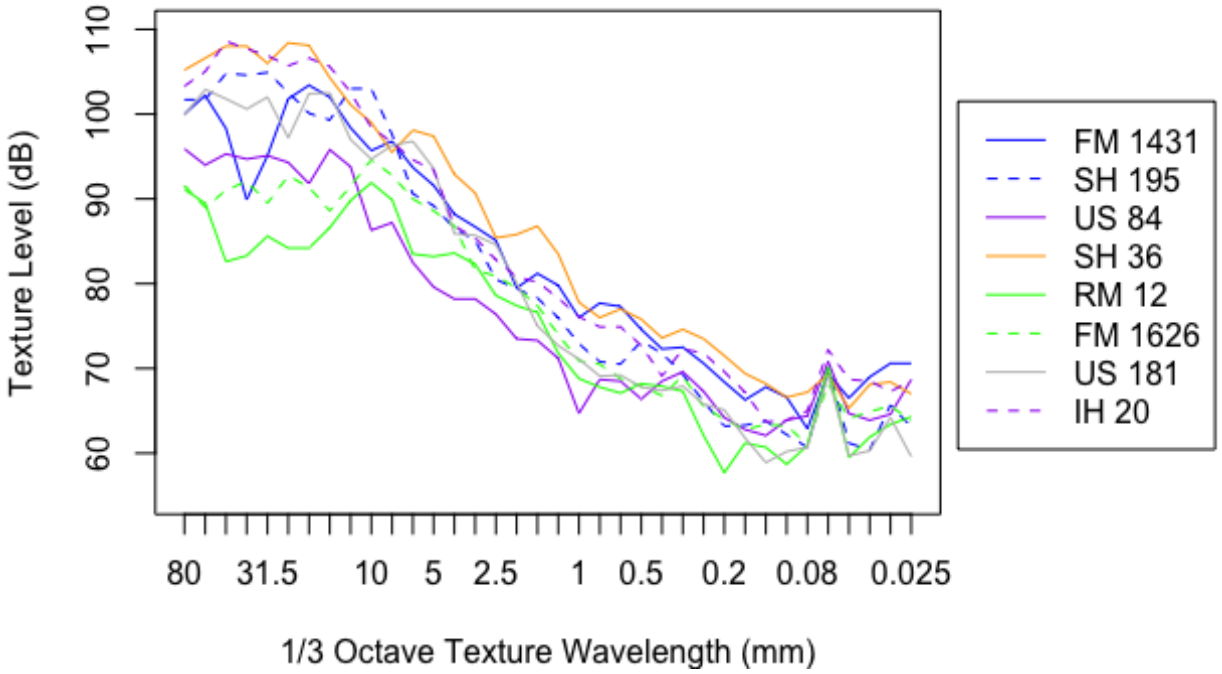

(d) Sample 1

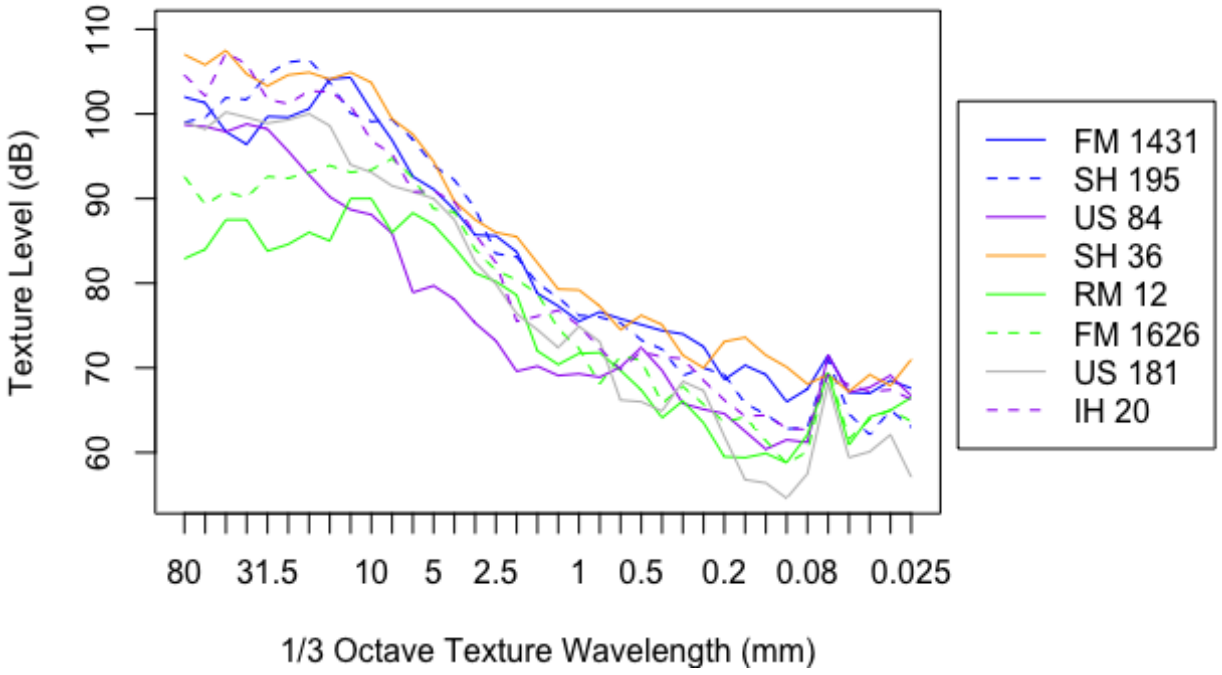

(e) Sample 2

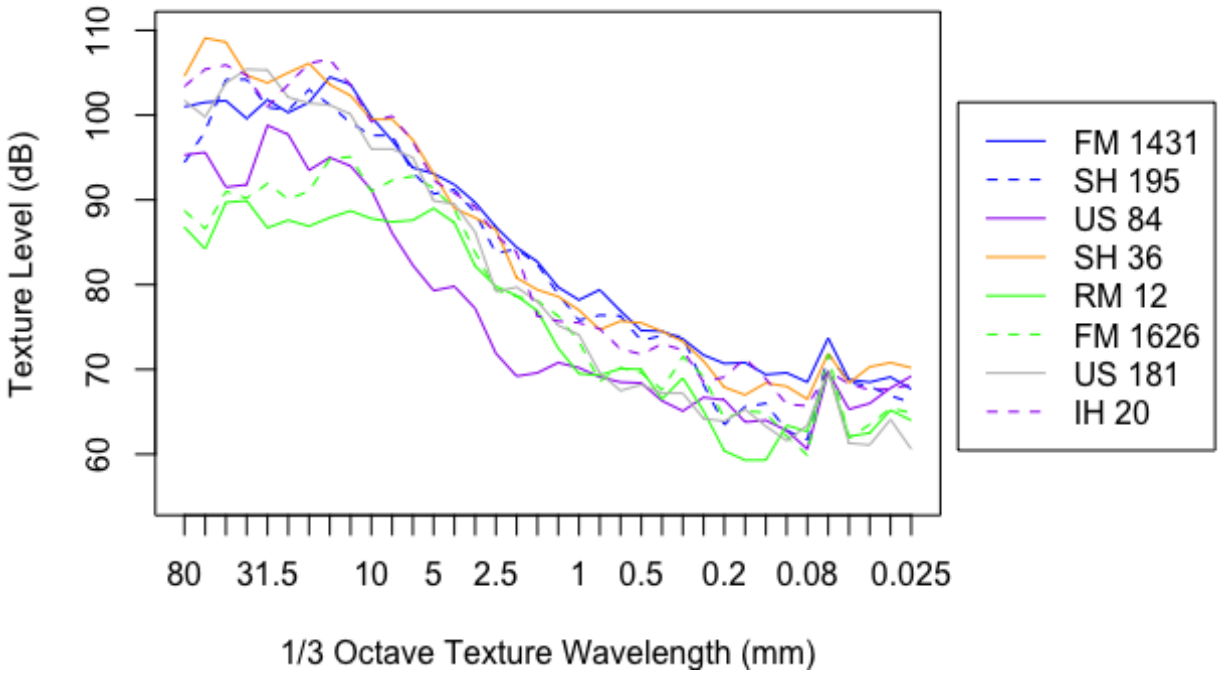

(f) Sample 3

Figure 6-6, the pavements have a high variability in the microtexture spectrum.

Linear Regression at Maximal Correlation, No Grouping

Across all three samples, the maximum positive correlation occurs around noise level of 630 Hz and texture level of 50 mm, while the maximally negative correlation is not concentrated at a single location: local minima in correlation coefficients are spread all around over the domain from 0.25 to 8 mm and the range from 1000 to 5000 Hz across the three samples. As a result, for the purpose of a more detailed analysis of the positive correlation between low frequency noise and long wavelength texture, the frequency of 630 Hz and the wavelength of 50 mm were selected. However, to explore the negative correlation between high frequency noise and short wavelength texture, the most common critical values identified by Sandberg and Descornet (1980) were chosen, locating the noise frequency at 3150 Hz and the texture wavelength at 3.2 mm.

(a) A single variable linear regression was first conducted with the noise level at 630 Hz as the dependent variable and the texture level with 50 mm wavelength as the independent variable. The regression results with the corresponding parameters and goodness-of-fit measures are shown in Table 6-4. The plots with noise level vs. texture level are shown in Low Frequency Noise Level vs. Sample 3 Large Scale Texture Level

Figure 6-13.

	Sample 1	Sample 2	Sample 3
Intercept	41.93	27.76	40.03
Coefficient	0.5111	0.6541	0.5263
Adjusted R_2	0.6403	0.6597	0.4453

Table 6-4: Regression Results for Low Frequency Noise vs. Large Scale Texture, No Grouping

From both the regression results and the plots, it can be observed that noise level at frequency of 630 Hz correlates positively with texture level at 50 mm, though the overall goodness-of-fit was not high.

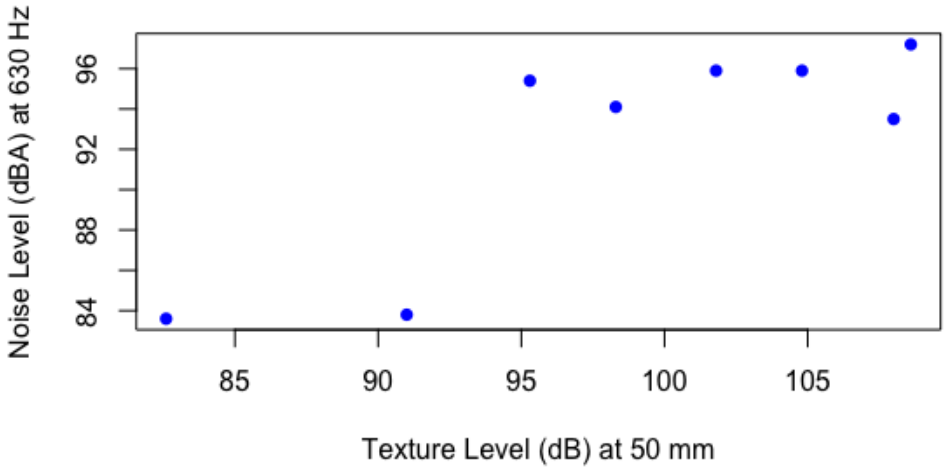

(b) Low Frequency Noise Level vs. Sample 1 Large Scale Texture Level

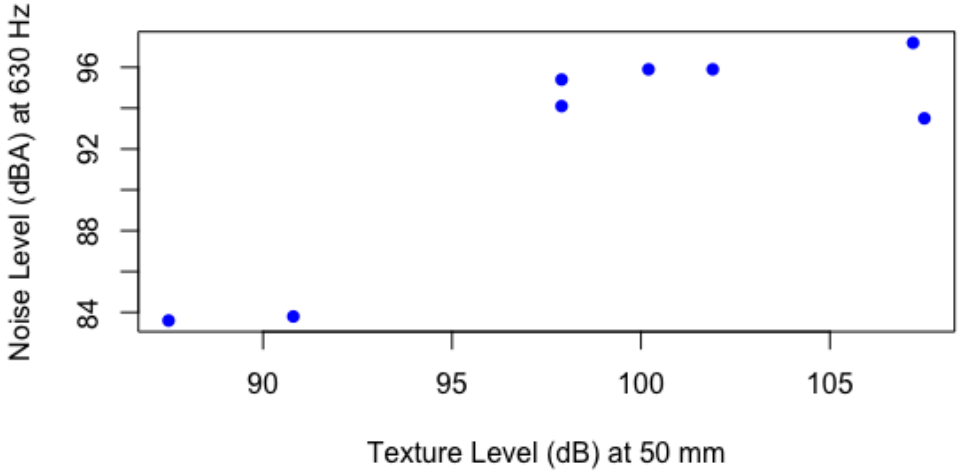

(c) Low Frequency Noise Level vs. Sample 2 Large Scale Texture Level

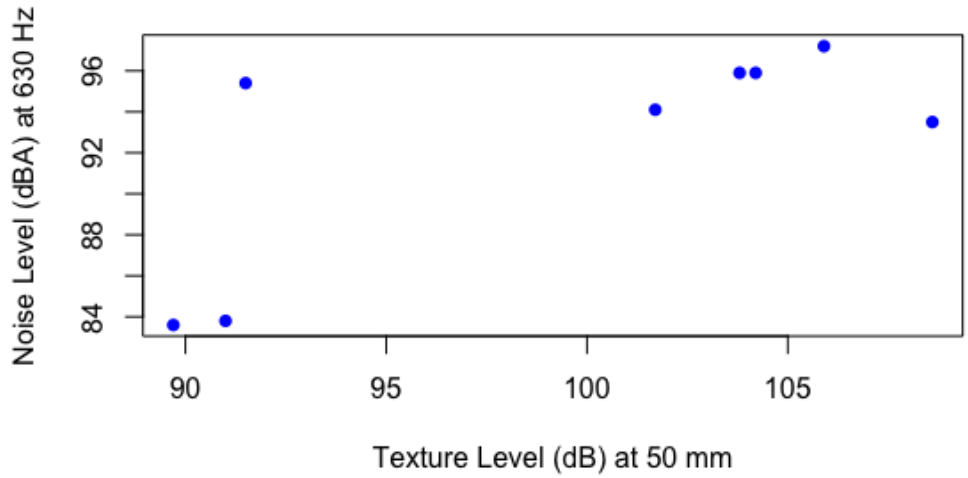

(d) Low Frequency Noise Level vs. Sample 3 Large Scale Texture Level

Figure 6-13: Low Frequency Noise vs. Large Scale Texture, No Grouping

A similar procedure was repeated for high frequency noise at 3150 Hz and texture with 3.2 mm wavelength, without grouping the pavements. The regression results are as shown in Table 6-5. The plots are as shown in Figure 6-14. From both the regression results

and the plots, it can be seen that the ungrouped goodness-of-fit for the negative correlation is not high either.

	Sample 1	Sample 2	Sample 3
Intercept	138.96	126.82	119.46
Coefficient	-0.7059	-0.5662	-0.4687
Adjusted R^2	0.6815	0.5348	0.3222

Table 6-5: Regression Results for High Frequency Noise vs. Small Scale Texture, No Grouping

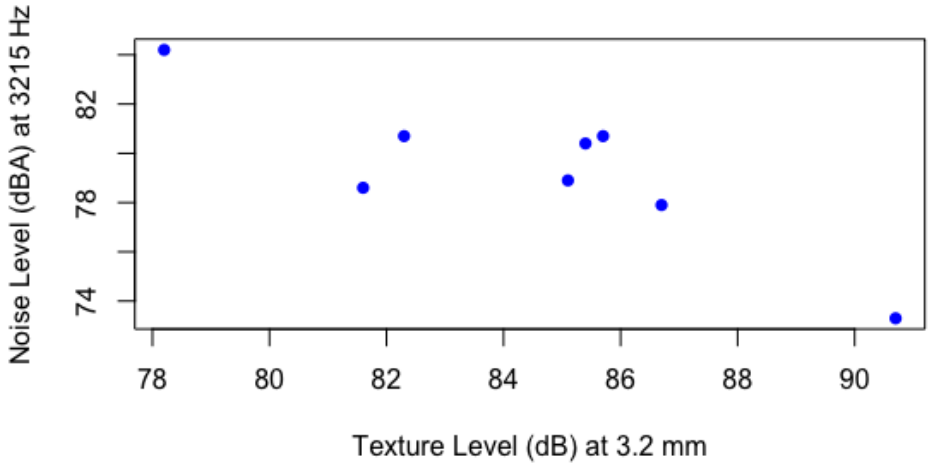

(a) High Frequency Noise Level vs. Sample 1 Small Scale Texture Level

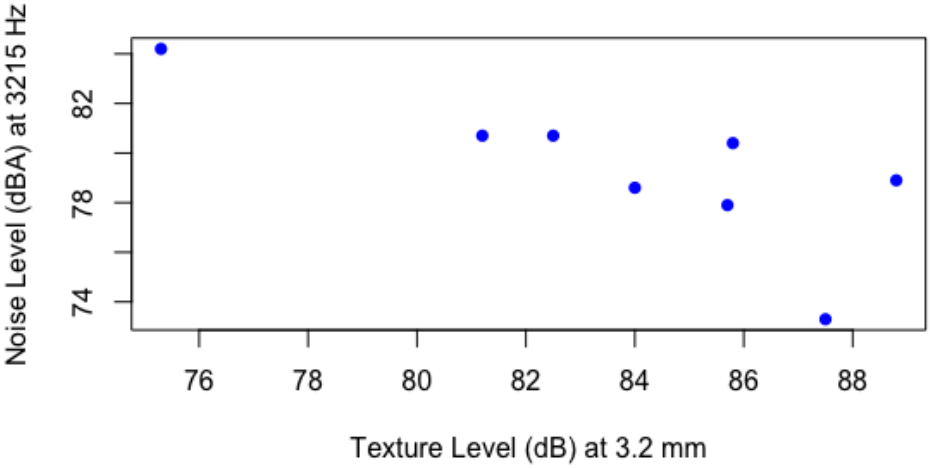

(b) High Frequency Noise Level vs. Sample 2 Small Scale Texture Level

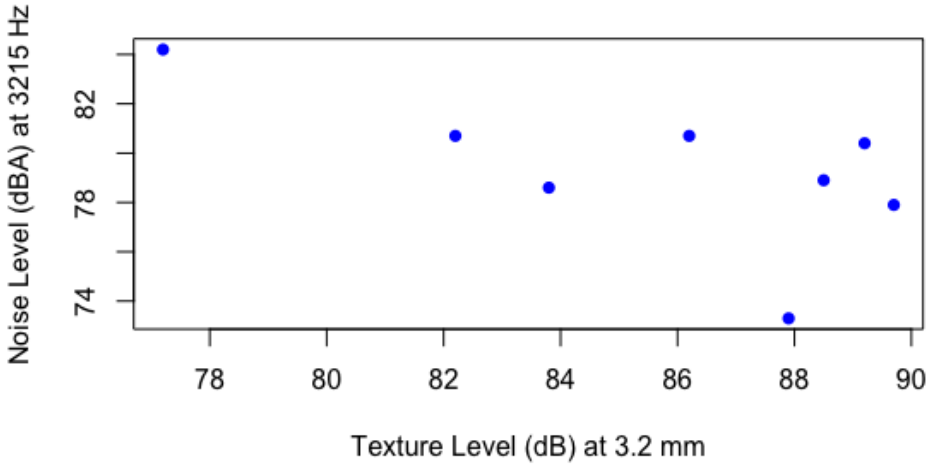

(c) High Frequency Noise Level vs. Sample 3 Small Scale Texture Level

Figure 6-14: High Frequency Noise vs. Small Scale Texture, No Grouping

Linear Regression at Maximal Correlation, with Grouping

As it has been discussed, texture alone is not sufficient to determine the tire/pavement noise. For example, Anfosso-Lédée and Do (2002) noticed that porous pavements tend to behave differently in noise generating patterns. It can be helpful to separate the pavements into different groups. From the plots, the pavements are separated

into three groups: SH 36 (Type C), RM 12 (TOM), and FM 1626 (TOM) as Group 1, SH 195 (PFC), FM 1431 (PFC), IH 20 (seal coat), and US 181 (NovaChip) as Group 2, and US 84 (seal coat) as Group 3.

When the data were grouped, the regression results and plots are as shown in Table 6-6 and Figure 6-15. The three groups are assumed to have the same coefficient but different intercepts. Intercept 1 is for the three pavements in Group 1, represented by the blue dots in Figure 6-16, intercept 2 is for Group 2, represented by the red dots, and intercept 3 is for Group 3, represented by the green dot. When separated into two groups, the model's overall goodness-of-fit improved for all three samples. With the same level of texture, it can be seen that pavements in Group 1 tend to generate the lowest level of noise, with Group 2 being louder than Group 1, and Group 3 even louder.

	Sample 1	Sample 2	Sample 3
Intercept 1	49.83	40.77	34.59
Intercept 2	54.88	46.41	39.34
Intercept 3	57.70	47.93	45.70
Coefficient	0.3956	0.4849	0.5432
Adjusted R_2	0.9382	0.9685	0.9957

Table 6-6: Regression Results for Low Frequency Noise vs. Large Scale Texture, Three Groups

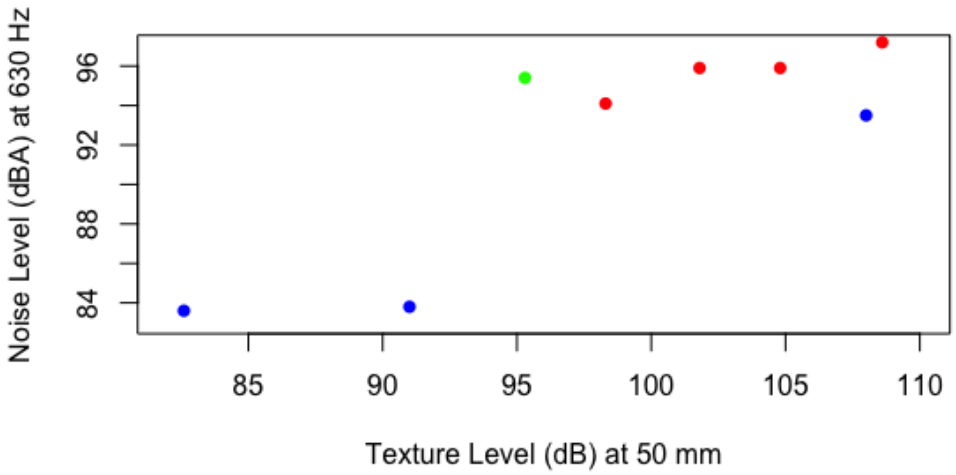

(a) Low Frequency Noise vs. Sample 1 Large Scale Texture

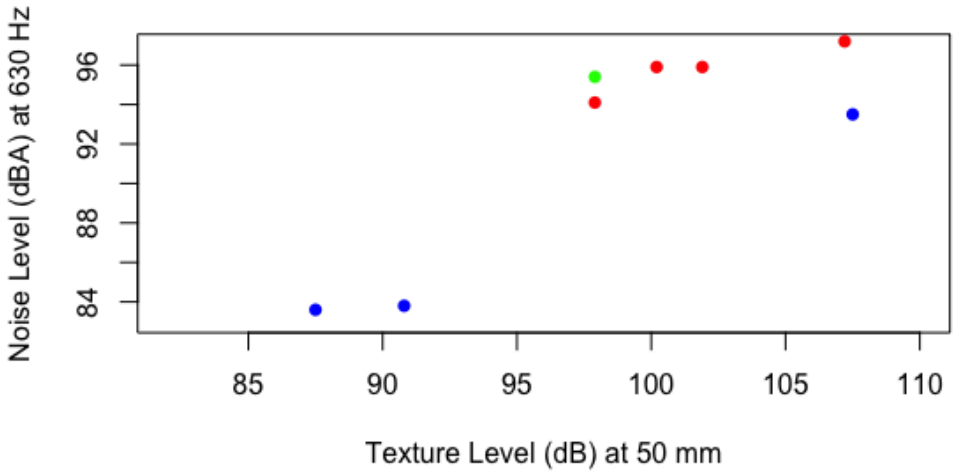

(b) Low Frequency Noise vs. Sample 2 Large Scale Texture

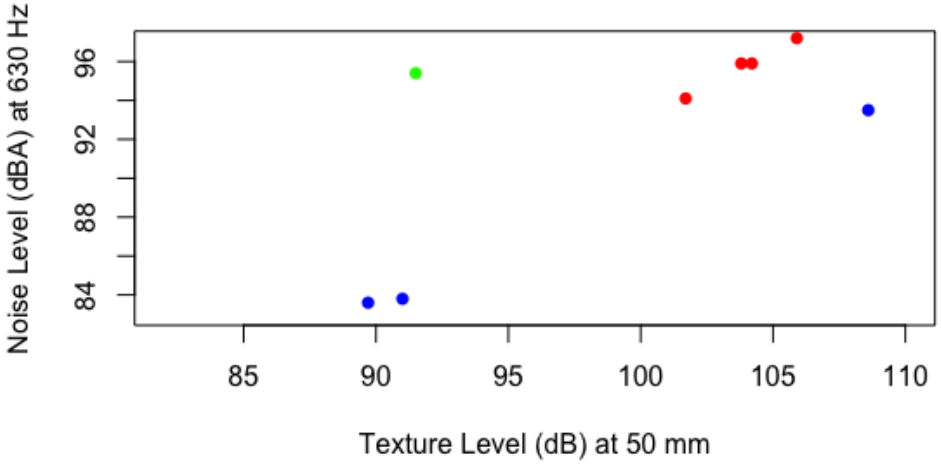

(c) Low Frequency Noise vs. Sample 3 Large Scale Texture

Figure 6-15: Low Frequency Noise vs. Large Scale Texture, with Grouping

Analysis with grouping was the next step for the negative correlation between high-frequency noise and short wavelength texture. Interestingly, US 84, which was showing a different pattern from all the rest of the pavements in the low frequency range, appeared to behave similarly to the pavements in Group 1, and thus it was grouped into Group 1 for this analysis.

	Sample 1	Sample 2	Sample 3
Intercept 1	147.98	140.07	159.14
Intercept 2	150.34	143.09	164.85
Coefficient	-0.8266	-0.7423	-0.9657
Adjusted R_2	0.8187	0.7377	0.8736

Table 6-7: Regression Results for High Frequency Noise vs. Small Scale Texture, Two Groups

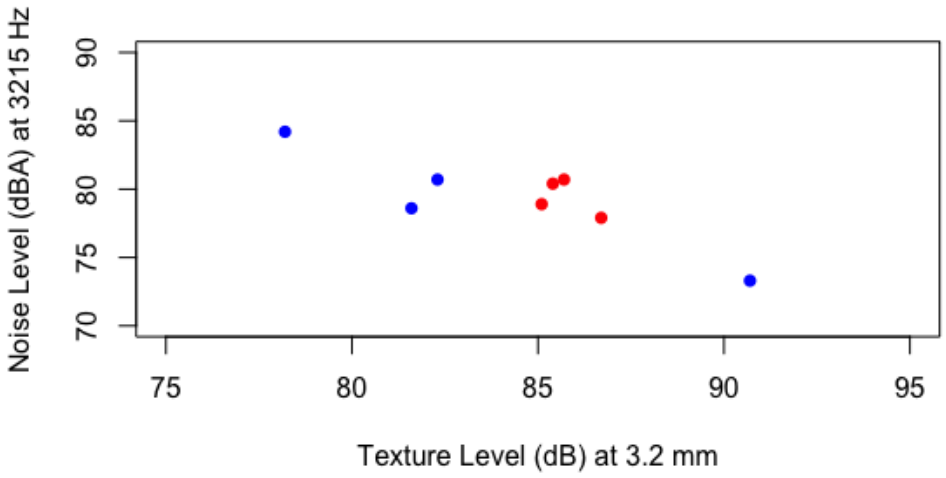

(a) High Frequency Noise vs. Sample 1 Small Scale Texture

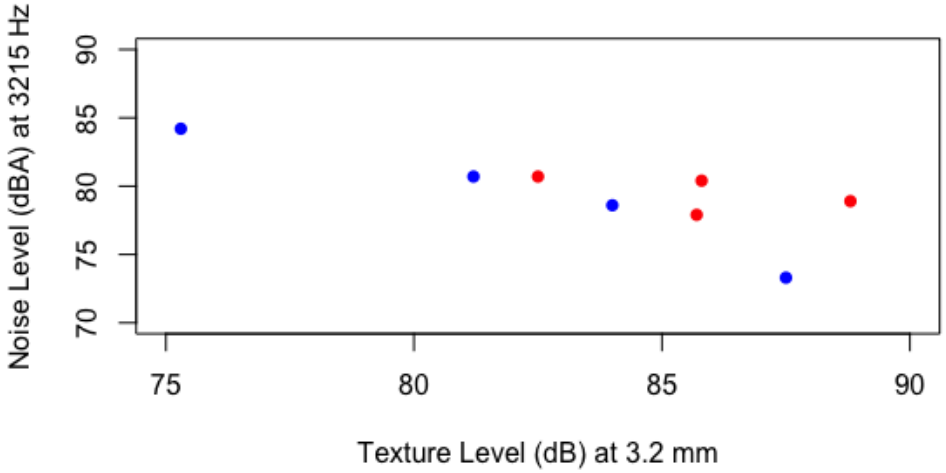

(b) High Frequency Noise vs. Sample 2 Small Scale Texture

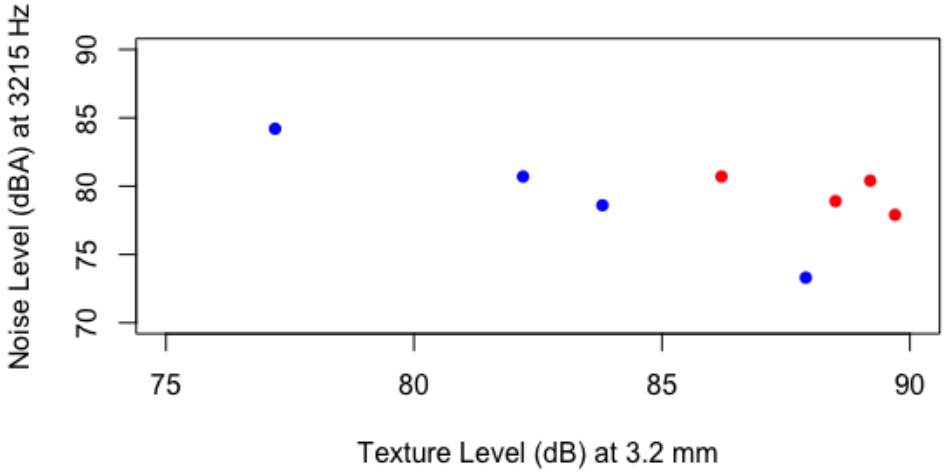

(c) High Frequency Noise vs. Sample 3 Small Scale Texture

Figure 6-16: High Frequency Noise vs. Small Scale Texture, with Grouping

When a linear relationship is to be found between noise and texture level at the critical frequencies and wavelengths, grouping the pavements by their type while enforcing the same slope improved the linear fit in both frequency spectra. This indicated that, with unit increase in texture level, the unit increase/decrease in noise is consistent across all sampled pavements, but at a given texture, different pavements might generate a different level of noise.

Friction-Noise Correlation

As for each measuring device, three friction measurements are made at each section, but only one noise measurement. To ensure a one-to-one correlation between friction and noise, the arithmetic average was taken for each of the testing site's three friction measurements from each testing method (BPN, MicroGrip Tester, and Grip Tester). The single variable linear regression models with BPN, MicroGrip Number (MGN), and Grip Number (GN) each being dependent variable, and noise level as independent variable, are shown in Table 6-8. The friction results from different measuring devices plotted against noise level are as shown in Figure 6-17, with blue dots representing PFC pavement, orange for Type C dense graded, green for thin overlay mix (TOM), grey for NovaChip, and purple for seal coat.

	Coefficient (dBA^{-1})	Intercept	Adjusted R^2
BPN vs. Noise	0.490	-8.558	-0.1445
MGN vs. Noise	-0.02692	3.391	0.04414
GN vs. Noise	-0.009426	1.351	-0.2177

Table 6-8: Regression Result for Friction vs. Noise

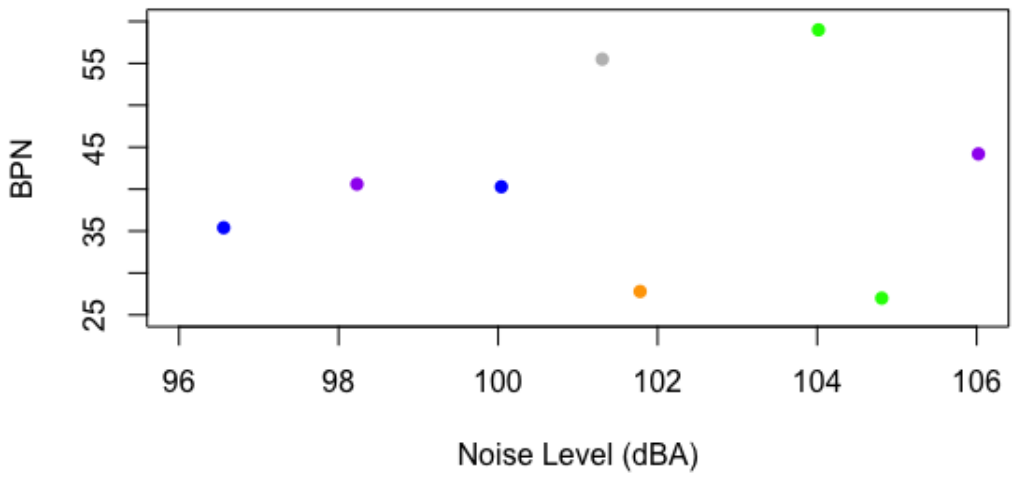

(a) British Pendulum Number vs. Noise Level

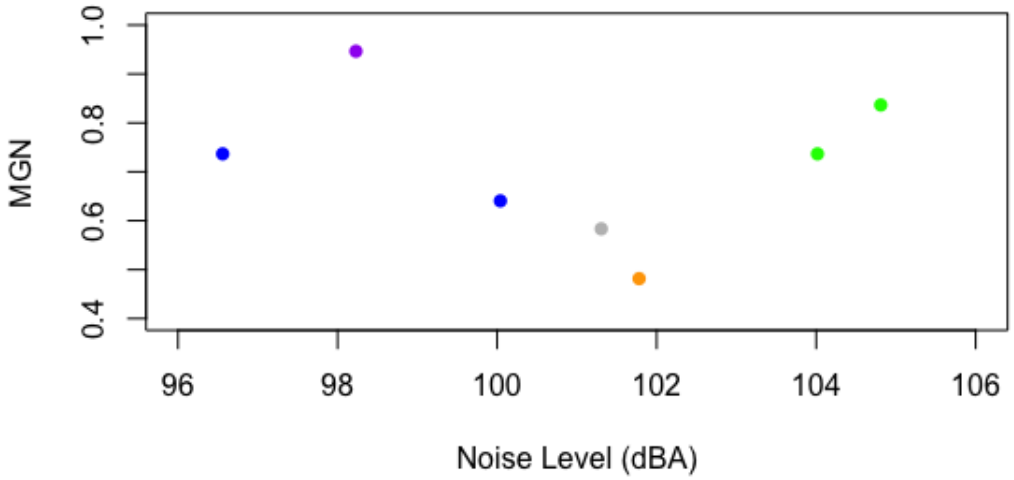

(b) MicroGrip Number vs. Noise Level

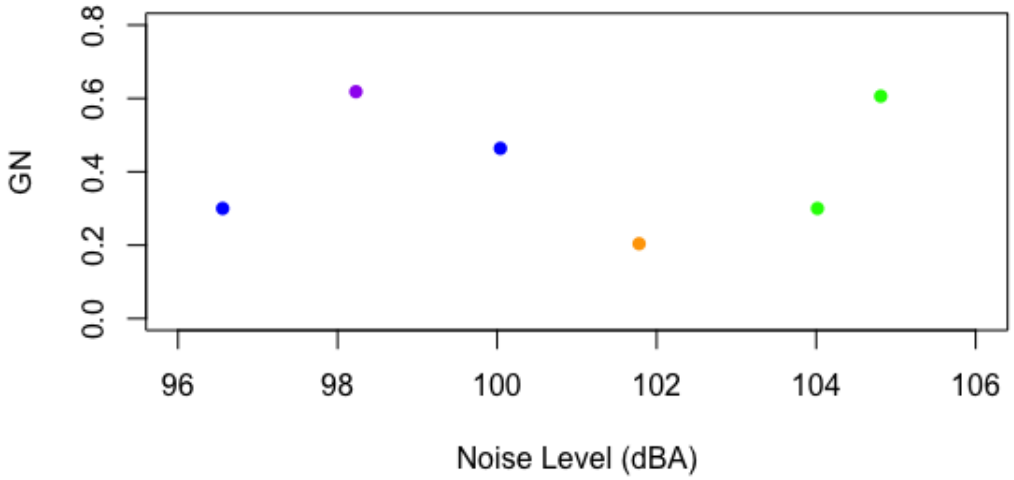

(c) Grip Number vs. Noise Level

Figure 6-17: Friction vs. Noise Plots

Friction-Texture Correlation

The first attempt was done for each friction measurement device along each section, directly correlating the three friction measurements to the three texture measurements. The regression results are as shown in Table 6-9, and plots shown in Figure 6-18.

	Coefficient (mm^{-1})	Intercept	Adjusted R^2

BPN vs. MPD	-6.929	50.803	0.1527
MGN vs. MPD	-0.1556	0.8526	0.209
GN vs. MPD	-0.1572	0.6002	0.3301

Table 6-9: Regression Result for Friction vs. Texture

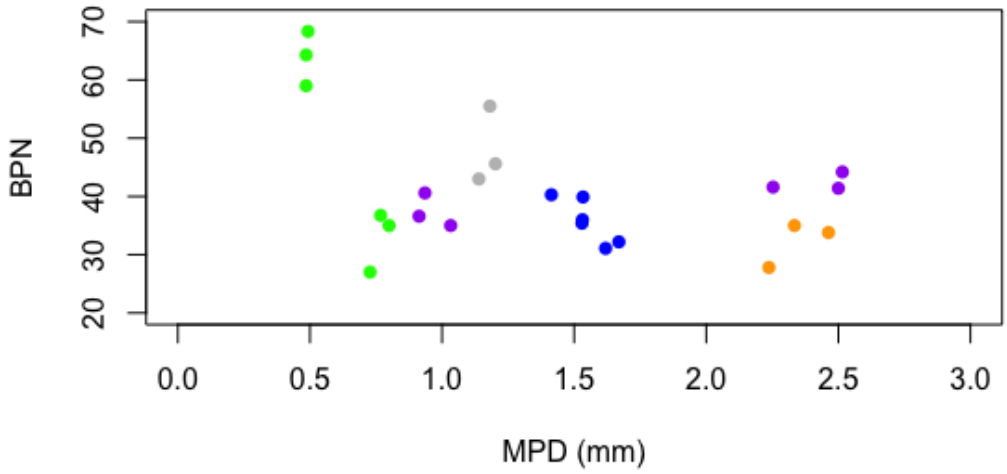

(a) British Pendulum Number vs. Mean Profile Depth

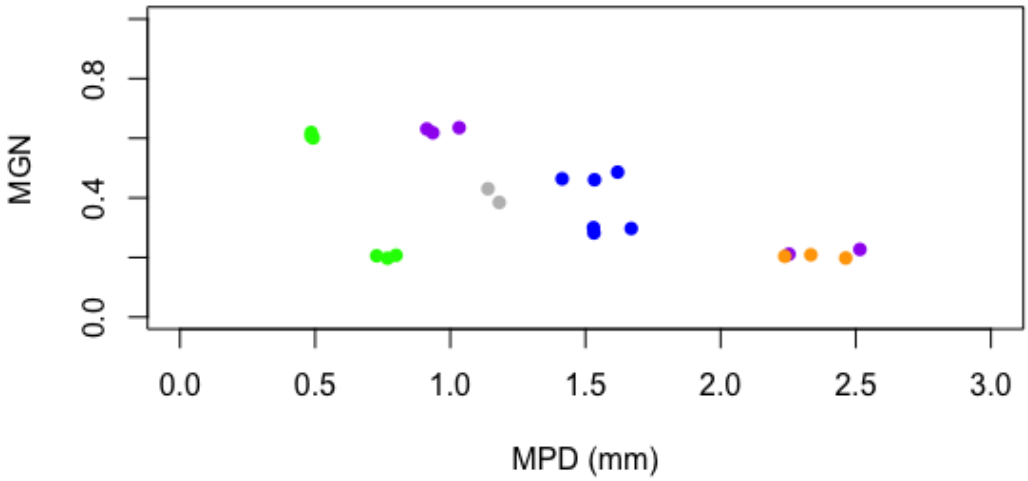

(b) MicroGrip Number vs. Mean Profile Depth

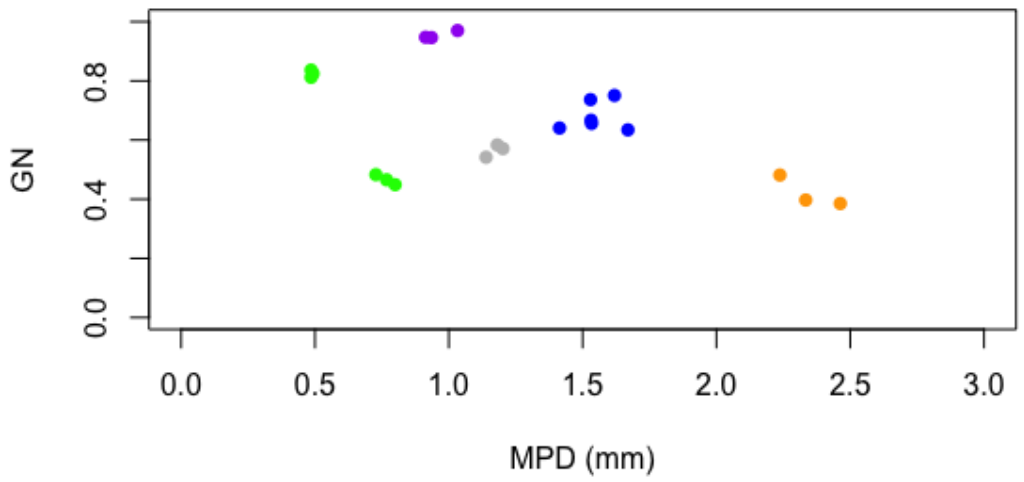

(a) Grip Number vs. Mean Profile Depth

Figure 6-18: Friction vs. Texture Plot

In 1992, Permanent International Association of Road Congress (PIARC) sponsored a study in order to allow conversion among friction measures used worldwide with representatives from 16 countries participating. After conducting measurements at 54 sites across the United States and Europe with 51 different testing systems, including ones measuring friction such as locked-wheel, fixed-slip, ABS, variable-slip, side-force, pendulum, and some prototype devices, and those measuring texture such as the sand patch, laser profilometers, an optical system, and outflow meters, the International Friction Index (IFI) was developed (Hall et al., 2009), consisting of a speed constant and a friction number at 60 km/h. The speed constant, determined by a macrotexture measurement either MPD or MTD, can be calculated as follows:

$$S_P = 14.2 + 89.7\,MPD \qquad 6\text{-}9$$

Or

$$S_P = -11.6 + 113.6\,MTD \qquad 6\text{-}10$$

From GripTester measurements, the coefficient of friction at 60 km/h should be calculated as follows:

$$PSNG = 4.1 \cdot \left(\frac{MTD}{0.0254}\right)^{-0.47} \quad 6\text{-}11$$

$$F_{60} = SN \cdot \exp\left(\frac{-50.6}{S_P}\right) \quad 6\text{-}12$$

While from BPT measurements, the coefficient of friction at 60 km/h can be calculated using this equation:

$$F_{60} = 0.0436 + 0.0095 \cdot BPN \cdot \exp\left(\frac{-50}{S_P}\right) \quad 6\text{-}13$$

	Coefficient (mm^{-1})	Intercept	Adjusted R^2
FN60 (BPN) vs. MPD	-0.02621	0.3260	0.05005
FN60 (MGN) vs. MPD	-0.07519	0.5022	0.1244
FN60 (GN) vs. MPD	-0.08578	0.3565	0.2761

Table 6-10: Regression Result for IFI vs. Texture

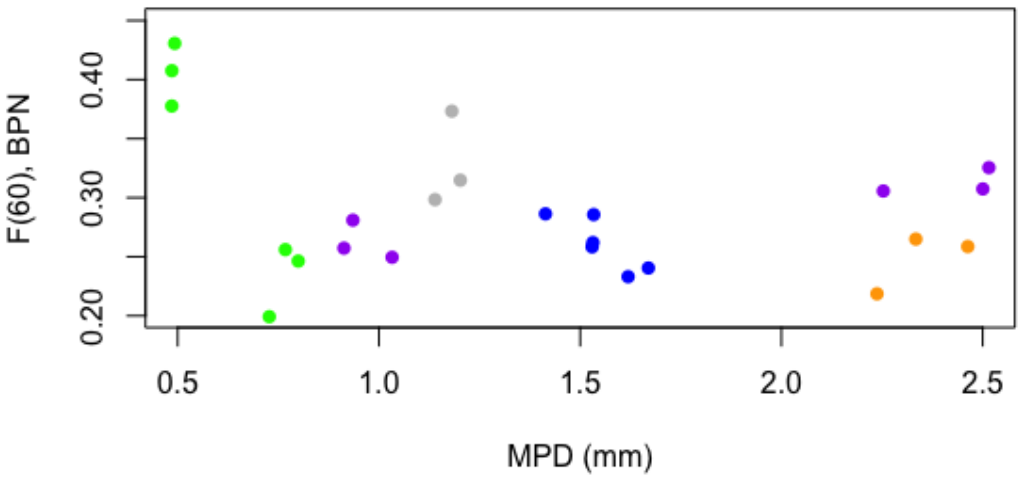

(a) IFI Based on BPN vs. MPD

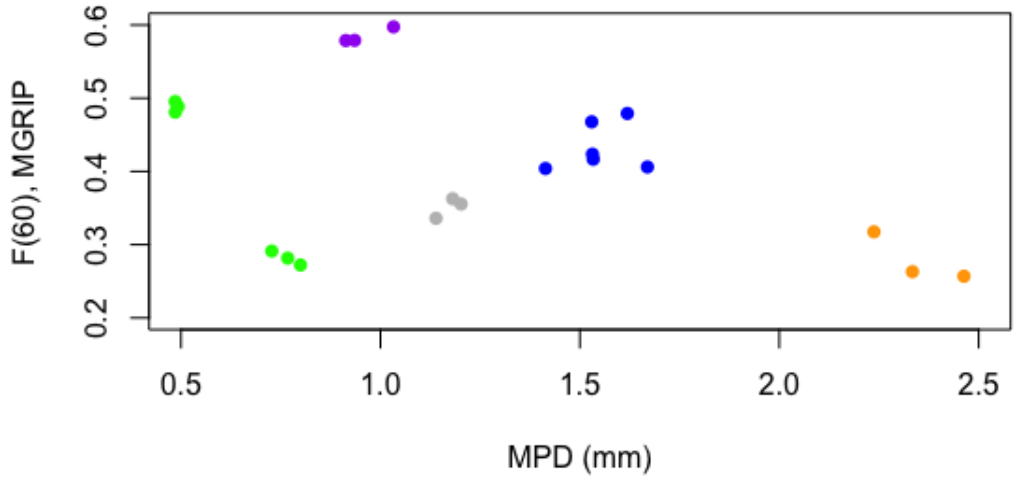

(b) IFI Based on MGN vs. MPD

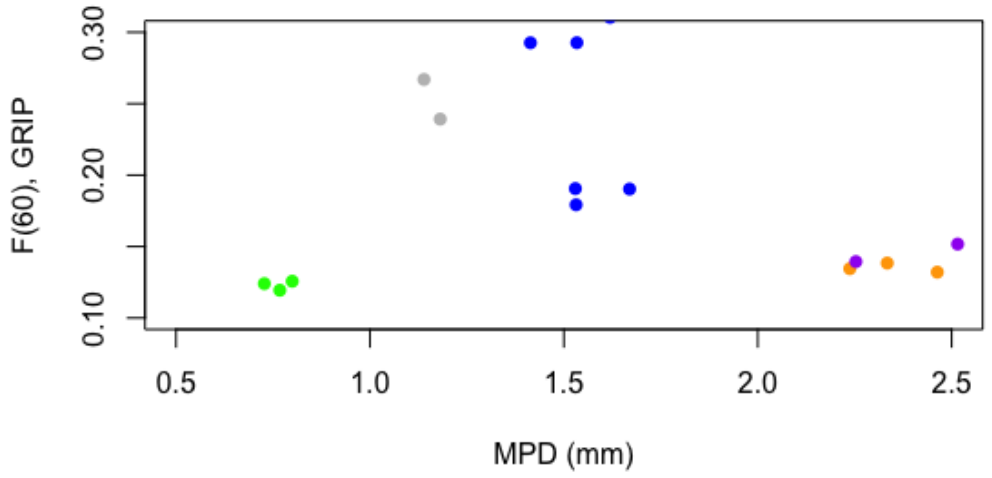

(c) IFI Based on GN vs. MPD

Figure 6-19: IFI vs. Texture Plot

The goodness-of-fit does not improve even when the IFI is used in place of the original measurement outputs, and the coefficient remains negative, which is quite counterintuitive, as it is typically found that a higher level of texture tends to provide better skid resistance. The IFI concept did never became popular in the US and only to a very limited extent in Europe as several studies have found that the proposed relationships do not apply locally.

POTENTIAL IMPROVEMENT IN FRICTION-TEXTURE CORRELATION

One of the reasons for the poor correlation found between friction and texture from the data collected is the inconsistency of measurement location in the data collection process. As friction and texture are measured separately, it is very difficult to ensure that both measurements are taken at exactly the same point. As early as 1978, when Leu and Henry developed a model to characterize skid resistance with microtexture and macrotexture, they suggested a simultaneous measurement of macrotexture and skid number from a single test without interrupting traffic, while acknowledging that obtaining microtexture using non-contacting, high-speed methods was not possible with the technology at that time. In 1983, Arnberg developed the laser road surface tester, addressing the need for developing a reliable, integrated measuring device operating at highway speed, and capable of obtaining data for several characteristics simultaneously, and thus maximizing the efficiency of the roadway surface evaluating process. As technology advances, not only has measuring both macrotexture and skid resistance together become possible, but attempts have been made to incorporate microtexture as well. In 2004, the Florida Department of Transportation (FDOT) conducted a study to

assess the feasibility of collecting data on both surface texture and friction characteristics of pavement sections while operating at highway speed (Jackson et al., 2007).

Device Setup

To enhance the efficiency and safety when collecting data on surface characteristics, researchers at the University of Texas at Austin (UTA) have developed a measuring device, as shown in Figure 6-20. A laser-sensor was incorporated to the GripTester, to ensure the corresponding friction and texture measurements are conducted at the exact same point and under the same environmental conditions.

Figure 6-20: Texture-Friction Measuring Device

As the GripTester is able to measure friction in terms of Grip Number at speeds up to 62 mph, the laser sensor captures the profile of the surface up to a width of 330 mm in the transverse direction, and the texture parameters can be calculated as shown in Table 4-1.

Specification

The GripTester is designed to capture the drag and load force which, in turn, are used to calculate the Grip Number that is averaged and recorded over every meter of travel. The laser scanner was set to collect transverse profiles at a longitudinal interval of approximately 40 mm. Based on the frequency of the laser sensor, it has a transverse resolution of 0.161 mm, indicating that each two consecutive points along a transverse profile have a horizontal distance of 0.161 mm between each other., The laser sensor also measures with a vertical resolution of 5.0 microns, meaning the minimum deviation from the flat surface that it can capture is 5 microns. While an entire transverse profile of 330 mm width consists of 2048 data points, only the 622 points that correspond to the 100-mm wide wheelpath of the GripTester were analyzed to correlate with friction.

Outputs

Data were collected along a total of 19 sections, each being 500 to 1,000 m in length, with different types of pavement surface. Details regarding each of the sections are as shown in Table 6-11. Wherever the sections start with the same letter, they are located along the same road, divided into different sections due to either surface pavement type change or wheelpath change.

Section	Number of GN points	Initial GN	Terminal GN	Mix Type
A1	800	0.34	0.35	Seal Coat (Heavily Distressed)
A2	800	0.37	0.37	Seal Coat (Heavily Distressed)

A3	620	0.32	0.34	Seal Coat (Heavily Distressed)
B1	650	0.73	0.75	Seal Coat
B2	700	0.71	0.86	Seal Coat
B3	500	0.67	0.79	Seal Coat
D1	821	0.4	0.37	Dense Graded Mix
D2	779	0.37	0.35	Dense Graded Mix
E1	584	0.55	0.59	TOM
E2	500	0.51	0.49	PFC
E3	502	0.36	0.42	PFC
E4	600	0.53	0.61	PFC
F1	500	0.6	0.31	PFC
F2	879	0.4	0.47	PFC
F3	963	0.47	0.42	PFC
F4	668	0.4	0.38	PFC
G1	519	0.24	0.32	Dense Graded Mix
G2	581	0.32	0.36	Dense Graded Mix
G3	600	0.4	0.42	Seal Coat

Table 6-11: Section Description for New Data Collection

To ensure consistency in data, since the GripTester also records load, speed, and waterflow along with measured GN, the friction measurements were filtered so that only when the load is between 150 and 300 (N), speed is above the 10% percentile of the speed along the section, and water flow is between 20 and 50 L/min, is the GN measurement considered valid. Figure 6-21: Example GripTester output along a section before and after filtering shows one example section with GN before and after filtering based on the three criteria.

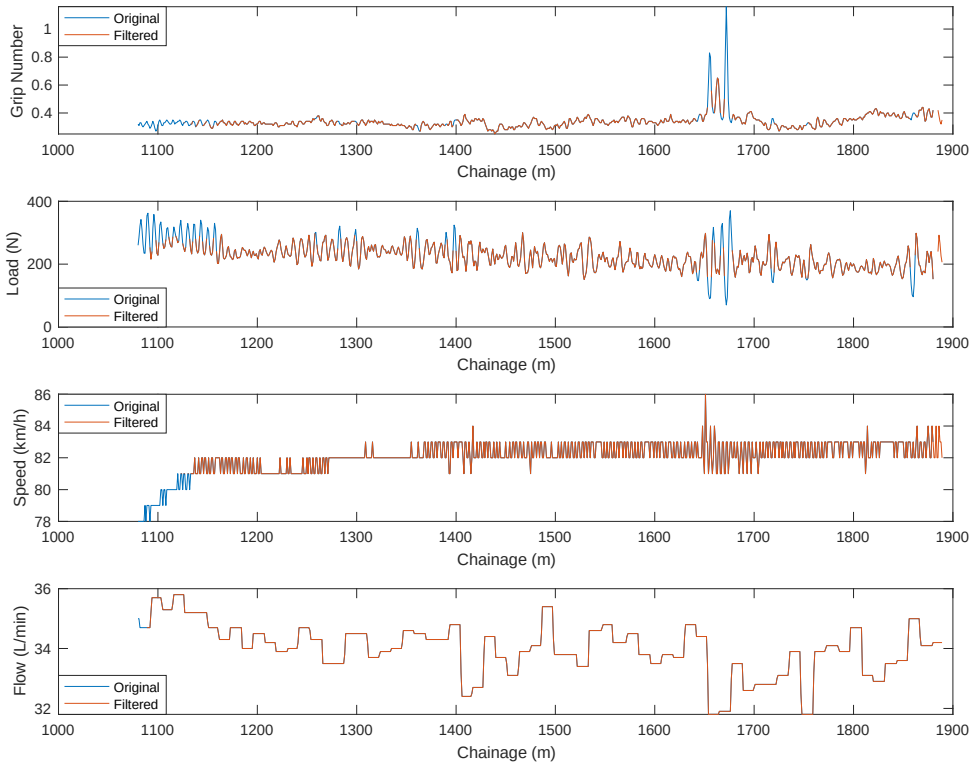

Figure 6-21: Example GripTester output along a section before and after filtering

The profile data is first run through a filter that replaces points with null measurements where a zero change in elevation is found both from its previous to itself,

and from itself to the next. It is then filtered based on a peak detection algorithm that defines a peak by a starting change in elevation, average slope, and ending change in elevation. Since two consecutive points along a transverse profile are 0.161 mm apart, and the 90th percentile of change in elevation is 0.21 mm, if a set of points starts and ends with a change in elevation of no less than 0.21 mm in opposite direction, with the total horizontal distance between the starting and ending points no more than 1.0 mm (or six data points) apart, and an average absolute slope across both directions no less than 0.21 mm/0.161 mm = 1.304, then it is considered a peak. From the point before the beginning change in elevation all the way up to the point after the ending change in elevation are replaced with null. The full peak-detection algorithm can be found in the code in the Appendix. Figure 6-22 shows an example profile before and after the points identified as flat section and peaks being removed.

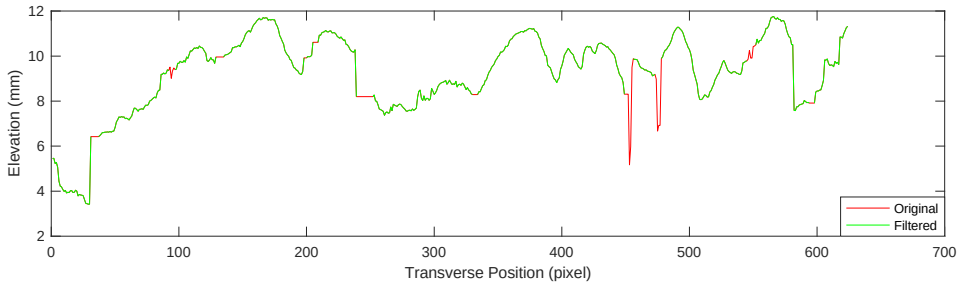

Figure 6-22: Example of a Transverse Profile before and after Filtering

The profiles with flat lines and peaks filtered out are then selected based on number of points removed. If more than 62 points are removed from a profile, consisting of over 10% of its total points, then the entire profile is considered invalid and removed from the dataset. Out of a total of 314,169 profiles, 119,002 were removed based on this criterion.

Correlating Jointly Collected Friction and Texture Data

Using the profile data collected with the laser scanner and processed with the aforementioned steps, texture parameters were calculated to correlate with friction. These include MPD, second, third, and fourth moments, RMS, skewness, and kurtosis. All moments calculated are central, indicating that the mean is removed. These statistics are calculated for each profile, and then averaged to correlate one-to-one with friction.

When friction and texture data were matched, there were 25 texture profiles corresponding to one friction measurement. However, due to profile removal, the number of profiles each GN corresponds to are no longer equal. A weight is then assigned to every entry to account for this difference, which is proportional to the number of profiles whose statistics are averaged to correspond to one GN. Using these weights, the correlation across all the calculated parameters are shown in **Error! Reference source not found.**.

	MPD (mm)	Second Moment	Third Moment	Fourth Moment	RMS	Skewness	Kurtosis
MPD (mm)	1.00						
Second Moment	0.86	1.00					
Third Moment	-0.13	-0.43	1.00				
Fourth Moment	0.05	0.09	-0.66	1.00			
RMS	0.91	0.98	-0.38	0.08	1.00		
Skewness	0.30	0.07	0.680	-0.60	0.12	1.00	
Kurtosis	-0.02	-0.01	-0.49	0.79	-0.01	-0.74	1.00

Table 6-12: Correlation Matrix across Texture Parameters Calculated

It can be seen that there was a strong correlation between MPD and second moment, as well as between third and fourth moments. There was also some level of correlation between second and third moments. The correlation between MPD and third moment, as well as that between second and fourth moments, however, was not too high. Because least square linear regression assumes independence across the predictors, it is advisable not to keep highly correlated variables in the same model.

Another factor to consider is speed. Although it is desirable to measure friction at constant speed, variations are inevitable due to geometry and other traffic in the roadway. As a result, capturing the effect from the varying speed on measured friction might also provide some insight. As shown in **Error! Reference source not found.**, there is a clear trend that as speed increases, the measured GN decreases. Also, when the pavement types are analyzed separately, from data points identified with seal coat and dense graded mix, the two mix types with a wider range of speed distribution, this decreasing trend was found to become less steep as speed increases. A better linear relationship may be obtained through a non-linear transformation such as taking a natural log of speed and plotting grip number against it.

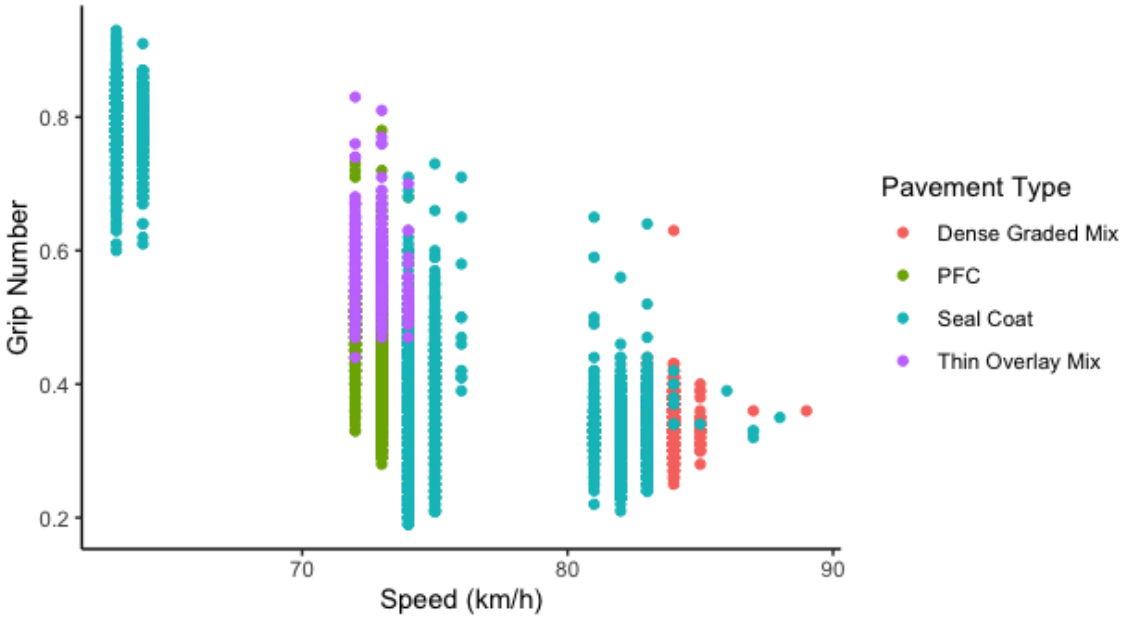

Figure 6-23: Grip Number Plotted against Speed

Pavement surface characteristics should also be accounted for as the relationship may be different for different mixture types. As the 19 sections have five distinct surface mixes, accounting for the effects from the type of pavement surface can potentially provide better predicting power for friction compared to a model based on texture and speed alone. Furthermore, to ensure that no single surface type becomes over- or under-represented when fitting the model due to its sample size, each entry was weighted by the inverse of the total GN points within its mix type category. This weight is then multiplied to the weight based on profile number to produce the final weight as input for the regression model.

Out of all the texture parameters calculated, RMS appears to correlate best with friction. **Error! Reference source not found.** shows the model output. It can be seen that friction correlates negatively with speed. The most statistically significant variable is the natural log of speed, with a slope of -1.795. Since the tests were all conducted at highway

speed, this conclusion cannot be extended into speeds lower than 63 km/h, which is the minimum speed captured in the dataset. For instance, when speed increases from 70 km/h to 80 km/h, natural log of speed increases by 0.1335, and an expected decrease in GN is estimated to be 0.24. While when speed increases from 80 km/h to 90 km/h, its natural log increases by 0.1178. With the same 10-km/h increase in speed, GN is expected to decrease by only 0.21 compared to 0.24. RMS, which varies between 0.225 and 3.350 in the data, has a positive coefficient of 0.0564, indicating that friction correlates positively with this texture parameter, with effect up to 0.176 in GN. Compared to the base case of dense graded mix, with everything else held constant, PFC and seal coat tend to generate lower friction, while TOM higher.

	Coefficient	Std. Err.	P-Value
Constant	8.2647	0.03960	0.0000
log(Speed (km/h))	-1.7945	0.00893	0.0000
RMS	0.0564	0.00329	0.0000
PFC	-0.2088	0.00352	0.0000
Seal Coat	-0.1079	0.00231	0.0000
TOM	-0.0248	0.00191	0.0000
Number of Observations	10,617		
Residual Standard Error	0.004677		
Adjusted R_2	0.8683		

Table 6-13: Model Output without Accounting for Presence of Distress

As noted in Table 6-11: Section Description for New Data Collection, there are three sections, totaling in 2220 GN points where the pavement with seal coat surface is

heavily distressed. If presence of distress is added as another indicator variable, the model outputs are as shown in **Error! Reference source not found.**. With the presence of distress, the GN measured experiences a statistically significant increase. The difference between PFC and Seal Coat is not as significant after taking into account the presence of distress.

	Coefficient	Std. Err.	P-Value
Constant	11.9912	0.0604	0.0000
log(Speed (km/h))	-2.6386	0.0138	0.0000
RMS	0.0770	0.0027	0.0000
PFC or Seal Coat	-0.3351	0.0037	0.0000
TOM	-0.1411	0.0022	0.0000
Distress	0.2325	0.0031	0.0000
Number of Observations	10,617		
Residual Standard Error	0.004078		
Adjusted R_2	0.8998		

Table 6-14: Model Output Accounting for Presence of Distress

However, since seal coat is the only mix type that has both distressed and non-distressed sections to compare, this finding does not realistically reflect what happens to friction when a pavement section experiences distresses, and no conclusion can be generalized to other types of mixes experiencing other distress situations. It is, though, an indication that friction varies with not only pavement type, but condition as well, which can potentially change over time as different distresses develop.

Chapter 5: Conclusion

From the 1/3 octave band to 1/3 octave band linear regression between noise and texture, it was found that noise correlates the strongest with texture with wavelengths 2.5 to 31.5 mm, which include texture wavelengths within the first decade of macrotexture. The correlation appears to be positive, indicating that pavements with a higher level of texture tends to generate more noise.

With the correlation mapping approach, across all different types of pavements sampled, thin overlay mix (TOM) has not only relatively lowered texture, but also generates less noise given the same texture level. The two permeable friction course (PFC) pavements sampled in this study, however, though found by many previous works to be quieter compared to other pavement types, do not produce less noise in either low or high frequency spectrum. Moreover, given the same texture level of short and long wavelength, the two PFC pavements tend to generate more noise at both high and low frequency spectra, respectively. It seems that the noise of PFC surfaces is more friendly to the road user but it contains a lot of energy.

One of the seal coat surface pavement sections, which was located on US 84, behaves differently at the two frequency ranges. With the same level of long wavelength texture, it produces the highest level of low frequency noise, significantly higher than the two other groups. When considering noise in the high frequency spectrum, however, its noise-texture correlation belongs to the quieter group, given the same level of short-wavelength texture. This further confirms the idea that tire/pavement noise is a superposition of noise generated by different mechanisms, independent of each other.

The correlation between noise and friction has not been found to be significant, which is consistent with what many previous researchers have claimed, and is a further

indication that constructing a pavement that generates a low level of noise while providing sufficient skid resistance is viable, and a compromise does not necessarily have to be made between the two. However, this also means that using noise measurement as an alternative to friction measurement might not yield the results we were expecting.

The correlation between friction and texture also varies both across different pavement types and within pavement types. Between the two PFC pavements, the MPD does not differ much, but large differences were found in friction measurement from the GripTester. The two seal coat pavements have similar level of texture overall, while IH 20 does not have sufficient measurement in friction, it performs slightly better in providing friction as measured by the BPT than US 84, which has very high friction levels measured by both the Micro-GripTester and the GripTester. The two TOM pavements differ much in texture level, Grip Number, and BPN.

Overall, TOM pavements tend to generate the lowest level of noise, while providing moderate to high level of friction. If this pattern is to be consistently found in future studies, this type can be a competitive choice for pavement selection. However, TOM mixtures are relatively new and their long-term performance still needs to be assessed. PFC provides a good level of friction in general as well, while being slightly louder compared to TOM. Neither PFC nor TOM have much texture, but their ability to provide skid resistance is satisfactory even with a lower texture, compared to dense graded mixes. NovaChip and fine seal coats also have the characteristic of providing good friction with low texture level, though they are relatively loud compared to the two previous types. Moreover, since only one of each type was sampled, it is not easy to draw a conclusion simply based on the current data. Type C dense graded pavements seem to generate less noise given the texture level, but their texture does not provide as much friction as the other types of pavement do.

Some findings of this study have been consistent with what previous researchers have proposed or discovered, for example, the positive correlation between low frequency noise and long wavelength texture and the negative correlation between high frequency noise and short wavelength texture. But there are findings that contradict previous research conclusions, such as PFC pavements being relatively loud. These disagreements can be due to other pavement factors not accounted for, such as age, stiffness, surface thickness, etc. Keeping track of at least the year each pavement was constructed might be a sensible approach for further analysis, as many pavement characteristics are time dependent.

The poor correlation between friction and texture is partially due to the fact that the measurement locations where the two pavement characteristics were tested were not exactly matched. By utilizing the new equipment developed at the University of Texas at Austin, a higher level of accuracy and precision in aligning of texture and friction measurements resulted in a much higher correlation. The second moment was found to be the texture parameter that correlate the best among the ones calculated, with a 0.01 increase in GN for every unit increase in second moment. Speed was also found to play an important role. Within the highway speed range, GN decreases by 0.2 with every 10 km/h increase in speed. While this is higher than findings from previous studies, the range of speeds in this study was limited so this gradient should be taken with caution.

Regarding surface mix type, with everything else held constant, TOM was found to provide the highest friction, followed by dense graded mix, then seal coat, and lastly PFC. The presence of different levels of distress may also be a factor to consider while estimating friction. With an adjusted R_2 over 80%, the analysis showed that much variability in friction can be explained by speed, texture, and pavement type, and reveals the potential of collecting texture profile at highway speed to achieve full coverage of network-level friction.

Appendix (or Appendices)

```
function outPut = peaklength(v, width)
outPut = v;
length = size(v,1);
gap = diff(v,1,2);
thres = 0.21;
changePrev = [zeros(length,1),gap];
changeNext = [gap,zeros(length,1)];
noChange = (changePrev == 0 & changeNext == 0);
%if there are at least two locations where the change in elevation
between
%two consecutive points are greater than the defined threshold;
[jumpsAndDropsRow, jumpsAndDropsCol] = find(changePrev >= thres |
changePrev <= -thres);
[jumpsAndDropsRow I] = sort(jumpsAndDropsRow);
jumpsAndDropsCol = jumpsAndDropsCol(I);
numOfChanges = size(jumpsAndDropsRow,1);
i = 1;
j = 1;
rm = zeros(size(v,1),size(v,2));
while i + j < numOfChanges
    if jumpsAndDropsRow(i) == jumpsAndDropsRow(i+j) &&
changePrev(jumpsAndDropsRow(i),jumpsAndDropsCol(i)) *
changePrev(jumpsAndDropsRow(i+j),jumpsAndDropsCol(i+j)) < 0 &&
jumpsAndDropsCol(i+j) - jumpsAndDropsCol(i) <= width &&
sum(abs(changePrev(jumpsAndDropsRow(i),jumpsAndDropsCol(i):jumpsAndDrop
sCol(i+j)))) >= thres * (jumpsAndDropsCol(i+j) - jumpsAndDropsCol(i)) *
2
        rm(jumpsAndDropsRow(i),jumpsAndDropsCol(i)-
1:min(jumpsAndDropsCol(i+j)+1,622)) = 1;
        j = j + 1;
    end
    i = i + 1;
    j = 1;
end
outPut(rm == 1) = NaN;
outPut(outPut == -97.4) = NaN;
outPut(noChange) = NaN;

prevPoint = [zeros(length,1),outPut(:,1:end-1)];
nextPoint = [outPut(:,2:end),zeros(length,1)];
prevNan = isnan(prevPoint);
nextNan = isnan(nextPoint);
outPut(prevNan == 1 & abs(changeNext) > 1) = NaN;
outPut(nextNan == 1 & abs(changePrev) > 1) = NaN;

      end
```

References

Abbott, P. G. S., & Phillips, M. (1996, September). Vehicle noise levels derived from the statistical pass-by method and road surface texture. In *NOISE CON* (pp. 217-222).

Ahammed, Mohammad & Tighe, Susan. (2010). Pavement surface friction and noise: Integration into the pavement management system. Canadian Journal of Civil Engineering. 37. 1331-1340. 10.1139/L10-076.

American Association of State Highway and Transportation Officials (AASHTO). (2008). AASHTO Guide for Pavement Friction, first ed., Washington DC.

American Association of State Highway and Transportation Officials (AASHTO). (2015). Standard method of test for measurement of tire/pavement noise using the on-board sound intensity (OBSI) Method, first ed., Washington DC.

American Association of State Highway and Transportation Officials (AASHTO). (2015). Standard method of test for determining the influence of road surfaces on traffic noise using the continuous flow traffic time-integrated method (CTIM), first ed., Washington DC.

Anfosso-Lédée, F., & Do, M. T. (2002). Geometric descriptors of road surface texture in relation to tire-road noise. *Transportation research record*, *1806*(1), 160-167.

Arnberg, P. W. (1983). *Laser road surface tester: A system for simultaneous measurement of rut depth, roughness, macrotexture and friction*. Statens väg-och trafikinstitut.

ASME B46.1 (2009). Surface Texture (Surface Roughness, Waviness, and Lay) (ASME).

ASTM E1845 (2009). Standard Practice for Calculating Pavement Macrotexture Mean Profile Depth. American Society for Testing and Materials (ASTM).

ASTM E1911 (2009). Standard Test Method for Measuring Paved Surface Frictional Properties Using the Dynamic Friction Tester. American Society for Testing and Materials (ASTM).

ASTM E1960 (2015). Standard Practice for Calculating International Friction Index of a Pavement Surface. American Society for Testing and Materials (ASTM).

ASTM E2157 (2015). Standard Test Method for Measuring Pavement Macrotexture Properties Using the Circular Track Meter. American Society for Testing and Materials (ASTM).

ASTM E2380 (2015). Standard Test Method for Measuring Pavement Texture Drainage Using an Outflow Meter. American Society for Testing and Materials (ASTM).

ASTM E303 (1998). Standard Test Method for Measuring Surface Frictional Properties Using the British Pendulum Tester. American Society for Testing and Materials (ASTM).

ASTM E867 (2012). Standard Terminology Relating to Vehicle-Pavement Systems. American Society for Testing and Materials (ASTM).

Baran, R. G., & Henry, J. J. (1983). *Tire noise and its relation to pavement friction* (No. HS-037 873).

Berglund, B., Lindvall, T., & Schwela, D. H. (2000). New WHO guidelines for community noise. noise & vibration worldwide, 31(4), 24-29.

Bernhard, R, Wayson, R.L. (2005). An introduction to tire/pavement noise of asphalt pavement. Institute of Safe, Quiet and Durable Highways, Purdue University.

Blackburn, R. et al., 1978. Effectiveness of Alternative Skid Reduction Measures. Reports No. FHWA-RD-79-22, 23, 24, 25. Federal Highway Administration, Washington, DC.

Braun, M. E., Walsh, S. J., Horner, J. L., & Chuter, R. (2013). Noise source characteristics in the ISO 362 vehicle pass-by noise test: Literature review. *Applied Acoustics*, *74*(11), 1241-1265.

Burchett, J.L., and Rizenbergs, R.L. (1982). Frictional Performance of Pavements and Estimates of Accident Probability. Pavement Surface Characteristics and Materials. ASTM Special Technical Publication 763. C.M Hayden, Ed., American Society of Testing and Materials, Philadelphia, 73-97.

Chandler, J. W. E., Phillips, S. M., Roe, P. G., & Viner, H. E. (2003). Quieter concrete roads: construction, texture, skid resistance and noise. TRL report, 576.

Chen, D. (2020). Evaluating asphalt pavement surface texture using 3D digital imaging. *International Journal of Pavement Engineering*, *21*(4), 416-427.

De Fortrier Smit, A. (2008). *Synthesis of NCAT Low-Noise HMA studies.*. Auburn: National Center for Asphalt Technology, pp.NCAT Report 08-01.

Descornet, G. (1989). A criterion for optimizing surface characteristics. *Transportation Research Record*, (1215).

Do, M. T., & Cerezo, V. (2015). Road surface texture and skid resistance. *Surface Topography: Metrology and Properties*, *3*(4), 043001.

Domenichini, L., Fracassa, A., Torre, F.L., Loprencipe, G., Ranzo, A., & Scalamandrè, A. (1999). Relationship between road surface characteristics and noise emission.

Ejsmont, J. A., Ronowski, G., Świeczko-Żurek, B., & Sommer, S. (2017). Road texture influence on tyre rolling resistance. *Road Materials and Pavement Design*, *18*(1), 181-198.

Elsenaar, P. M. W., Reichert, J., & Sautery, R. (1977). Pavement characteristics and skid resistance. *Transportation research record*, *622*, 1-25.

European Environment Agency. (2019). Exposure of Europe's population to environmental noise

Flintsch, G. W., De León, E., McGhee, K. K., & AI-Qadi, I. L. (2003). Pavement surface macrotexture measurement and applications. *Transportation Research Record*, *1860*(1), 168-177.

Flintsch, G.W., McGhee K.K., Izeppi, K.L., and Najafi, S. (2012). The Little Book of Tire Pavement Friction.

Federal Highway Administration, "Surface Texture for Asphalt and Concrete Pavements" Technical Advisory 5040.36, Federal Highway Administration, Washington, DC, 2005

Fwa, T. F., Choo, Y. S., & Liu, Y. (2003). Effect of aggregate spacing on skid resistance of asphalt pavement. *Journal of Transportation Engineering*, *129*(4), 420-426.

Giles, C., Sabey, B., & Cardew, K. H. (1962, January). Development and performance of the portable skid-resistance tester. In *Symposium on Skid Resistance*. ASTM International.

Haider, M., Descornet, G., Sandberg, U., & Pratico, F. G. (2007, September). Road traffic noise emission: recent developments and future prospects. In Proc. 4th Int. SIIV Congress.

Hall, J.W., K.L. Smith, J.C. Wambold, T.J. Yager and Z. Rado (2009). Guide for Pavement Friction. NCHRP Web-Only Document 108. National Cooperative Highway Research Program, Washington, D.C.

Harland, D. G. (1974). Rolling noise and vehicle noise (No. 652 Lab Rpt.).

Hayes, G. G., Ivey, D. L., & Gallaway, B. M. (1983). Hydroplaning, hydrodynamic drag, and vehicle stability. In *Frictional Interaction of Tire and Pavement*. ASTM International.

Heckl, M. (1986). Tyre noise generation. Wear, 113(1), 157-170.

Henry, J.J. (2000). Evaluation of Pavement Friction Characteristics. NCHRP Synthesis 291. National Cooperative Highway Research Program, Washington, D.C.

Hoerner, T., Smith, K., United States, & Applied Pavement Technology, I. (2002). High performance concrete pavement: pavement texturing and tire-pavement noise. Retrieved from http://hdl.handle.net/2027/uc1.31822036169753

Horne, W. B., & Buhlmann, F. (1983). A method for rating the skid resistance and micro/macrotexture characteristics of wet pavements. In *Frictional Interaction of Tire and Pavement*. ASTM International.

Hu, L., Yun, D., Liu, Z., Du, S., Zhang, Z., & Bao, Y. (2016). Effect of three-dimensional macrotexture characteristics on dynamic frictional coefficient of asphalt pavement surface. *Construction and Building Materials*, *126*, 720-729.

ISO 11819-1 (1997). Acoustics – Method for Measuring the Influence of Road Surfaces on Traffic Noise – Part 1: Statistical Pass-By Method. International Organisation for Standardisation (ISO), Geneve, Switzerland

ISO 11819-2 (1997). Acoustics – Method for Measuring the Influence of Road Surfaces on Traffic Noise – Part 2: Close Proximity Method. International Organisation for Standardisation (ISO), Geneve, Switzerland.

ISO 13473-4 (2008). Characterization of pavement texture by use of surface profiles – Part 4: Spectral analysis of surface profiles. International Organisation for Standardisation (ISO), Geneve, Switzerland.

Jackson, N. M., Choubane, B., Holzschuher III, C. R., & Gokhale, S. (2007). Measuring Pavement Friction Characteristics at Variable Speeds for Added Safety. In *Symposium on Pavement Surface Condition/Performance Assessment: Reliability and Relevancy of Procedures and TechnologiesAmerican Society for Testing and Materials*.

Kandhal, P. S. (2004). Asphalt pavements mitigate tire/pavement noise. *Hot Mix Asphalt Technology*, *9*(2), 22-31.

Kogbara, R. B., Masad, E. A., Kassem, E., Scarpas, A. T., & Anupam, K. (2016). A state-of-the-art review of parameters influencing measurement and modeling of skid resistance of asphalt pavements. *Construction and Building Materials*, *114*, 602-617.

Kogbara, R. B., Masad, E. A., Woodward, D., & Millar, P. (2018). Relating surface texture parameters from close range photogrammetry to Grip-Tester pavement friction measurements. *Construction and Building Materials*, *166*, 227-240.

Kouchaki, S., Roshani, **H., Hernandez, J.B.**, Prozzi, J.A., *Field Investigation of Relationship Between Pavement Surface Texture and Friction*, 97th Annual Meeting of the Transportation Research Board, Washington, DC, January 7-11, 2018.

Kuijpers, A., & Van Blokland, G. (2001, August). Tyre/road noise models in the last two decades: a critical evaluation. In *INTER-NOISE and NOISE-CON Congress and Conference Proceedings* (Vol. 2001, No. 2, pp. 2494-2499). Institute of Noise Control Engineering

Kummer, H. W. (1966). Unified Theory of Rubber and Tire Friction. Eng. *Res. Bull. B-94, The Pennsylvania State University*, 100-101.

Kuttesch, J. S. (2004). *Quantifying the relationship between skid resistance and wet weather accidents for Virginia data* (Doctoral dissertation, Virginia Tech).

Leu, M. C., & Henry, J. J. (1978). Prediction of skid resistance as a function of speed from pavement texture measurements. *Transportation Research Record*, *666*, 7-13.

Li, L., & Wang, K. C. (2016). Geometric texture indicators for safety on AC pavements with 1 mm 3D laser texture data. *International Journal of Pavement Research and Technology*, *9*(1), 49-62.

Liu, Qingfan, and Shalaby, Ahmed. "Relating Concrete Pavement Noise and Friction to Three-Dimensional Texture Parameters." International Journal of Pavement Engineering 18.5 (2017): 450–458. Web.

Mahmoud, E., Gates, L., Masad, E., Erdoğan, S., and Garboczi, E. (2010). Comprehensive Evaluation of AIMS Texture, Angularity, and Dimension Measurements. J. Mater. Civ. Eng., 22(4), 369–379.

Maguire, D.J., P.H.D. & Carme, C., P.H.D. (2015). "LOUDNESS tells you nothing", Ishn, vol. 49, no. 8, pp. 34.

Masad, E. (2005). Aggregate Imaging System (AIMS): Basics and Applications. Texas: Texas Transportation Institute. FHWA/TX-05/5-1707-01-1.

McDaniel, R. (2014). Hot Mix Asphalt Surface Characteristics Related to Ride, Texture, Friction, Noise and Durability. West Lafayette.

McGhee, K. (2012). Virginia quiet pavement study. SURF, Norfolk, VA.

Meyer, W. E., Hegmon, R. R., & Gillespie, T. D. (1972). Locked-wheel pavement skid tester correlation and calibration techniques. *NCHRP Research Results Digest*, (38).

Miller, T., Swiertz, D., Tashman, L., Tabatabaee, N., & Bahia, H. U. (2012). Characterization of asphalt pavement surface texture. *Transportation research record*, *2295*(1), 19-26.

Milton, J. C., Shankar, V. N., & Mannering, F. L. (2008). Highway accident severities and the mixed logit model: an exploratory empirical analysis. *Accident Analysis & Prevention*, *40*(1), 260-266.

Msallam, M., Asi, I., & Abudayyeh, D. (2017). Safety Evaluation (Skid Resistance) of Jordan's National Highway Network. *Jordan Journal of Civil Engineering*, *11*(2).

Ohiduzzaman, M., Sirin, O., Kassem, E. and Rochat, J. (2016). State-of-the-Art Review on Sustainable Design and Construction of Quieter Pavements—Part 1: Traffic Noise Measurement and Abatement Techniques. Basel: Molecular Diversity Preservation International and Multidisciplinary Digital Publishing Institute (MDPI).

Ongel, A., & Harvey, J. (2010). Pavement characteristics affecting the frequency content of tire/pavement noise. *Noise Control Engineering Journal*, *58*(6), 563-571.

Petropoulos, G. P. (2007). Multi-parameter analysis and modelling of engineering surface texture. *Journal of Achievements in Materials and Manufacturing Engineering*, *24*(2), 91-100.

Rasmussen, R., Benhard, R., Sanberg, U., and Mun, E.P. (2007). The little book of quieter pavements. Washington, D.C.: U.S. Federal Highway Administration.

Rizenbergs, R.L., Burchett, J.L., Napier, C.T., and Deacon, J.A. (1976). Accidents on Rural Interstate and Parkway Roads and Their Relation to Pavement Friction. Transportation Research Record 584, Transportation Research Board, National Research Council, Washington, D.C., 22-36.

Roe, P. G., Parry, A. R., & Viner, H. E. (1998). High and Low Speed Skidding Resistance: the Influence of Texture Depth." TRL Report 367. *Transport Research Laboratory. Crowthorne*.

Rymer, B. C., Donavan, P., & Kohler, E. R. (2010). *Tire/pavement noise levels related to roadway friction improvement* (No. 10-2896).

Sandberg, U. (1980). Road surface influence on tire/road noise-Part I Descornet. *G., Sandberg, U: Road surface influence on tire/road noise-Part II VTI preprint*, (56).

Sandberg, U. (1998). Influence of Road Surface Texture on Traffic Characteristics Related to Environment, Economy, and Safety: A State-of-the-Art Study Regarding Measures and Measuring Methods, VTI Report 53A-1997, Swedish National Road Administration, Borlange, Sweden.

Sandberg, U. (1987), "Road traffic noise—The influence of the road surface and its characterization", Applied Acoustics, vol. 21, no. 2, pp. 97-118

Sayers, M.W., Gillespie, T.D., and Paterson, D.O. (1986). Guidelines for Conducting and Calibrating Road Roughness Measurements. Work Bank Technical Paper Number 46. The World Bank, Washington, D.C.

Seong, J. C., Park, T. H., Ko, J. H., Chang, S. I., Kim, M., Holt, J. B., & Mehdi, M. R. (2011). Modeling of road traffic noise and estimated human exposure in Fulton County, Georgia, USA. Environment international, 37(8), 1336-1341.

Serigos, P., De Fortier Smit, A. and Prozzi, J. (2014). Incorporating Surface Microtexture in the Prediction of Skid Resistance of Flexible Pavements. *Transportation Research Record: Journal of the Transportation Research Board*, 2457(1), pp.105-113.

Serigos, P., Buddhavarapu, P., Gorman, G., Hong, F. and Prozzi, J. (2016). *The contribution of Micro and Macro-Texture to the Skid Resistance of Flexible Pavement*. Austin: Center for Transportation Research, Report No. SWUTC/16/600451-00085-1.

Smit, A., Prozzi, J., Manuel, T., Natalia, Z. and Buddavarapu, P. (2016). *Designing Quieter Pavement Surfaces*. Austin: Center for Transportation Research, Technical Report No: 0-6819-1.

Texas Department of Transportation (n.d.), 3D Texture Measurement: “Development and Field Evaluation of a Texture Measurement System Based on Continuous Profiles from a 3D Scanning Instrument”.

Thomas, L. (2008). MK2 D-type Maintenance Manual. Issue 4, Findlay, Irvine Limited, Scotland.

Van Keulen, W., Duškov, M (2005). Inventory study of basic knowledge on tyre/road noise. IPG Report DWW-2005-022, Delft, the Netherlands.

Wambold, J. C., Antle, C. E., Henry, J. J., Rado, Z., Descornet, G., Sandberg, U., Gothié, M. and Huschek S. (1995). International PIARC Experiment to Compare and Harmonize Skid Resistance and Texture Measurements (Paris: PIARC) Publication number 01.04.T.

Xiao, J., Kulakowski, B. T., & EI-Gindy, M. (2000). Prediction of Risk of Wet-Pavement Accidents: Fuzzy Logic Model. Transportation Research Record, 1717(1), 28–36. https://doi.org/10.3141/1717-05

Yan, Y., Ran, M., Sandberg, U., Zhou, X., & Xiao, S. (2020). Spectral Techniques Applied to Evaluate Pavement Friction and Surface Texture. *Coatings*, *10*(4), 424.

Zeller, P. (2009). Handbuch Fahrzeugakustik (Handbook vehicle acoustics). *Vieweg+ Teubner, Wiesbaden*.

Zuñiga Garcia, Natalia (2017). Predicting Friction with Improved Texture Characterization. University of Texas at Austin.